FILM COOLING ENHANCEMENT WITH SURFACE RESTRUCTURE

by

Shuping Chen

BS, Tsinghua University, P. R. China, 1990

MS, Xi'an Jiaotong University, P. R. China, 1993

Submitted to the Graduate Faculty of

the Swanson School of Engineering in partial fulfillment

of the requirements for the degree of

Doctor of Philosophy

University of Pittsburgh

2008

UNIVERSITY OF PITTSBURGH

SWANSON SCHOOL OF ENGINEERING

This dissertation was presented

by

Shuping Chen

It was defended on October 3, 2008

and approved by

Dr. Gerald H. Meier, Professor, Department of Mechanical Engineering and Materials Science

Dr. Laura Schaefer, Assistant Professor, Department of Mechanical Engineering and Materials Science

Dr. Sung K. Cho, Assistant Professor, Department of Mechanical Engineering and Materials Science

Dissertation Director: Dr. Minking K. Chyu, Professor,

Department of Mechanical Engineering and Materials Science

Copyright © by Shuping Chen
2008

FILM COOLING ENHANCEMENT WITH SURFACE RESTRUCTURE

Shuping Chen, PhD

University of Pittsburgh, 2008

Discrete-hole film cooling is used extensively in turbine components. In past decades, many research works concerning this technique have been published. Recently, efforts have been directed at seeking technologies that would increase film cooling effectiveness. Particularly, surface reshaping through protective coatings, such as a thermal barrier coating (TBC), is very attractive to turbine designers because extra machining work is not needed for its application. In the present work, film cooling enhancement with surface restructure is experimentally studied using an infrared (IR) imaging technique.

The first surface structure studied is the surface with flow-aligned blockers. The studied configurations include single-hole and three-hole-row structures. The single-hole case is used for studying the effects of blocker design parameters, which include blocker height (0.2D, 0.4D, and 0.6D), distance between two neighboring blockers (0.8D, D, and 1.2D), blocker length (2", 4", and 6"), and blowing ratio M (0.43 and 0.93). The design with the best performance is chosen for the three-hole-row cases.

The second surface shape studied, is the so-called upstream ramp, which is placed in front of a row of film cooling holes. Investigated geometrical parameters include upstream ramp angles (8.5^o, 15^o, and 24^o) and blowing ratio M (0.29, 0.43, 0.57, 0.93, and 1.36). Detailed local film cooling effectiveness and heat transfer coefficient are measured using an IR imaging technique.

The third film cooling concept is the so-called trenched film cooling holes, i.e., film cooling holes sitting in a transverse groove. The film cooling structure for this experimental test consists of a three-hole row embedded in a trench 0.5D in depth and 2D in width, where D is the diameter of the holes. Five blowing ratios (0.29, 0.43, 0.57, 0.93, and 1.36) are tested. Based on the tested results, the three film cooling schemes are also compared.

To implement the experimental work, a test system, which employs a FLIR infrared system to obtain local heat transfer characteristics of both two- and three-temperature problems, is developed. Detailed theoretical issues of data reduction and experimental procedures are presented.

TABLE OF CONTENTS

LIST OF TABLES

LIST OF FIGURES

NOMENCLATURE

Roman Letters

A	Area
D,d	Diameter of film cooling hole
h	Heat transfer coefficient
H	Blocker height
k	Thermal conductivity
L	Length of blocker
M	Blowing ratio
q	Heat flux
Re	Reynolds number
t	Time
T	Temperature
W	Width between two blockers
x,X	Coordinate, distance from the downstream edge of film cooling holes
z	Coordinate

Greek Letters

α	Thermal diffusivity, ramp angle
μ	Dynamic viscosity
ρ	Density
τ	Time
η	Film cooling effectiveness
φ	cooling effectiveness

Subscripts

av	Spanwise averaged
aw	Adiabatic wall
c	Coolant
f	Film cooling flow
i	Initial
m	Main stream
o	Reference, baseline, without film cooling injection case
r	Reference
w	Wall

Abbreviations

BBAR	Broad band antireflection
IR	Infrared
TLC	Thermo-chromic liquid crystal

ACKNOWLEDGEMENTS

Many people provided assistance during this endeavor. First, I want to acknowledge my advisor, Dr. Minking K. Chyu, for his support, encouragement, and patient guidance throughout my dissertation work.

I also thank Drs. Gerald H. Meier, Laura Schaefer, and Sung K. Cho for being my committee members. Thank you for your time, encouragement, and valuable advice. The work done by the staff of the machine shop in the school of engineering was invaluable during construction of the test facility. My thanks are also extended to the faculty and staff members in the Department of Mechanical Engineering.

Special thanks go to my colleagues in the heat transfer group, Emmanuel Olayede, Sin Chien Siw, Danny Mazzotta, and Pavin Ganmol, for their support, help, and inspiration. Thank you to Sin Chien Siw and Danny Mazzotta for helping me to run tests, even over the weekend, during the final two weeks. Thank you for your time and effort.

1.0 INTRODUCTION

1.1 BACKGROUND

The desire to improve the thermal efficiency and power output of modern jet engines has increased turbine inlet temperature up to 2000 K (Martini and Schulz, 2004). This operating temperature is far above the permissible temperature of currently available thermal-resistive materials. Therefore, a cooling technique has to be established to prevent the thermal degradation of turbine components.

Gas turbine cooling designs can be categorized into two different approaches: internal cooling and external cooling. In internal cooling, coolant is forced into and directed through the cooling flow circuits inside turbine components. The coolant is normally the compressed air bled from the compressor. Forced convective heat transfer is the dominant mechanism to transport thermal energy from the component body into the coolant. External cooling, on the other hand, injects or bleeds coolant from a coolant manifold inside components directly into a hot gas stream to protect the exposed component surfaces. External cooling is designed to mitigate heat transfer from a hot gas stream to a component. Examples of this type of cooling include schemes such as film cooling, transpiration cooling, and trailing edge discharge cooling. Turbine researchers always look for heat transfer designs to increase the heat transfer rate in internal cooling but reduce the heat transfer rate in external cooling.

One of the most effective external cooling methods employed in gas turbine airfoil cooling is film cooling. The idea is to introduce a secondary flow with a low temperature into the boundary layer on the surface to be protected. This second flow forms a thin film, which is expected to attach on the surface, as a buffer zone between hot gas stream and airfoil surface. There are two ways to introduce a second flow: slot injection and discrete-hole injection (Figs. 1.1 and 1.2 (reproduced from Yu, 1993).

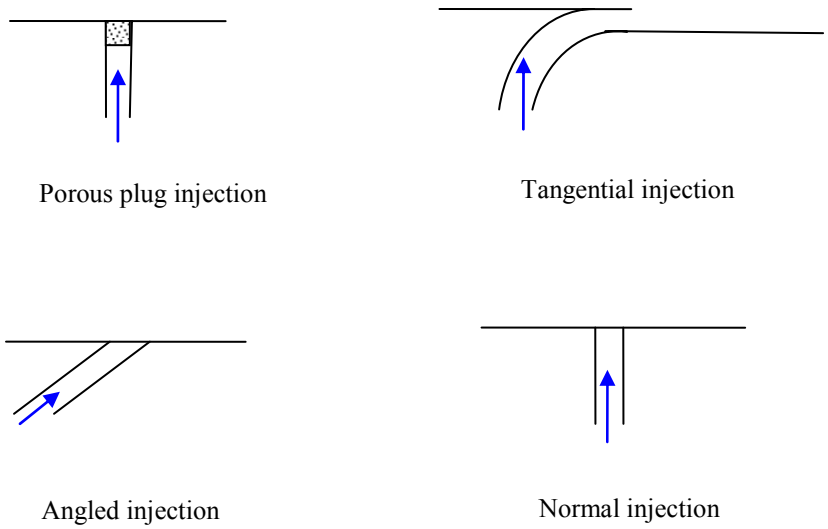

Figure 1.1 Various slot injection configurations (Yu, 1993)

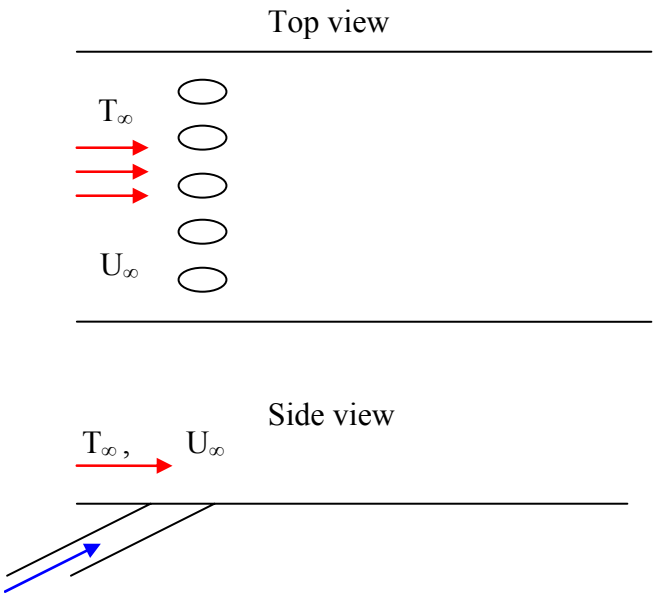

Figure 1.2 Film cooling injection from discrete holes

The flow associated with slot injection film cooling is two dimensional; therefore, it is also called two-dimensional film cooling. The early research work regarding film cooling started from this relatively simple flow regime. Goldstein (1976) authored a thorough review about two-dimensional film cooling. Slot injection film cooling, particularly tangential injection, provides excellent coverage of the protected surface because of uniform laterally spreading coolant and long distance streamwise attachment. However, since gas turbines operate at very high temperatures, stress is always an issue. It is impractical to put slots in a turbine component. In consequence, film cooling is applied through discrete-hole injection in practical applications. Discrete-hole film cooling is also called three-dimensional film cooling, since the associated flow is highly three-dimensional, particularly in the region near film cooling holes. It is a commonly used technique for cooling of turbine airfoils and combustor liners.

Due to the complex flow and heat transfer phenomena in discrete-hole film cooling, there has been extensive research on this topic for the past several decades. Factors that have significant effects on film cooling performance include: film hole internal fluid dynamics (Obot et al., 1979; Pietrzyk et al.,1989; Thole et al. 1998; Wilfert and Wolff, 2000); turbulence and vortices production (Haven and Kurosaka, 1997; Goldstein and Jin, 2001); approaching flows prior to hole entry (Gillespie et al. 1996; Burd and Simon, 1997; Gritsch et al, 1998); hole shaping (Goldstein et al., 1974; Papell, 1984; Makki and Jakubowski, 1986; Berger and Liburdy, 1998; Cho et al., 2001); hole inclination and orientation (Foster and Lampard, 1980; Ligrani et al., 1992; Schmidt et al., 1996; Kohli and Bogard, 1999; Jung and Lee, 2000; Ahn et al, 2000; Lee et al., 2002); hole spacing and length-to-diameter ratio (Lutum and Johnson,1999; Hale et al., 2000); density ratio (Pederson et al., 1977; Teekaram et al., 1989; Ammari et al., 1990; Sinha et al., 1991; Salcudean et al., 1994); blowing ratio (Bergeles et al., 1977; Forth and Jones, 1988; Vedula and Metzger, 1991; Ekkad et al., 1997); momentum flux ratio and mainstream turbulence intensity (Jumper et al., 1991; Menhendal and Han, 1992; Drost et al., 1997; Saumweber et al., 2003); mainstream acceleration (Kim et al,. 2005); external surface curvature (Schwarz et al., 1990); and external surface roughness (Goldstein et al., 1985; Barlow and Kim, 1995; Schmidt et al.,1996). This active research trend continues, striving for new techniques for improving film cooling performance to approach that in an ideal tangential slot injection (Fig. 1.3, reproduced from Bunker, 2005).

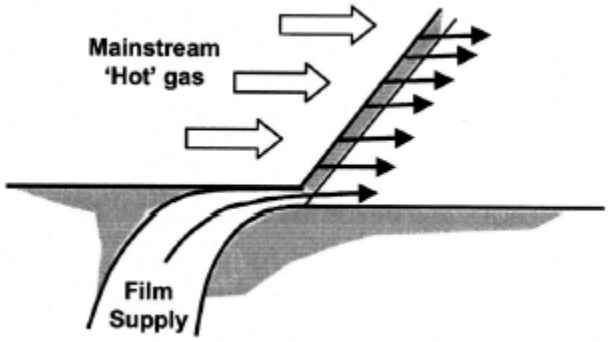

Figure 1.3 Ideal tangential slot injection film cooling (Bunker, 2005)

Three concepts of film cooling based on surface restructure have been suggested in recent years, though there is no concrete data. They are: (1) downstream flow-aligned blocker; (2) upstream ramp; (3) trench. Details about these film cooling concepts are included in Section 1.3. The common advantage among them is that their structures can be formed by protective coating, such as thermal barrier coating (TBC), without additional machining work, and therefore no stress issue. The first two are presented via computational flow dynamics (CFD) by Na (Na and Shih, 2006) and Shih (Shih et al., 2006), respectively. Their simulation results indicate that the structures significantly improve film cooling effectiveness. However, the first one has not been experimentally investigated and little research has been published on the second. There are some literature regarding the third, but the results are far from conclusive.

The work in the present dissertation focuses on the experimental study of the aforementioned three film cooling concepts. Particularly, the three film cooling schemes are compared based on the experimental results. The infrared (IR) imaging technique for the measurement of heat transfer coefficient and film cooling effectiveness is also established via this work.

1.2 PREVIOUS STUDIES

A discrete film cooling hole is typically cylindrical or diffusion fan-shaped with 30^{o}-35^{o} inclination relative to the protected surface along the streamwise direction (Bunker, 2006). Full coverage thermal protection can prevail, if coolant flow attaches onto the protected surface and never penetrates and dissipates in the hot mainstream. However, such an ideal film cooling performance is always compromised because of main flow/film cooling flow interaction. Studies of coolant jets by Fric and Roshko (1994) reported the vortical structure in the wake of a transverse jet. As illustrated in Fig.1.4 (reproduced from Fric and Roshko, 1994), four types of vortex structure are observed: (1) the jet shear-layer vortices; (2) the system of horseshoe vortices; (3) the developing counter-rotating vortex (CRV) pair; and (4) the wake vortices.

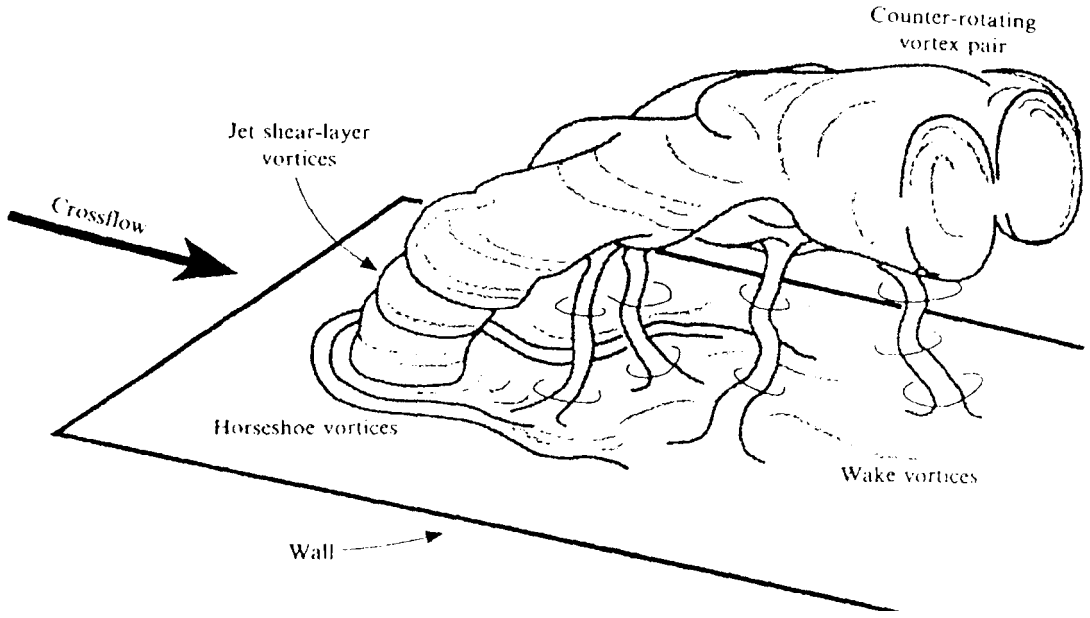

Figure 1.4 Schematic of vortical structure associated with a jet in cross flow (Fric and Roshko, 1994)

This complex flow pattern reflexes mainstream-jet interaction and significantly affects film cooling performance. Particularly, the CRV pair, also called "kidney vortices," tends to lift coolant flow off the protected surface and to entrain hot gases underneath. As a result, coolant flow penetrates and dissipates quickly into the main flow stream, and degraded protection is inevitable. To directly address this issue, there have been studies using altering vortices structure, variation of the geometry of film cooling hole, or both.

Zaman and Foss (1996) studied the effect of attaching a tab over a jet nozzle on the penetration and spreading of the jet. They found that the presence of a tab over the upstream edge of a jet produces anti-kidney vortices, which alleviates the jet's lift-off and penetration effect (Fig.1.5).

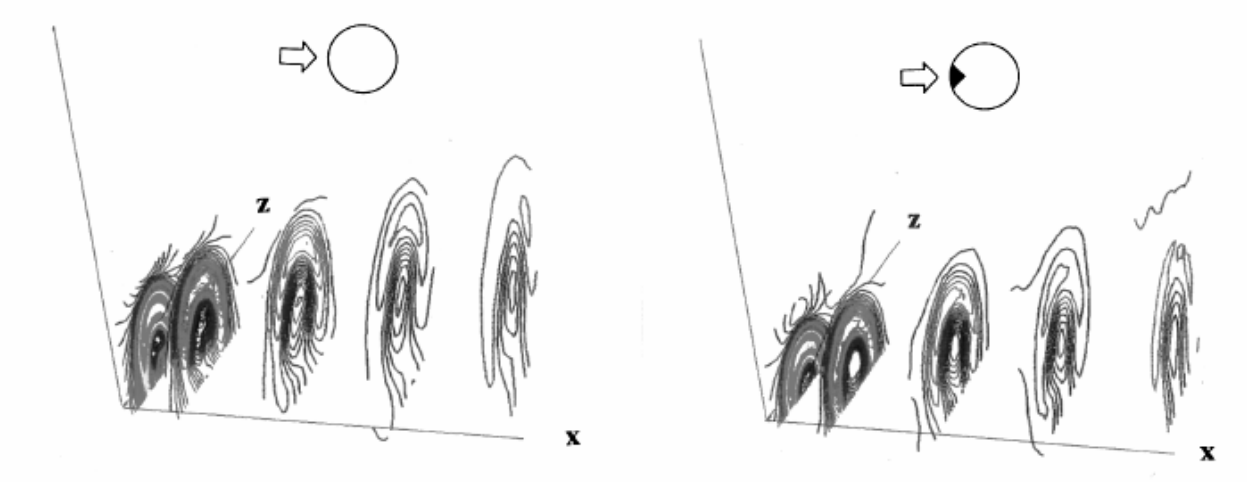

Figure 1.5 Perspective views of mean velocity, which indicates the penetration height (Zaman and Foss, 1996)

Haven and Kurosaka (1996) reported improvement in jet coverage using an approach based on vortex cancellation. Specifically, they placed a vane producing a pair of canceling vortices inside a jet passage. The canceling vortices weaken the kidney vortices and reduce the coolant lift-off. Even for a completely detached jet, the cancellation brings it closer to the surface (Fig.1.6).

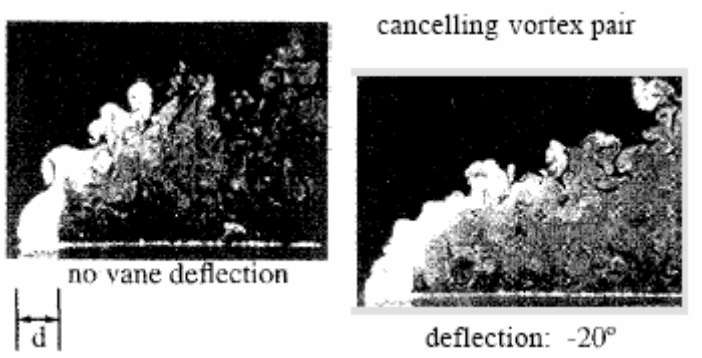

Figure 1.6 Vane introduced anti-kidney vortex reducing the lift-off effect of kidney vortex pair (Haven and Kurosaka, 1996)

Shih et al. (1999) presented a computational work about placing a strut within each film cooling hole to modify the vortex structure. Haven et al. (1997) and Hyams et al. (1997) studied the effect of the vortices in a shaped hole on film cooling performance. Okita and Nishiura (2006) proposed an arrowhead-shaped hole for improving film cooling effectiveness. Fric and Campbell (2002) studied a so-called cratered film cooling hole whose shape near the exit region was recessed to a shallow cylinder (Fig. 1.7). Their results revealed substantial improvement in film cooling effectiveness.

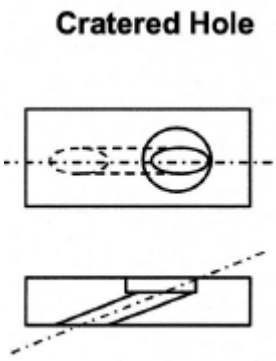

Figure 1.7 Cratered hole (Bunker, 2005)

Bunker (2002) further modified the design into a two-dimensional trench in which film cooling holes are embedded. The measured data suggested a 50-75% increase in film cooling effectiveness relative to that achieved by a standard circular-hole. Also suggested was the idea that the trench can be formed by thermal barrier coating (TBC) without additional machining work. The study indicated that a narrow and shallow trench performs better than a deeper and wider one.

Based on Bunker's work, Lu et al. (2005) studied four trench configurations (Fig. 1.8) using a transient IR thermography technique to obtain spatial distribution of film cooling effectiveness and heat transfer coefficient. Three blowing ratios of M=0.5, 1.0, and 1.5 were tested. They observed that Cases 2 and 4 performed better with only a slight increase in heat transfer.

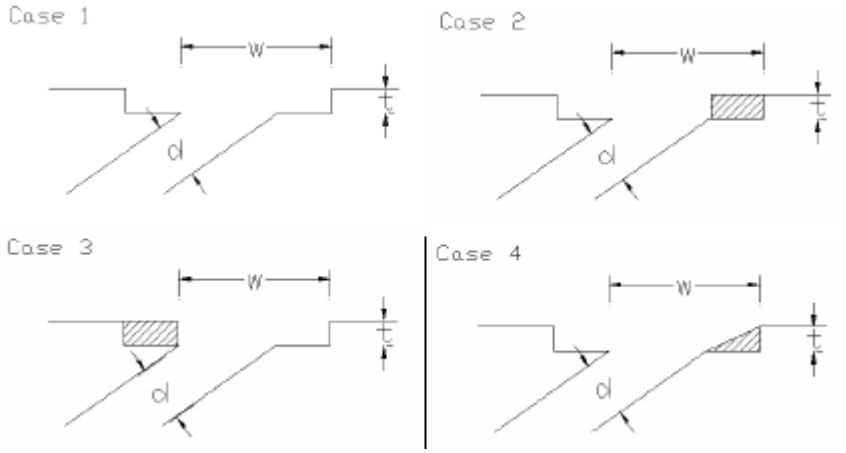

Figure 1.8 Schematics of four trench configurations studied by Lu et al. (2005)

Waye and Bogard (2006) reported their work about nine trench configurations (Fig. 1.9) in an airfoil cascade test. They used a steady IR thermography technique; thus, only film cooling effectiveness was presented. They found that the vertical walls at both the upstream edge and downstream edge of film cooling holes are crucial to improving film cooling effectiveness, which is consistent with the observation made in Lu et al.'s (2005) work. Therefore, Case 2 is the optimal configuration.

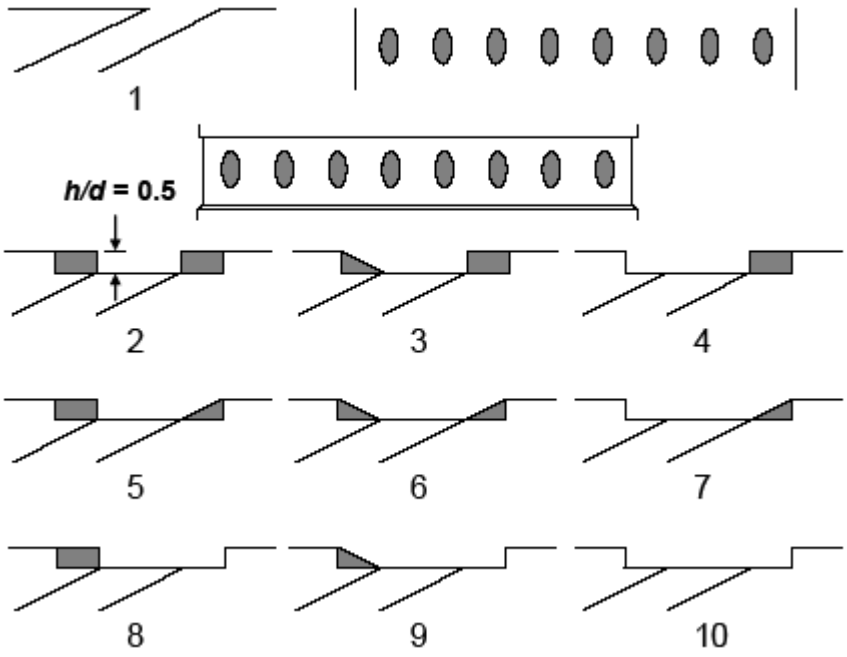

Figure 1.9 Schematics of nine trench configurations studied by Waye and Bogard (2006)

Somawardhana and Bogard (2007) studied the effects of obstructions and surface roughness on film cooling effectiveness with a transverse trench. The trench configuration is the same as that shown in Fig.1.9 Case 2. They found that film cooling effectiveness with trench is higher than that of the traditional cylindrical hole without a trench. Harrison et al. (2007) presented the effects of a trench on the heat transfer coefficient. The configuration of the trench is very similar to that shown in Fig.1.9 Case 2, except that its depth is 1.0D. They found that the presence of a trench increases heat transfer coefficient overall. CFD predictions of film cooling effectiveness for trenches were also reported by Harrison and Bogard (2007).

Na and Shih (2006) proposed placing a ramp with a backward facing step upstream of the film cooling holes to modify the approaching boundary layer flow and its interaction with film cooling flow. Their computational results showed very promising effects on film cooling performance (Fig. 1.10).

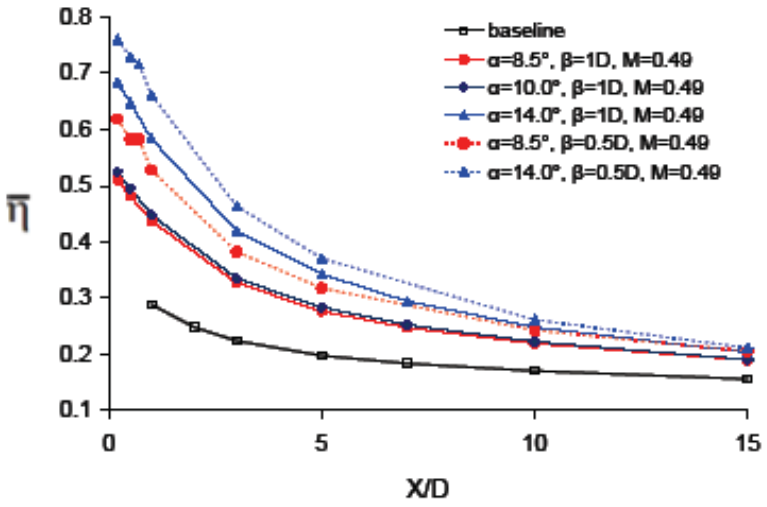

Figure 1.10 Spanwise averaged film cooling effectiveness with and without upstream ramp (Na and Shih, 2006)

In the same year, Shih et al. (2006) presented another cooling concept of placing flow-aligned blockers downstream of film cooling holes to prevent hot gases from entraining underneath kidney vortices via computational fluid dynamics. As shown in Fig 1.11, the computation results indicated great improvements in film cooling effectiveness.

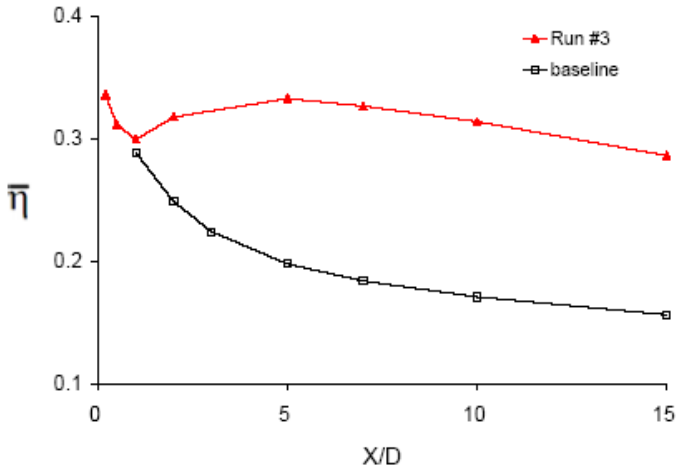

Figure 1.11 Spanwise averaged film cooling effectiveness with and without downstream flow-aligned blocker (Shih et al, 2006)

Barigozzi et al. (2007) studied the effects of an upstream ramp on cylindrical and fan-shaped hole film cooling performance. Their results indicated that the upstream ramp introduced strong aerodynamic loss and degraded film cooling performance, except that it improved film cooling at low blowing ratio for cylindrical holes.

1.3 PRESENT WORK STATEMENT

The aforementioned three film cooling concepts based on surface reshaping could be useful to turbine designers. One of the reasons is that these structures can be manufactured over the layer of thermal-barrier coating (TBC) provided on the external surface of an airfoil, without additional machining work. In the present work, these concepts are tested via a flat plate housed in a rectangular channel and compared based on the experimental results.

The idea of film cooling of flow-aligned blockers is depicted in Fig.1.12 (Shih et al., 2006).

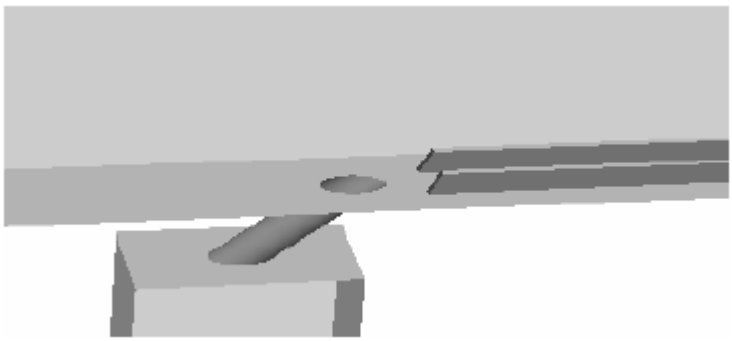

Figure 1.12 Schematic of the film cooling concept of flow-aligned blockers (Shih et al. 2006)

Two blockers sit in the downstream area of the film cooling hole. It is expected that the blockers will prevent hot stream from entraining underneath film cooling flow, thus improve film cooling performance. The study includes two phases. The first phase investigates the effect of blocker design parameters (height and length) and the distance between two blockers using a single film cooling hole. The second phase considers the effects of blowing ratio via a three-hole-row configuration, with the best performance design found in the first phase. While local film cooling effectiveness and heat transfer coefficient for all tested cases are measured by an IR imaging technique in the first phase, centerline and spanwise averaged film cooling effectiveness are compared with their counterparts in each design. In the second phase, both film cooling effectiveness and heat transfer coefficient are compared with the baseline cases. The overall heat flux reduction is also calculated to further evaluate film cooling performance.

Illustrated in Fig. 1.13 (Na and Shih, 2006) is the upstream ramp film cooling concept. The ramp modifies the approaching boundary layer flow and thus the mainstream/jet interaction, which consequently increases film cooling effectiveness. The study is two-fold in scope. First

the efficacy of the concept is experimentally validated. Second, the relationship among the major geometrical and flow parameters in the system is examined so that the design may be optimized.

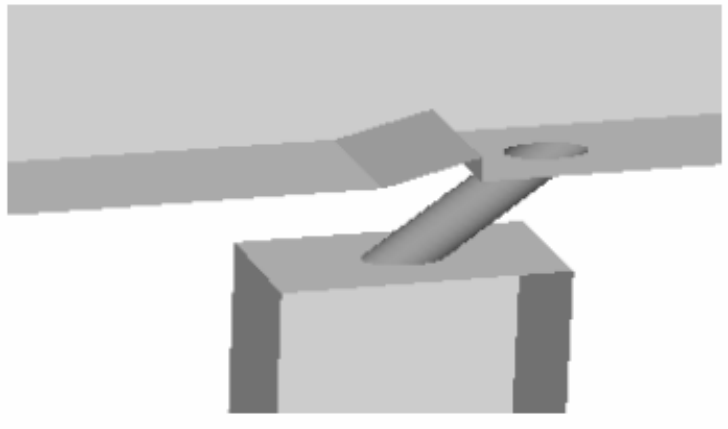

Figure 1.13 Schematic of the film cooling concept of upstream ramp (Na and Shih 2006)

To facilitate the study, local film cooling effectiveness η and heat transfer coefficient h are measured simultaneously using an IR imaging technique. The test matrix includes three upstream ramp angles at five different blowing ratios. For each case, the reduced heat flux relative to its corresponding baseline value, i.e., the heat flux without coolant protection, is also determined to assess the overall film cooling performance.

Figure 1.14 illustrates trenched film cooling holes in the experimental study. The trench is a two-dimensional narrow and shallow groove upon which film cooling holes sit. Both film cooling effectiveness and heat transfer coefficient are measured via a transient test. Five blowing ratios are tested. As in the above two studies, the overall heat flux reduction is calculated to further evaluate film cooling performance.

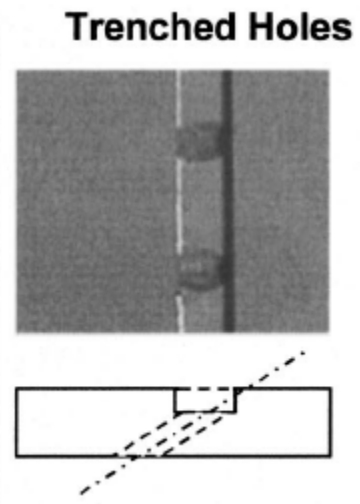

Figure 1.14 Trenched film cooling holes (Bunker, 2005)

2.0 FILM COOLING MEASUREMENT

2.1 INTRODUCTION

In the previous chapter, the research work of this dissertation, which covers studies on three film cooling concepts, is introduced. In this chapter, the method for film cooling measurement, as well as the definitions of the associated parameters, is introduced. In particular, the IR imaging technique developed by the author in the present dissertation work for both two- and three-temperature problems is addressed in detail.

2.2 FILM COOLING FUNDAMENTALS

The heat transfer model associated with film cooling is a so-called three-temperature problem, as illustrated in Fig. 2.1 (Figure is from Han et al., 1999)

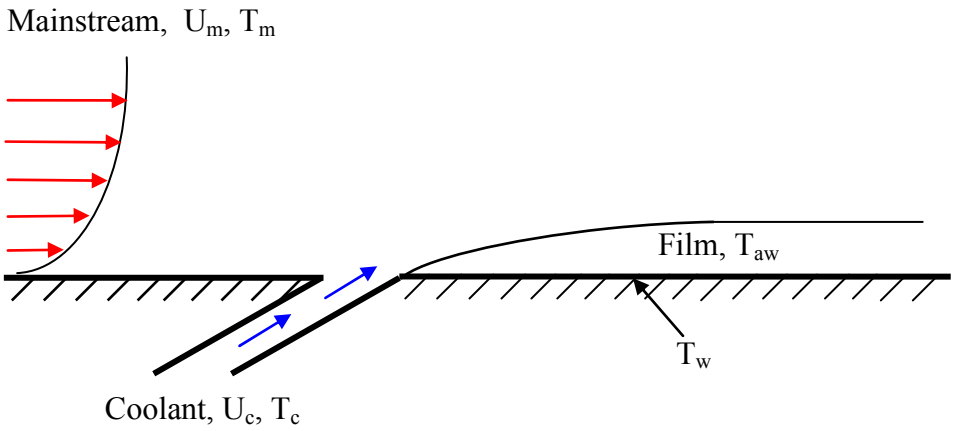

Figure 2.1 Schematic of film cooling concept (Figure is from Han et al., 1999)

Typically, the heat flux from flow to surface without film cooling is expressed as

$$q_o = h_o(T_m - T_w) \tag{2.1}$$

where h_o is the heat transfer coefficient on the surface, T_m is mainstream temperature, and T_w is surface temperature. In this case, T_m-T_w is the driving potential for heat transfer; thus it is called a two-temperature problem. While film cooling flow is injected on the surface, the flow downstream of a film cooling hole is a mixture of mainstream and coolant. It is the temperature of this mixed flow stream, not T_m or T_c, that drives heat transfer. The heat flux to surface can be described as

$$q = h(T_{aw} - T_w) \tag{2.2}$$

where h is the heat transfer coefficient with film cooling injection, T_{aw} ($T_m \geq T_{aw} \geq T_c$) is adiabatic wall temperature. In this case, both h and T_{aw} are unknowns. To solve for $T_{aw,}$ a non-dimensional temperature is defined as

$$\eta = \frac{T_m - T_{aw}}{T_m - T_c} \tag{2.3}$$

where η is the so-called adiabatic film cooling effectiveness, T_c is the temperature of coolant. Since the magnitude of T_{aw} varies from T_c to T_m, the value of η falls between from 0 to 1. When η=0, it implies that the adiabatic wall temperature is equal to the hot gas temperature, which also suggests that the surface is under no film protection. On the other hand, η=1 means that the adiabatic wall temperature is the coolant temperature, which indicates complete film protection.

In practical application, turbine designers are concerned with the reduction of heat load to the film protected surface. By combining film cooling effectiveness η and heat transfer coefficient h, the ratio of heat flux q to a film-protected surface to that of the corresponding baseline value without film cooling q_o, can be expressed as

$$q/q_o = (h/h_o)(1-\eta/\varphi) \tag{2.4}$$

where φ is the overall cooling effectiveness given by $\varphi = \frac{T_w - T_m}{T_c - T_m}$. The typical values of φ in actual engines range from 0.5 to 0.7 (Yu et al., 2002) in the main-body section. The average value of 0.6 is used in the calculation of the present studies. When film protection is effective, the value of q/q_o should be less than one. The situation of q/q_o = 0 represents a limiting case in which the local surface is fully protected by the cooling film.

From the above analysis, it is apparent that both η and h are needed for the evaluation of film cooling performance. A majority of studies focus only on film cooling effectiveness, assuming that heat transfer coefficient is rather uninfluenced by injection. However, such an assumption is only valid in the regions sufficiently far downstream. In the region near an ejection hole, the situation is expected to be different. The interaction between mainstream and coolant can significantly change the flow conditions, causing heat transfer coefficient to either decrease (Eriksen and Goldstein, 1974) or increase (Hay et al., 1985) relative to that in a no injection case.

As suggested in Section 1.1, the mass flow rate of coolant is one of the important factors affecting film cooling performance. The dimensionless coolant mass flow rate, normalized by the main stream mass flow rate, is given by the blowing ratio M

$$M = \frac{(\rho V)_c}{(\rho V)_m} \tag{2.5}$$

When the density ratio between the coolant and mainstream is about 1, which is the case in the present study, M is equivalent to the velocity ratio of coolant flow to main flow.

2.3 TRANSIENT TECHNIQUES FOR FILM COOLING MEASUREMENT

2.3.1 Transient liquid crystal method

Transient liquid crystal technique has been one of the standard techniques for determining heat transfer coefficient h and film cooling effectiveness η for turbine film cooling for several years. Vedula and Metzger (1991) developed the two-test method for simultaneously obtaining h and

η. Several studies have used this technique (Ekkad et al., 1997; Yu et al., 1998, 2002; Chen et al., 2006). Details of this method are described below because the same transient heat conduction model is used in the present IR imaging technique.

The transient liquid crystal technique is based on the one-dimensional transient heat conduction solution over a semi-infinite solid domain (Fig. 2.2). The local heat transfer coefficient can be inferred as the steady convective boundary condition over the surface exposed to the flow.

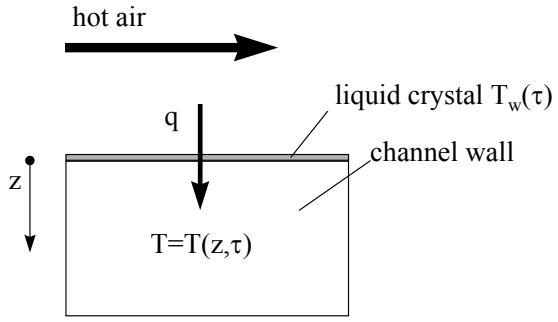

Figure 2.2 Schematic of one-dimensional transient heat transfer model

The equation governing the unsteady heat conduction is

$$k\frac{\partial^2 T}{\partial z^2} = \rho C_p \frac{\partial T}{\partial t} \tag{2.6}$$

The associated boundary and initial conditions are

$$-k\left.\frac{\partial T}{\partial z}\right|_{z=0} = h(T_w - T_r) \tag{2.7}$$

$$T\big|_{z=\infty} = T_i \tag{2.8}$$

$$T\big|_{t=o} = T_i \tag{2.9}$$

where T_i is the initial temperature of the test section, T_w is the local surface temperature, and T_r is the flow reference temperature. Equations (2.6)-(2.9) lead to a solution of T_w expressed as

$$\frac{T_w - T_i}{T_r - T_i} = 1 - \exp\left[\frac{h^2 \alpha t}{k^2}\right] \operatorname{erfc}\left[\frac{h\sqrt{\alpha t}}{k}\right] \tag{2.10}$$

In a typical heat convection system, the reference temperature T_r is readily available, i.e. equal to the temperature of the mainstream or bulk flow. As the time-varying liquid crystal images can provide a relation between T_w and t over the entire viewing domain, the distribution of local heat transfer coefficient, h, can be resolved from the above equation.

While the above approach is generally valid for resolving typical two-temperature convection problems, it is unsuitable for film cooling. As mentioned earlier, film cooling is a three-temperature problem, its thermal transport is governed by the temperatures of two participating streams and the surface exposed to the mixture of those streams. Thus, the reference temperature T_r in Eq. (2.10) is no longer a known quantity and needs to be solved simultaneously with the heat transfer coefficient. T_r is also termed the adiabatic wall temperature, T_{aw}, which is introduced to give an expression of film cooling effectiveness, as described in Section 2.2. This implies that two relations similar to Eq. (2.10) need to be established.

Based on the notion that the turbulent convection is predominantly controlled by flow dynamics rather than thermal conditions, two relations can be obtained by performing two different, but closely related, heat transfer tests under the same flow conditions. The resulting equations for the two unknowns h and T_{aw} are

$$\frac{T_w - T_{il}}{T_{aw} - T_{il}} = 1 - \exp\left[\frac{h^2 \alpha \tau_1}{k^2}\right] \operatorname{erfc}\left[\frac{h\sqrt{\alpha \tau_1}}{k}\right] \tag{2.11}$$

$$\frac{T_w - T_{i2}}{T_{aw} - T_{i2}} = 1 - \exp\left[\frac{h^2 \alpha \tau_2}{k^2}\right] \operatorname{erfc}\left[\frac{h\sqrt{\alpha \tau_2}}{k}\right] \tag{2.12}$$

In reality, one of the two tests, the "hot test", uses a film injection close to, but slightly lower than, the heated mainstream, while the "cold test" uses an unheated or slightly heated injection. A key criterion for selecting these test temperatures is to ensure that the two equations, Eqs. (2.11) and (2.12), are well coupled, so that when combined they yield a solution for the two unknowns.

In an actual experiment, a perfect step change of the applied flow temperature is usually not possible, and the reference temperature, in fact, is a function of time. This can be accounted for by modifying the solutions via superposition and Duhamel's theorem. The solution becomes:

$$T_w - T_i = \sum_{i=1}^{N} U(t - \tau_i) \Delta T_r \tag{2.13}$$

where

$$U(\tau - \tau_i) = 1 - \exp\left(\frac{h^2}{k^2} \alpha (\tau - \tau_i)\right) \operatorname{erfc}\left(\frac{h}{k}\sqrt{\alpha(\tau - \tau_i)}\right) \tag{2.14}$$

Since ΔT_r is directly related to the variations of the mainstream temperature, T_m, and injection temperature, T_c, by the definition of film cooling effectiveness η,

$$\Delta T_r = (1 - \eta)\Delta T_m + \eta \Delta T_c \tag{2.15}$$

substituting Eq. (2.15) into Eq. (2.13), the unknowns for the present system become film cooling effectiveness, η, and heat transfer coefficient, h.

2.3.2 The transient IR imaging technique for heat transfer measurement

The IR imaging technique involves the IR system, which can map the temperature of the surface viewed. Details of this system can be found in the IR system operation manual. Here only the procedures of running a test and getting solutions are introduced.

As for a two-temperature problem, the procedure for running a test is exactly the same as that in the transient liquid crystal method. The heat transfer coefficient is solved by using Eq. (2.10). In transient liquid crystal technique, usually only one T_w and corresponding lap time t are obtained. However, a series value of T_w and corresponding time t are available by using the IR system; thus, several equations similar to Eq. (2.10) are solved. The average of those h values is taken as the actual heat transfer coefficient so that uncertainty is minimized.

In the case of film cooling measurement, one test is sufficient for determining both η and h. During the test, only main flow is heated, while the coolant flow is kept at room temperature. As mentioned before, since the IR system provides local surface temperature distribution at a certain time interval, multiple equations (number of equations >>2) similar to Eq. (2.13) can be established via a single test. Optimal solutions of η and h are obtained by minimizing the uncertainty via least square method. Ekkad et al. (2004) reported their work using transient IR technique for film cooling measurement. However, only two frames are used for solving η and h in their work. They did not use this technique to get optimal η and h with minimized uncertainties. Details of the least square method used in the present study can be found in Appendix A. The code developed and written in Fortran by the author is in Appendix B.

2.3.3 The advantages and disadvantages of transient IR technique

IR imaging technique has many advantages.

1. A single test is sufficient for this technique; this reduces the number of tests and the uncertainties related to running two different tests at different times.

2. The test is not limited by the operating point, which the liquid crystal technique has. Liquid crystal cannot operate beyond 100^{o}C, whereas the IR technique has no such limitation, provided that the test plate material has low thermal conductivity to validate the transient semi-infinite conduction model.

3. The initial temperature distribution is available via the IR technique. It is very difficult to acquire this information in the liquid crystal technique.

4. The coolant does not need to be heated, as in the case of the two test method. This reduces experimental complexity and saves time.

5. Liquid crystal is based on sensing the reflective light and sensitive to the angle of illumination and viewing, while the IR technique does not need any special illumination.

6. Calibration for the IR technique is relatively more straight forward.

7. Multiple equations can be established via a single test, so that the least square method can be used to minimize uncertainty, which is not possible for the liquid crystal method.

The disadvantage of the IR technique is that the IR transparent window must be present for the IR camera, an unnecessary arrangement in the liquid crystal technique.

3.0 EXPERIMENTAL APPARATUS AND PROCEDURES

3.1 OVERALL TEST SETUP

The overall test setup is shown in Fig.3.1. The tests were conducted in SB81 Benedum Hall, at the University of Pittsburgh.

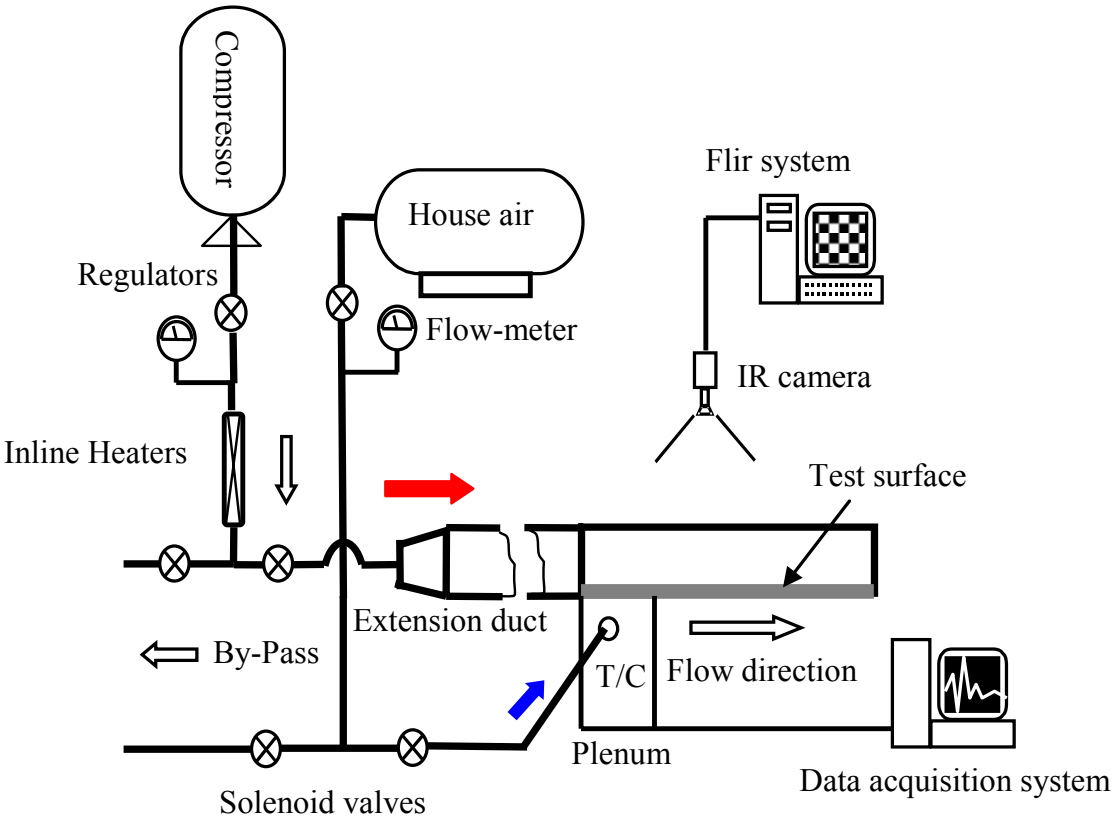

Figure 3.1 Schematic of the overall test setup

A 150-horsepower laboratory compressor provides the main flow. The flow rate is measured by a standard ASME orifice. After being metered, the flow goes through an inline 20 kW heater controlled by an auto-transformer, and the temperature of flow can be controlled accurately to a desired level. The heater, made by Chromalox, has a temperature range of 366-533K (200-500F). Upstream of the test section, there is a 762mm (30") long square duct with 89mm (3.5") per side. This relatively long duct serves as the developing section to ensure more uniform flow profile before reaching the test section. Film cooling flow is provided by house air and kept at room temperature. The flow is introduced to the filter integrated with a dryer after passing through a regulator valve. The clean and dried airflow is then metered by a rotameter before entering film cooling holes through a cubic shaped plenum of size 76.2x76.2x76.2mm (3"x3"x3"). One three-way valve is installed upstream of the extension duct in the main flow line, and another one is installed upstream of the plenum in the film cooling line. Before a transient test starts, both flows are diverted to bypass.

3.2 INFRARED (IR) IMAGING SYSTEM

The IR imaging system used in the present work is a FLIR system ThermaCAM SC40. The IR camera in this system can be controlled by a computer through software equipped with the system. The surface temperature data are also calculated by the software. Figure 3.2 shows an example of the temperature distribution of a viewed surface. Inside the camera, there is a Quantum Well Focal Plane Array (QWIP), which receives and records the infrared radiation between 8 and 9μm. Based on the radiation received, the temperature of the objects viewed is

determined. The resolution of the camera is 320x240 pixels in a viewing domain. The internal components of the camera are cooled to 70K by using a Stirling cooler. The camera has several temperature ranges between -20°C and 1500°C, and the temperature range can also be extended up to 2000°C with an optional filter. The accuracy of the camera as stated in its manual is ±2% of the chosen measurement range or ±2°C (2K), whichever is larger. The temperature range of -20°C to 80°C is used in the present study. The accuracy in this range is ±2°C.

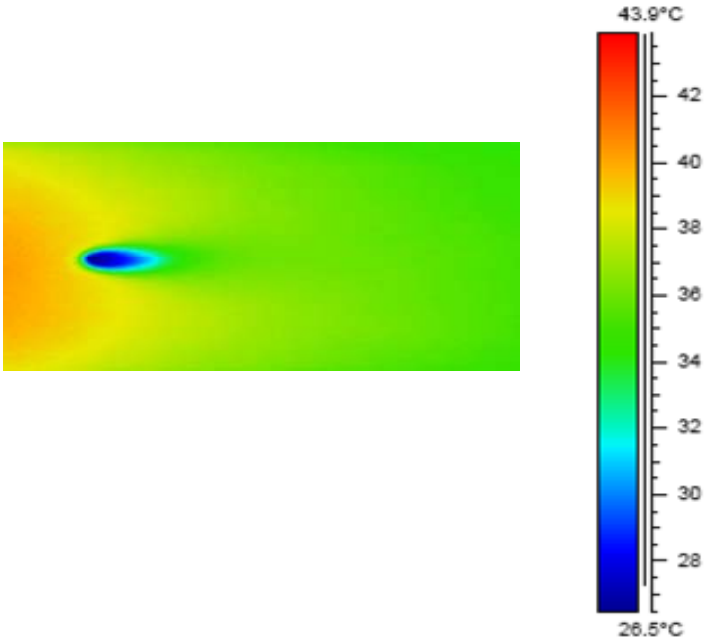

Figure 3.2 Surface temperature of single hole film cooling viewed by an IR camera

3.3 IR TRANSPARENT WINDOW

The flow must be confined to a channel for any test. This means that an IR camera has to see through the channel to measure the temperature of any inner surface. Typically, the test channel is made of Plexiglas, which is not IR transparent. Therefore, a special window, which does not absorb IR radiation, is needed. The special window used in the present study is a custom-designed Zinc Selenide CVD window made by CRYSTRAN, which is polished and coated with broad band antireflection (BBAR) on both sides. The size of this window is 101.6x152.4x8mm (4"x6"x0.315"). Its transmittance is shown in Fig. 3.3 (from the website of the specification of BBAR coated ZeSe CVD windows).

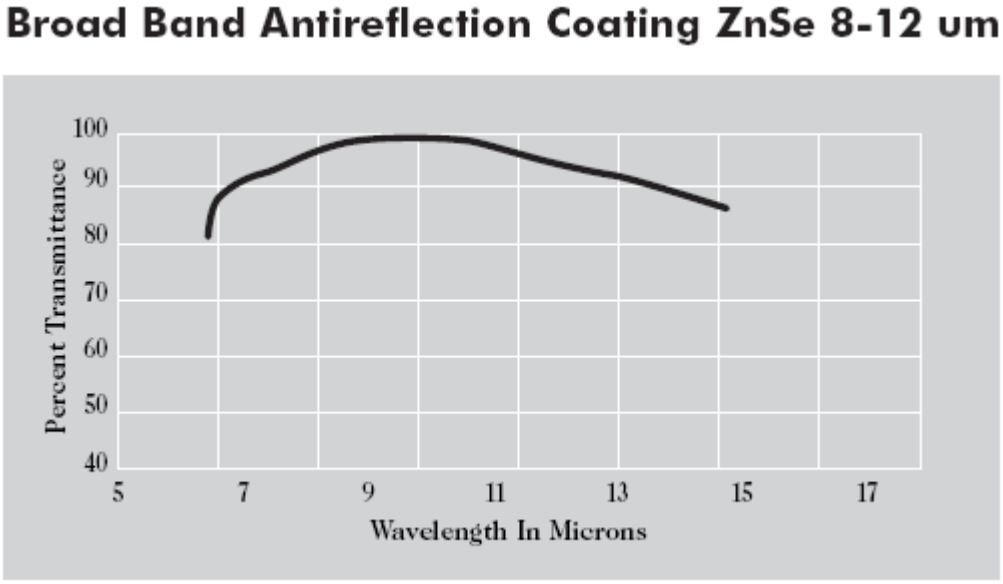

Figure 3.3 Transmittance of ZnSe CVD window with BBAR coated on both sides (from the website of the specification of BBAR coated ZeSe CVD windows)

3.4 TEST SURFACE PREPARATION AND SYSTEM CALIBRATION

To reduce uncertainty, large emissivity is usually preferred for IR imaging techniques. Therefore, the test surface is painted black after being cleaned and dried. An airbrush is used to spray ink on the surface, and the test plate is left overnight to dry completely before being assembled into the test section.

After the test section is installed in the test rig, the emissivity of the prepared test surface is determined through a calibration test. Temperature is measured using thermocouples attached on the surface, as well as by the IR camera. The test surface is then heated by hot air from a blower. The temperature is monitored during the heating up process, which subsequently achieves a steady state. The values of the temperature indicated by the thermocouples are compared with the temperatures obtained by the IR camera at locations very close to the thermocouple bead. Emissivity of the test surface is then adjusted until the IR system readings match the thermocouple readings within 0.1^{o}C. The emissivities of the prepared test surfaces viewed through the special window in the present study range from 0.93-0.97.

3.5 EXPERIMENTAL PROCEDURES

Temperature readings from the thermocouples for the main and coolant flows during a test are monitored by a data acquisition system. The data acquisition system used in this study is produced by National Instruments (NIDAQ). Before a test is started, the focus of the IR camera

is adjusted to view the surface in the proper image size. The IR camera needs to be warmed up before being connected to a computer, on which the software for controlling the camera is operated.

A test begins with the main flow valve being closed, and the three-way valves switched to the bypass mode. The film cooling flow valve is opened and adjusted to achieve the desired flow rate. The compressor providing the main flow is then turned on, while the main flow valve is kept closed. As the pressure upstream of the orifice, indicated by the pressure gauge, reaches 80psi, the three-way valve is opened and adjusted until the desired flow rate is reached. The heater is then turned on to heat the main flow to the required temperature. As the temperature of the main flow reaches the desired level, two flows are suddenly diverted to the test section. Simultaneously, the data acquisition system is triggered to record thermocouple readings. The recording of the temperature of the test surface by IR imaging is started before the flows are switched to the test section. This allows the IR camera to measure the initial temperature of the surface. To indicate the starting time of a test, a piece of aluminum paper is placed at the edge of the viewing domain in the test section as a marker. The moment that the marker is blown away indicates the start of a transient test. A transient test usually lasts for about three minutes. Then the recordings of thermocouple readings and surface temperature are stopped. Flows are again diverted to bypass, and the heater is turned off. When the temperature of the main flow is sufficiently low, the compressor is shut down. All the data are saved for post data reduction. A test run typically lasts 30 minutes.

3.6 DATA REDUCTION

The least square method is used to obtain the value of both η and h in data reduction. 15 frames of IR images are used for solving η and h in the present study. The first frame is acquired at the sixth second after the transient test is started. Then a frame is picked up every four seconds. The last frame is at the 62^{th} second. As mentioned before, the initial temperature of the test surface is obtained from the IR images recorded before the transient test is started. Several frames are used here to obtain the average values of the local temperatures.

3.7 FLOW CONDITIONS

Film cooling performance is affected by main flow characteristics, particularly the turbulence intensity and boundary layer thickness upstream of the film cooling injection site. Therefore, the flow conditions need to be characterized. The main flow velocity in the present study is 34.7m/s, which leads to a Reynolds number of 193,600 based on the hydraulic diameter of the square duct. Five blowing ratios, which are 0.29, 0.43, 0.57, 0.93, and 1.36, are tested in the present study. The corresponding Reynolds numbers for the film cooling flow are 3900, 5900, 7900, 13000, and 19000. The density ratio of the main flow to the film cooling flow is about 1. The main flow turbulence intensity is approximately 1.5%. The boundary layer velocity profile close to the position of a film cooling hole, without film cooling injection, is shown in Fig. 3.4. The

boundary layer thickness (where $u=0.99U_\infty$) is 13.97mm. Assuming a power law velocity profile of the form

$$\frac{u}{U_\infty} = \left(\frac{y}{\delta}\right)^{\frac{1}{n}} \tag{3.1}$$

the least square power regression yields n equal to 6.7. As shown in Fig. 3.4, the velocity profile has the characteristics of a fully turbulent boundary layer. The momentum thickness and displacement thickness are calculated to be 1.4mm and 1.8mm, respectively.

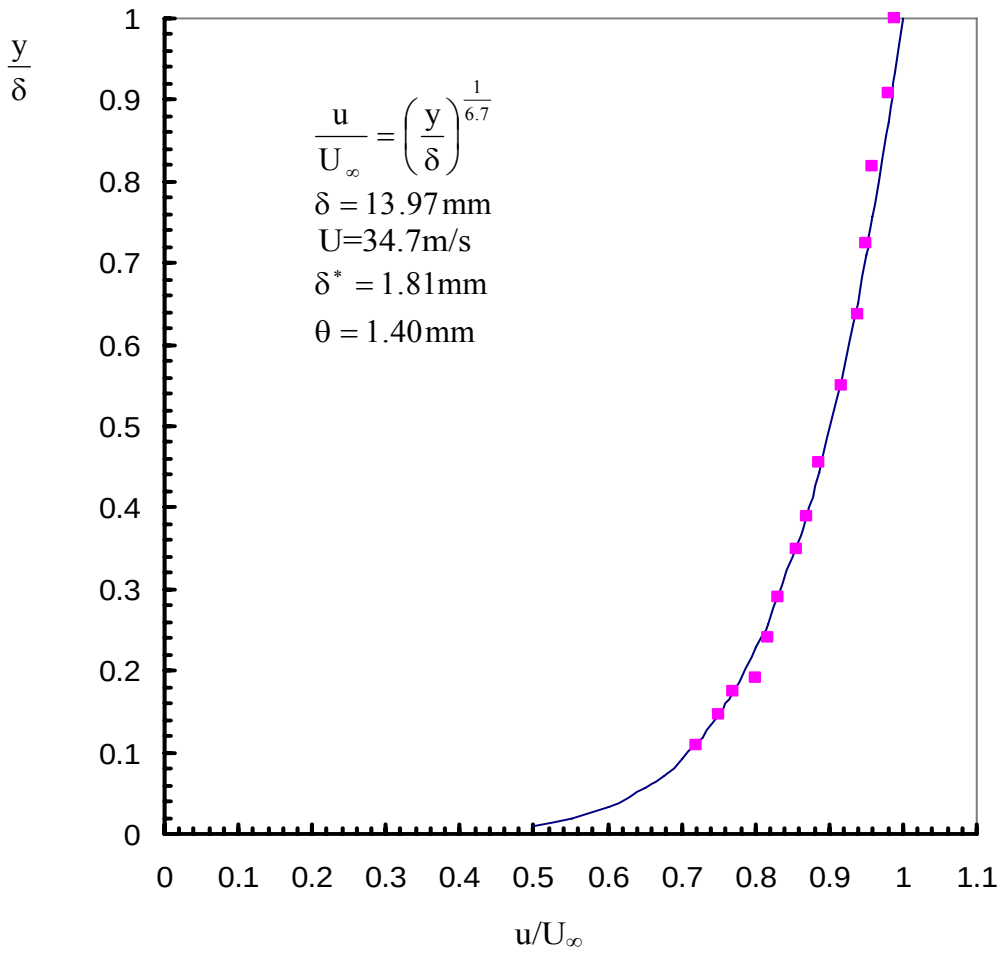

Figure 3.4 Boundary layer velocity profile upstream of film cooling holes, without film cooling injection

3.8 PRELIMINARY TESTS

To verify the results of the present facility, some preliminary tests were carried out on the regular cylindrical hole film cooling scheme, which is the baseline in the present study. Figure 3.5 shows the comparison of the present data to Kholi and Bogard (1997)'s results. The geometrical configuration they tested are quite similar to the present one, except it has a shorter hole length (2.8D) and a higher injection angle (35^o). The comparison is very favorable.

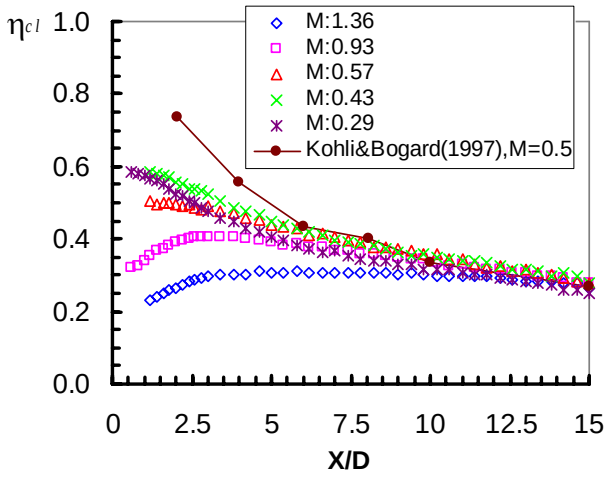

(a) Centerline film cooling effectiveness

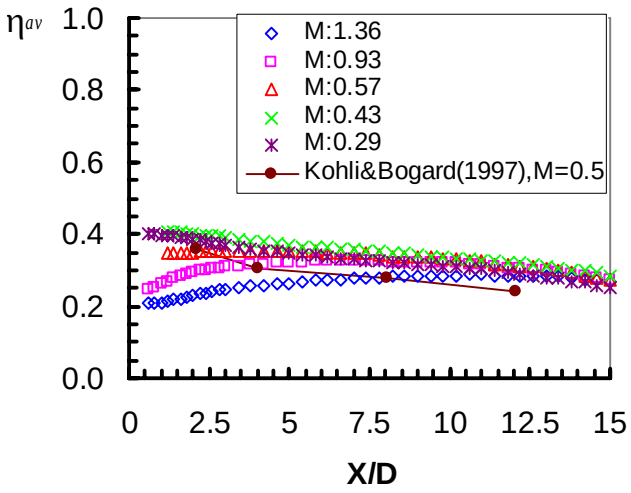

(b) Spanwise averaged film cooling effectiveness

Figure 3.5 Comparison of the present baseline to the published data

4.0 FILM COOLING PERFORMANCE OF DOWNSTREAM FLOW-ALIGNED BLOCKER

4.1 TEST MODEL

The test model in the present experimental study of film cooling performance of downstream flow-aligned blocker is shown in Fig.4.1. Film cooling holes are cylindrical and are inclined in a streamwise direction at 30^{o} related to the surface tangent. All holes are 6.35mm (0.25") in diameter. The length-to-diameter ratio is 10, which is significantly greater than that in a modern turbine to allow a study exclusively focused on the effect of flow-aligned blockers without significant effects from the hole-inlet condition. Three holes with the pitch of 3D form a film cooling row. Prism shaped flow-aligned blockers are placed at 1D downstream of film cooling holes. All blockers are 0.2D in thickness. In the case of parametric study with a single-hole structure, different test plates are machined, and only the hole and blockers in the middle are used.

The test plates are flat and made of Plexiglas, which has very low thermal conductivity (0.187W/mK) and is suitable for a transient test. Flow-aligned blockers are formed by milling off other parts from the plate. Figure 4.2 is a photo of the test plate for the three-hole row film cooling study. The test area is already painted black.

D: Diameter of film cooling hole, 0.25”

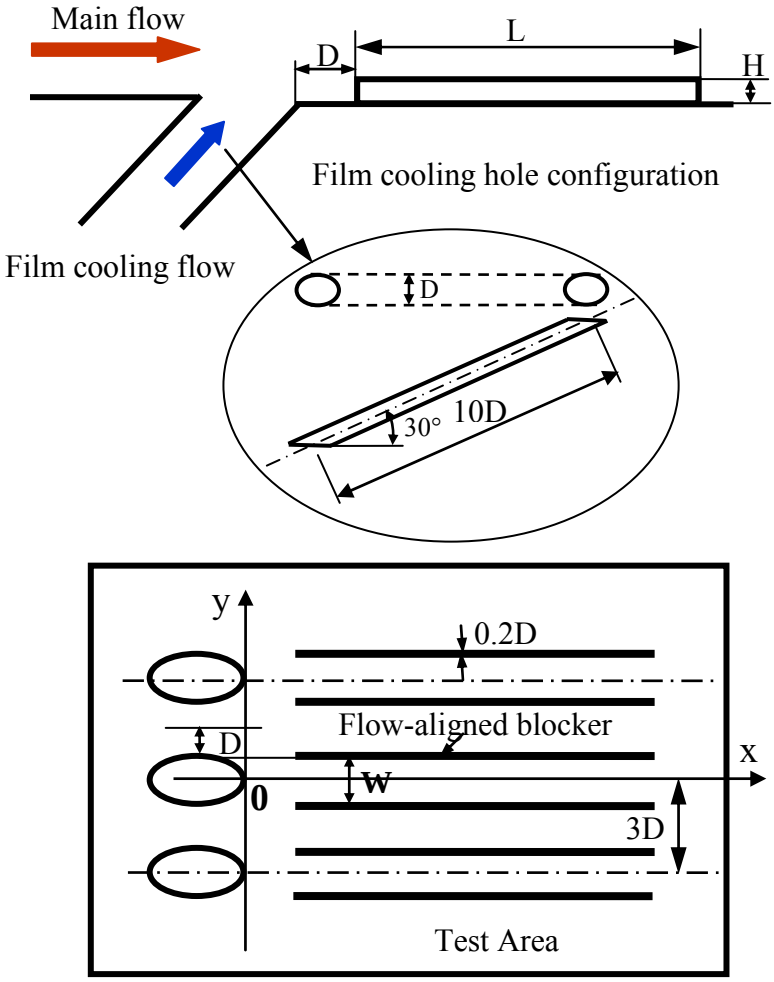

Figure 4.1 Schematics of the test model for the study on film cooling performance of downstream flow-aligned blockers

Test plate photo

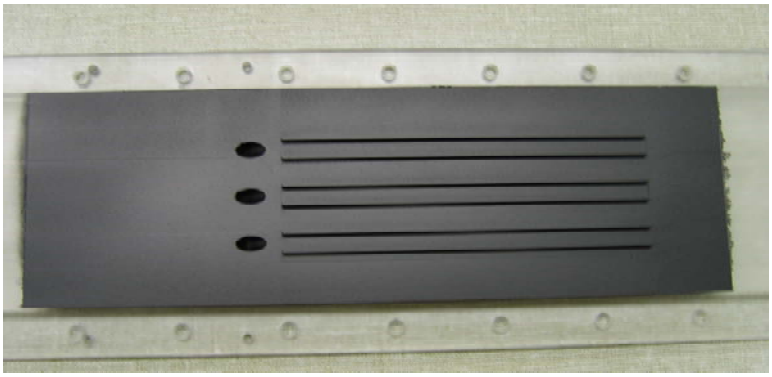

Figure 4.2 Photo of the test plate for three-hole row study

The design parameters studied include seven cases. The parameters of the seven different designs are shown in Table 4.1, where H and L represent the height and length of a blocker, respectively, and W is the width or transverse spacing between two neighboring blockers. Designs 1, 2, and 3 have different blocker heights. Designs 3, 4, and 5 possess different widths between two adjacent blockers, and variations of blocker length exist among Designs 3, 6, and 7. Therefore, totally, seven test pieces with different parameters of blocker are manufactured, and one base plate is machined (Fig. 4.3). The test piece is mounted into place by four screws in corners, which are far away from the domain of interest. The machining work is done carefully to ensure that the surface of the assembled test plate is smooth, particularly in the area between the film cooling hole and the leading edges of blockers. Figure 4.4 shows the photos of test pieces and the assembled test plate.

Table 4.1 Studied parameters

Parameter / Design No.	H	W	L
1	0.2D	D	24D
2	0.4D	D	24D
3	0.6D	D	24D
4	0.6D	0.8D	24D
5	0.6D	1.2D	24D
6	0.6D	D	8D
7	0.6D	D	16D

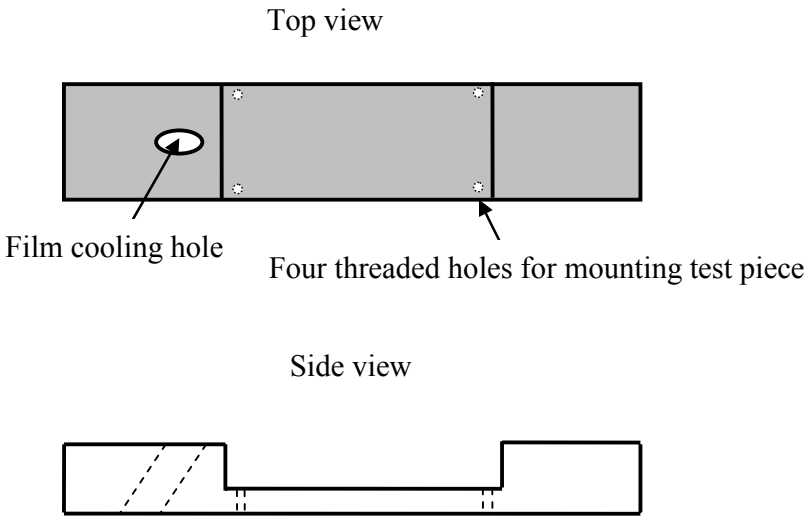

Figure 4.3 Schematic of the structure of the base plate

Figure 4.4 Photos of test pieces and the assembled test plate

The test section is a square Plexiglas duct of 406.4mm (16”) in length, with 89mm (3.5”) for each side. The bottom plate is removable, so that the test pieces can be assembled on it. A portion of the Plexiglas wall opposite to the bottom plate (test plate) is replaced by a Zinc Selenide CVD window for IR transparency. The test section is connected via flanges to the whole test rig (Fig. 4.5).

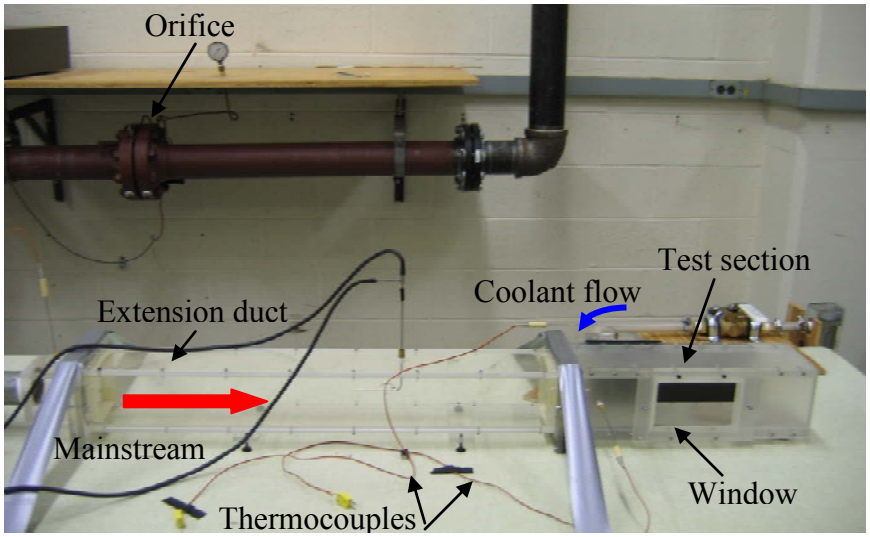

Figure 4.5 Photo of the test section connected to the test rig

4.2 RESULTS AND DISCUSSION

In this section, the experimental results are presented and discussed. Two blowing ratios, 0.43 and 0.93, are tested to study the blocker design parameters. After parametric study for single-hole film cooling, the design with the highest film cooling effectiveness is used for three-hole row film cooling performance evaluation.

4.2.1 The effect of blocker design parameters

The centerline and spanwise averaged film cooling effectiveness for all seven designs at two different blowing ratios are shown in Figs.4.6 and 4.7, respectively. For the two blowing ratios tested, Design 3 stands out in both centerline and spanwise averaged film cooling effectiveness values. The difference in either centerline or spanwise averaged film cooling effectiveness between the best and the worst is up to 50%. This is consistent with Shih and Na (2006)'s simulation result.

In addition, it is observed that the height of the blocker is an important parameter in the present study. As shown in Figs. 4.6 and 4.7, in both centerline and spanwise averaged film cooling effectiveness distribution, Design 1 with the lowest height has the lowest value among all the designs tested, and Design 2, with the second lowest height, has the second worst performance among all the designs tested. The effect of blocker height is much more obvious at the relatively higher blowing ratio of M=0.93. The film cooling effectiveness of the blocker with 0.6D in height is about 30% higher than that of the blocker with 0.2D in height at a blowing ratio M=0.43. However, at a blowing ratio of M=0.93, the film cooling effectiveness of the blocker with 0.6D in height is about 40% higher than that of the blocker with 0.2D in height. A 10% difference in the enhancement of film cooling effectiveness between the two blowing ratios is observed.

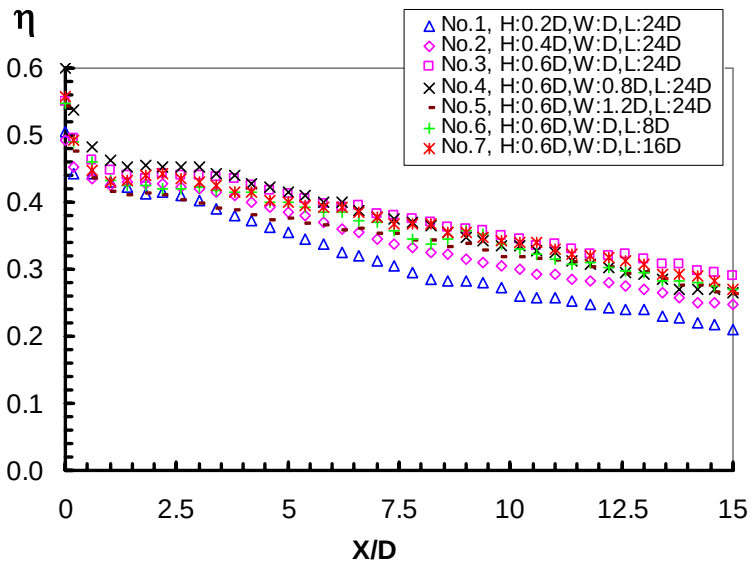

(a) Centerline

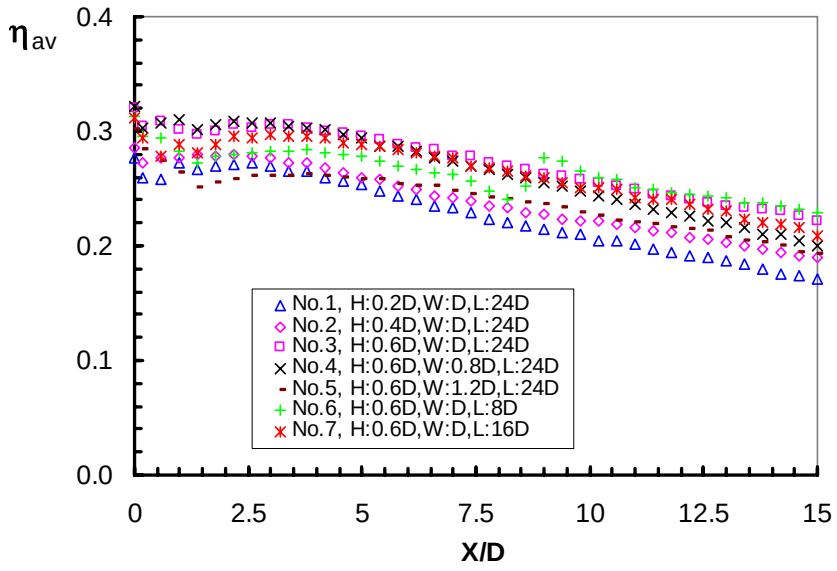

(b) Spanwise averaged

Figure 4.6 Centerline and spanwise averaged film cooling effectiveness for different designs of blockers at blowing ratio M=0.43

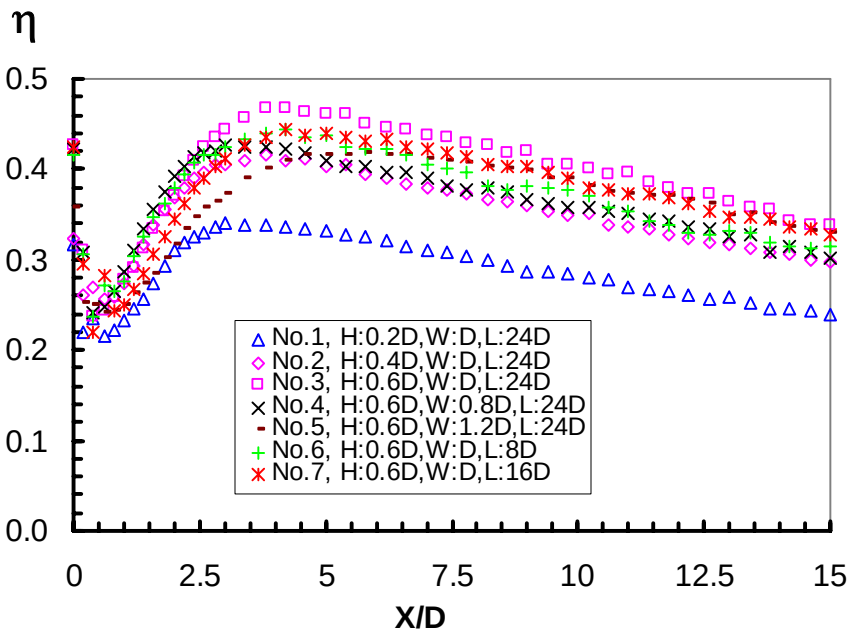

(a) Centerline

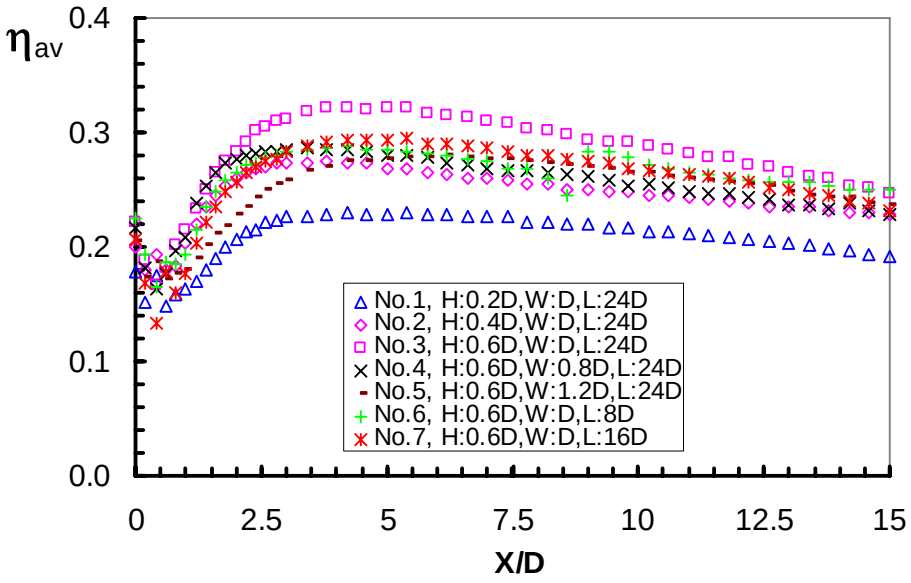

(b) Spanwise averaged

Figure 4.7 Centerline and spanwise averaged film cooling effectiveness for different designs of blockers at blowing ratio M=0.93

As mentioned earlier and outlined in Table 4.1, the only difference among Designs 3, 4, and 5 is the width. As shown in Figs. 4.6 and 4.7, the width between two blockers has a significant impact on film cooling effectiveness. Further evaluation of the current data suggests the existence of an optimal value in the width between blockers, which is around 1D in the present case. Comparative studies on designs 6, 7, and 3 reveal the effects of the blocker length on film cooling performance. The present results indicate that the blocker length of 24D has the highest film cooling effectiveness for both blowing ratios.

4.2.2 Film cooling performance of flow-aligned blockers

Film cooling performance of flow-aligned blockers is examined by making thermal measurement on a flat plate with a three-hole row. Based on the results of the design parameters studied, the geometry of Design 3, which has the best performance of single-hole test, is used for the test model design. The film cooling performance was evaluated with five deferent blowing ratios.

Film effectiveness Figure 4.8 shows the contour plots of local film cooling effectiveness for all five blowing ratios. The corresponding cooling effectiveness for the baseline cases without aligned blockers is also shown for comparison. Evidently revealed in these contour plots is that the flow-aligned blockers render higher film cooling effectiveness provided that the blowing ratio is greater than 0.43. The aligned blockers also extend the domain of higher η further downstream compared to the baseline cases.

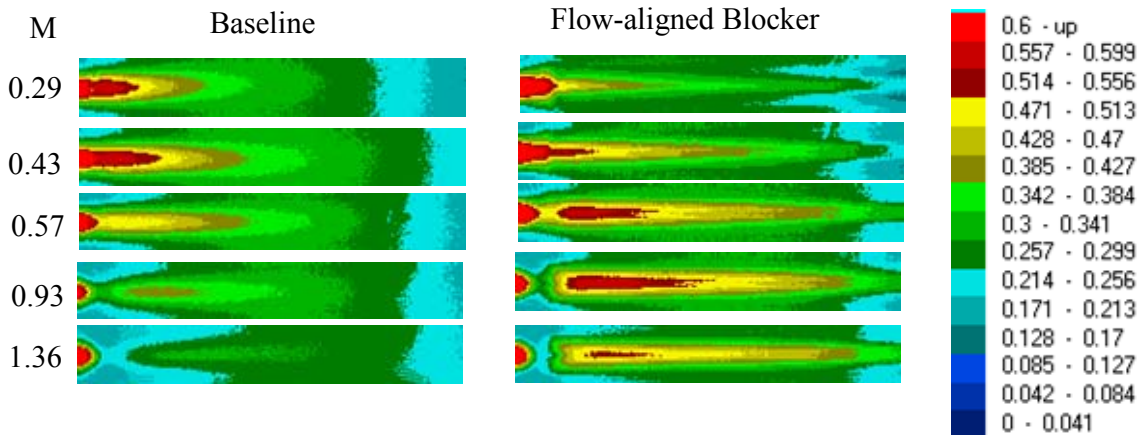

Figure 4.8 Local film cooling effectiveness distributions

To further quantify the effects of downstream flow-aligned blockers on film cooling effectiveness, the centerline and spanwise averaged film cooling effectiveness along streamwise locations with five different blowing ratios are also plotted in Figs. 4.9 and 4.10, respectively. Centerline film cooling effectiveness shows improvement with flow-aligned blockers for all the blowing ratios tested, except that at M=0.29, such an improvement is evident from X/D about 5 and toward downstream. The enhancement relative to the baseline case without blockers increases with the blowing ratio, with a maximum of up to 60% at M=1.36. A similar trend also prevails in the spanwise averaged data, as the maximum is about 45% at M=1.36. Overall, the effect of blocker-induced enhancement is significant, provided that M is greater than 0.43 and X/D > 1. X/D =1 represents the leading edges of the aligned blockers.

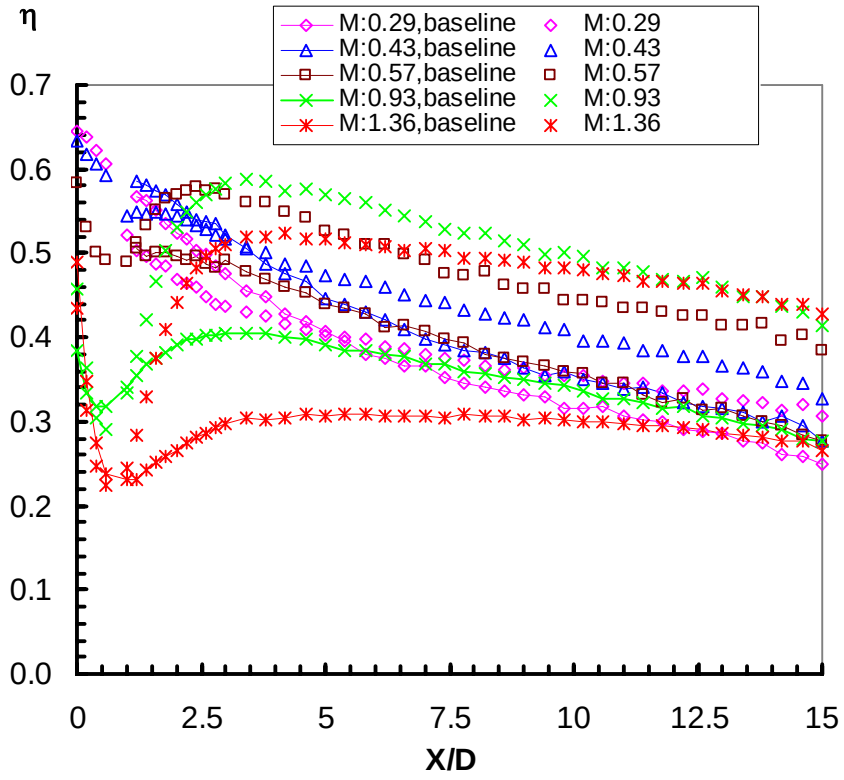

Figure 4.9 Streamwise distribution of the centerline film cooling effectiveness

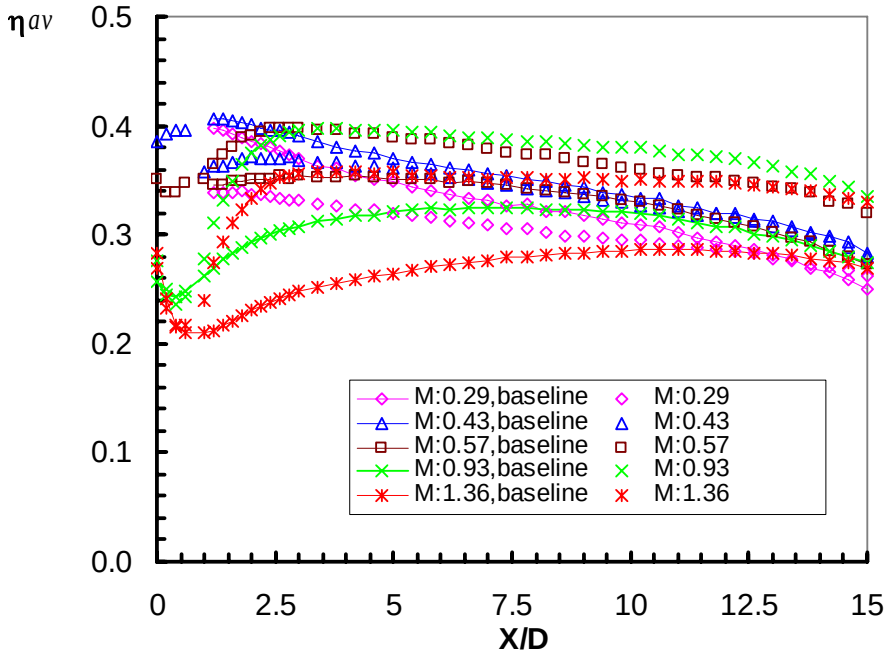

Figure 4.10 Streamwise distribution of the spanwise averaged film cooling effectiveness

One major design concern about film cooling is the spanwise coverage or lateral spread of coolant in the region not directly downstream to the film cooling holes. The inter-hole averaged film cooling effectiveness, which represents the cooling effect in the region between 0.5D to 1.5D from the centerline of a film cooling hole, is shown in Fig.4.11. Similar to Fig. 4.10, the presence of blockers also increases the film effectiveness for M>0.43. However, the level of enhancement is lower than that of the overall spanwise averaged value. For the cases with low blowing ratios, say M<0.43, the film effectiveness with the blockers is, in fact, lower than that of the cases without blockers. This implies that the aligned blockers reduce the spread of coolant toward the inter-hole region when blowing ratio is low.

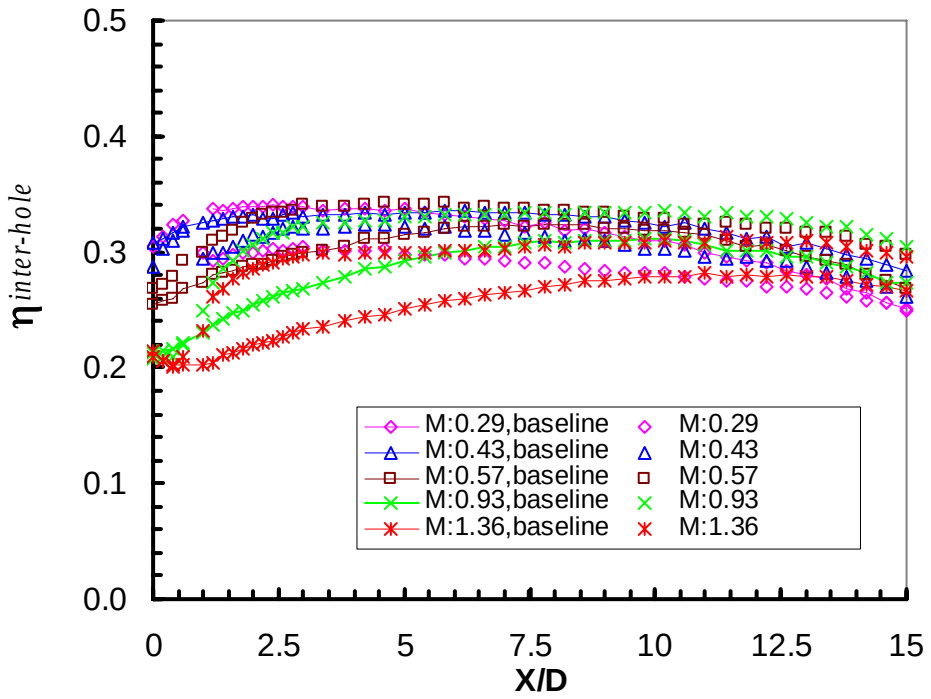

Figure 4.11 Streamwise distribution of the inter-hole spanwise averaged film cooling effectiveness

These aforementioned results collectively suggest that flow-aligned blockers can render significant improvement in film cooling effectiveness. This finding agrees with Shih and Na (2006)'s simulation result, but the improvement in the present experimental study is more evident when M>0.43.

Heat transfer coefficient The local heat transfer coefficients for downstream flow-aligned blocker and baseline cases at all five blowing ratios are shown in Fig. 4.12. In the center region between the two blockers, the values of heat transfer coefficient are lower than those in the corresponding baseline cases. This suggests the effectiveness of blockers in preventing the hot gas from entraining underneath the coolant jet. In the region near the leading edge of a flow-aligned blocker, the heat transfer coefficient increases substantially. This is similar to a common phenomenon of convective heat transfer with flow over an obstacle. Upstream to the leading edge of a blocker, flow separation is expected to prevail, due to an adverse pressure gradient. The higher turbulence level, accompanied with the flow shear generated with separation, is responsible for the increase in heat transfer coefficient. The elevated heat transfer on the blocker's top surface appears to be caused by the reattachment of the flow separated from the sharp corner to the blocker's top surface.

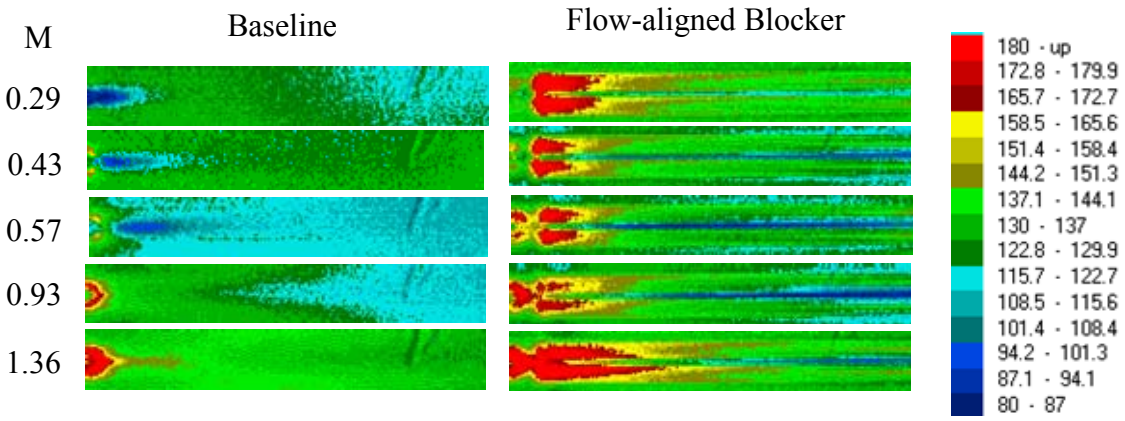

Figure 4.12 Local heat transfer coefficient distribution

To further evaluate the heat transfer variation affected by the aligned blockers, the ratio of the heat transfer coefficient h with film cooling to its counterpart h_o without film cooling is calculated. The centerline heat transfer coefficient ratios for all the blowing ratios tested and baseline cases are shown in Fig. 4.13.

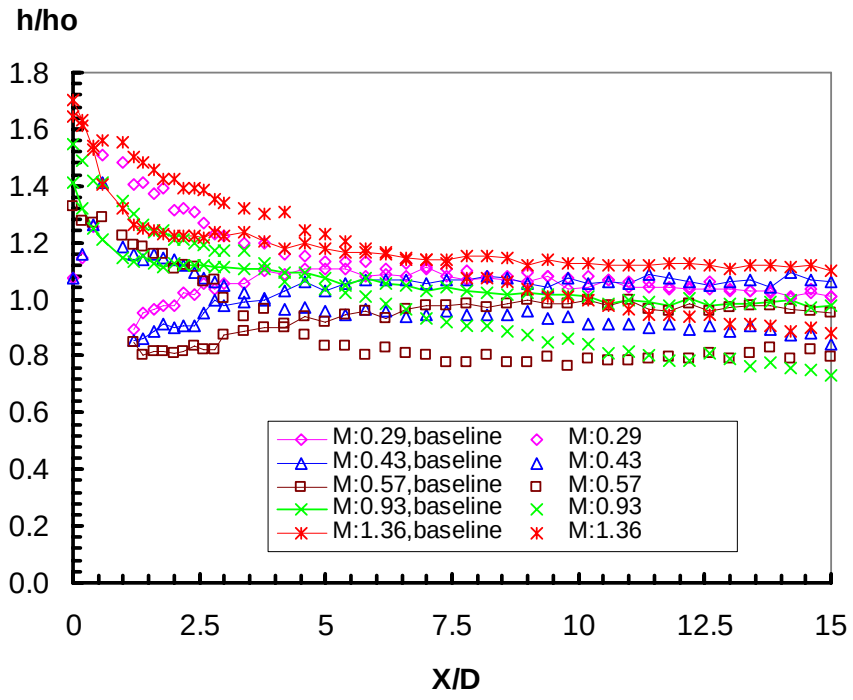

Figure 4.13 Streamwise distribution of the centerline heat transfer coefficient

The baseline value obtained here agrees well with that reported in the literature (Eriksen and Golstein, 1974; Hay et al., 1985). At a low blowing ratio and near the film cooling hole region, the heat transfer coefficient with injection is lower than that without injection. This trend reverses at a higher blowing ratio, as film cooling injection enhances the heat transfer, particularly in the near-hole region. There are two competing factors responsible for the above phenomenon. First, injection adds flow mass and linear momentum normal to the wall, which thickens the boundary layer. A thicker boundary layer presents more heat convection resistance between mainstream and the coolant film protected wall. This is prevalent at a low blowing ratio. Second, the interaction of main flow/coolant injection causes active momentum exchange, along with excessive shear and turbulence generated between the participating streams. This is especially the case when the blowing ratio or jet exit velocity is sufficiently high. When the blowing ratio or jet exit velocity is low, the first factor is dominant near the centerline, while the

second factor prevails along the side edge of a film cooling hole (Fig.4.14). This observation is based on the fact that the spanwise averaged heat transfer coefficient ratios increase slightly compared with their values at centerline (Fig. 4.15).

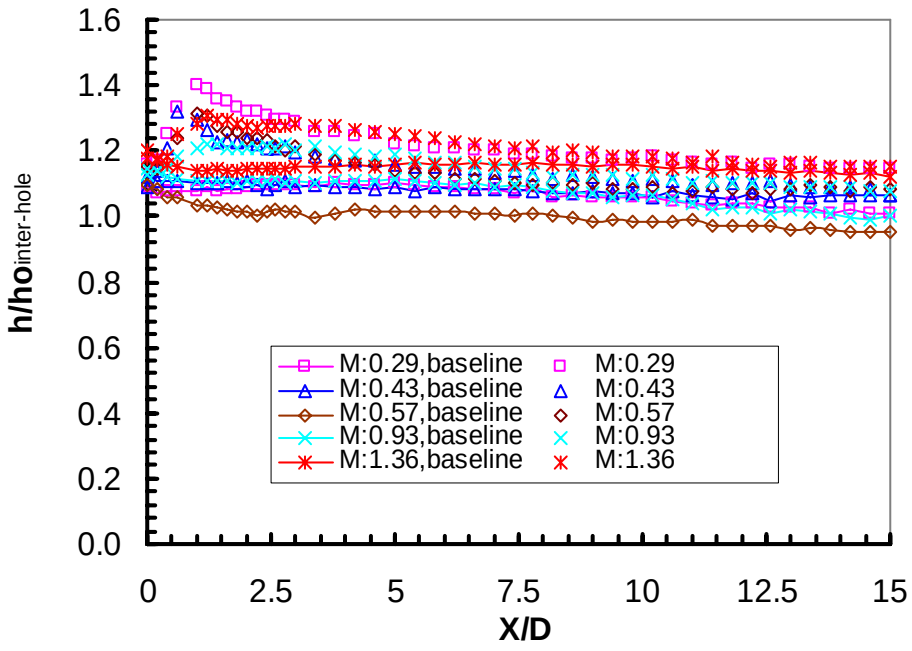

Figure 4.14 Streamwise distribution of the inter-hole averaged heat transfer coefficient

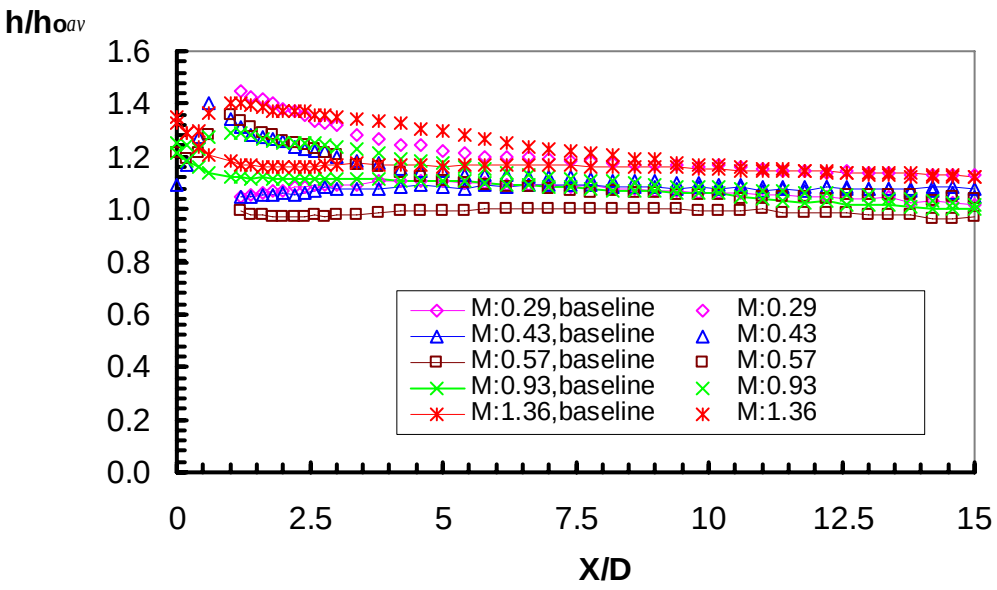

Figure 4.15 Streamwise distribution of the spanwise averaged heat transfer coefficient

As shown in Figs. 4.13 and 4.15, in the region sufficiently downstream to the film cooling holes, say X/D≥7.5, the presence of flow-aligned blockers reduces the magnitude of h by about 20% along the centerline. However the effect of blockers on the spanwise averaged heat transfer coefficient is rather insignificant (Fig. 4.15). Meanwhile, in the region near the injection hole or near the leading edge of a blocker, say X/D<5, the magnitude of the heat transfer coefficient is substantially higher compared to the corresponding baseline case. A blocker here serves as a surface mounted obstacle which induces boundary layer separation and reattachment, and hence increases heat transfer coefficient. This also suggests that blockers with variations in frontal configuration may alter the characteristics of heat transfer coefficient in the influenced region.

Reduced heat flux As mentioned in Section 2.2, the ratio of heat flux for cases with film cooling injection to those without film cooling q/q_o is an important parameter to measure the performance of film cooling. The streamwise distributions of centerline, inter-hole averaged and

spanwise averaged heat flux ratio are plotted in Figs. 4.16, 4.17, and 4.18, respectively. In general, the values of q/q_o on centerline are relatively low when X/D>5 for all the blowing ratios tested. Very evident is that, the values of q/q_o at centerline are relatively low when X/D>2.5 at blowing ratio M>0.29. The heat flux ratio q/q_o decreases about 70% at a blowing ratio of 1.36. The spanwise averaged value of q/q_o decreases at a blowing ratio M>0.43 when X/D>5. As the blowing ratio increases, say M>0.57, the q/q_o decreases as X/D>2.5. The largest reduction in q/q_o is about 20% at blowing ratio M=1.36. The inter-hole averaged value of q/q_o shows a decrease as M>0.57. One concern is about the q/q_o values of centerline and spanwise averaged in the region near the leading edge of a blocker (0<X/D<1.3). These values show some increase compared to those in the baseline cases. This is because the film cooling effectiveness exhibits virtually the same level, while the heat transfer coefficient increases. As suggested earlier, this phenomenon may be alleviated by implementing more streamlined blockers.

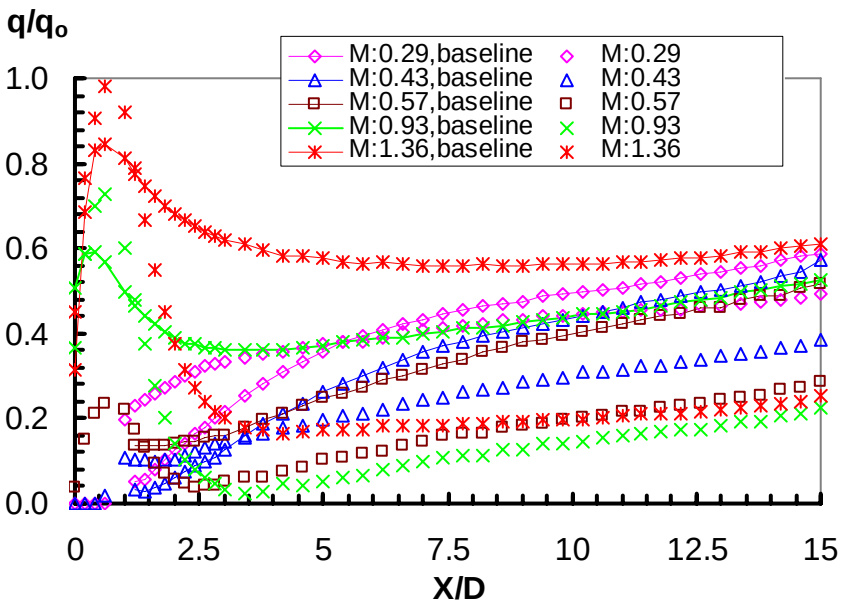

Figure 4.16 Streamwise distribution of the centerline heat flux ratio

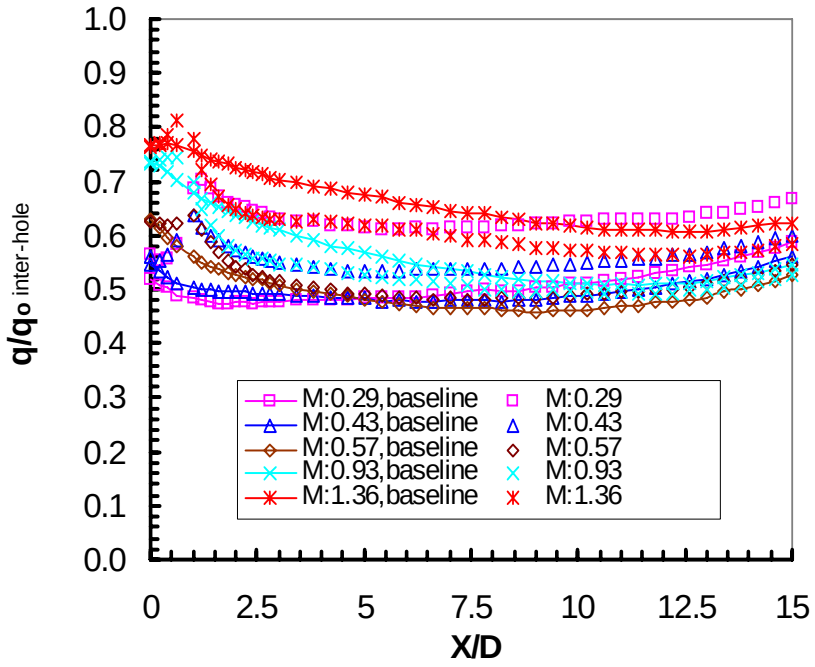

Figure 4.17 Streamwise distribution of the inter-hole averaged heat flux ratio

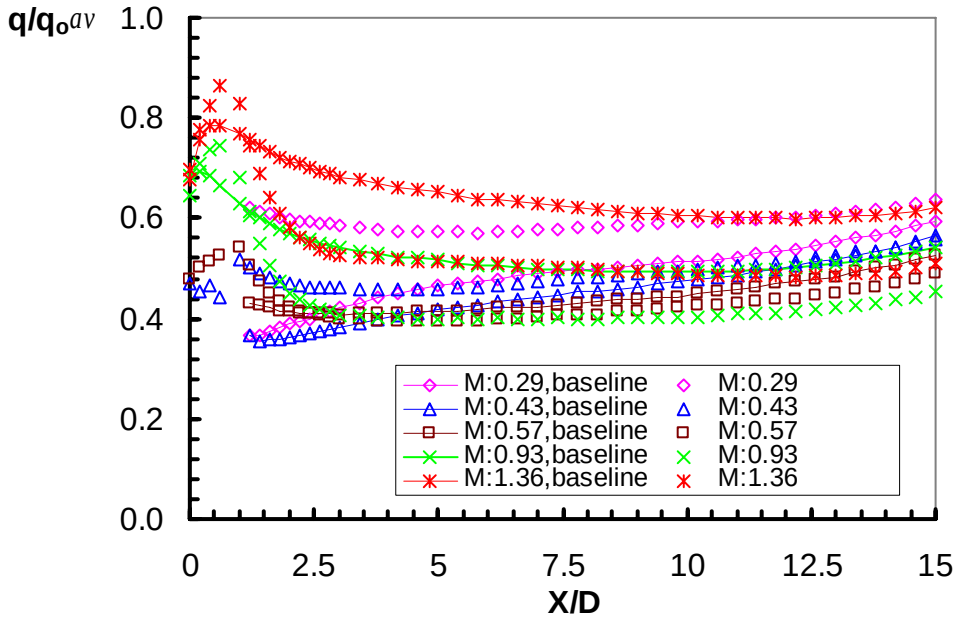

Figure 4.18 Streamwise distribution of the spanwise averaged heat flux ratio

4.3 CONCLUSIONS

This study represents the first experimental work in exploring the concept of placing flow-aligned blockers downstream of film cooling holes to temper the level of hot gas entrainment. Blocker design parameters are studied using a single-hole configuration, and film cooling performance is investigated using a three-hole row configuration. Local film cooling effectiveness and heat transfer coefficient distributions are measured using an IR imaging technique.

Seven designs are tested at two different blowing ratios. Design 3 shows the best performance, with the highest values in both centerline and spanwise averaged film cooling effectiveness. The single-element study suggests that the blocker's height, length, and the space between adjacent blockers are important design parameters, strongly affecting the convective transport phenomena over the element- influenced region.

For the three-hole row study based on Design 3, five blowing ratios are investigated. When $M>0.43$, the increase of centerline and spanwise averaged film cooling effectiveness starts from X/D around 1, coinciding with the streamwise location of blocker's leading edge. The enhancement of film cooling effectiveness increases with blowing ratio, with the maximum about 60% and 46% for the centerline and the spanwise averaged values, respectively, at $M=1.36$. This suggests that implementing flow-aligned blockers can be a viable approach to improve film cooling effectiveness as $M>0.43$.

The magnitudes of heat transfer coefficient with aligned blockers are at the same levels as those in the baseline cases. However, their centerline values when $X/D\geq7.5$, i.e. sufficiently downstream are, in fact, lower than those in the baseline cases, with a reduction up to 20%. On

the contrary, the heat transfer coefficient in the region near the leading edge of the blocker increases, due likely to the high turbulence level associated with flow separation and reattachment.

The heat flux ratio q/q_o decreases when blowing ratio $M>0.57$, with a largest reduction of 70% in centerline value and 20% in spanwise averaged value. The value of q/q_o in the region near the leading edge of the blocker ($0<X/D<1.3$) increases slightly, due to unchanged film cooling effectiveness and increased heat transfer coefficient.

5.0 FILM COOLING PERFORMANCE OF UPSTREAM RAMP

5.1 TEST MODEL

A schematic view of the test model with an upstream ramp is shown in Fig.5.1. The film cooling hole configuration is the same as that of the study with downstream flow-aligned blockers, as discussed previously in Chapter 4. The upstream ramp, 2D in length, is placed at a distance of 1.0D upstream to the edge of film cooling holes. To examine the effects of ramp geometry, the present study considers three different ramp angles, i.e. 8.5^{o}, 15^{o}, and 24^{o}. Since all the ramps have the same longitudinal base, the height of the backward facing step differs among different ramps, varying with the ramp angle.

D: Diameter of film cooling hole, 0.25”, α: 8.5^{o},15^{o},24^{o}

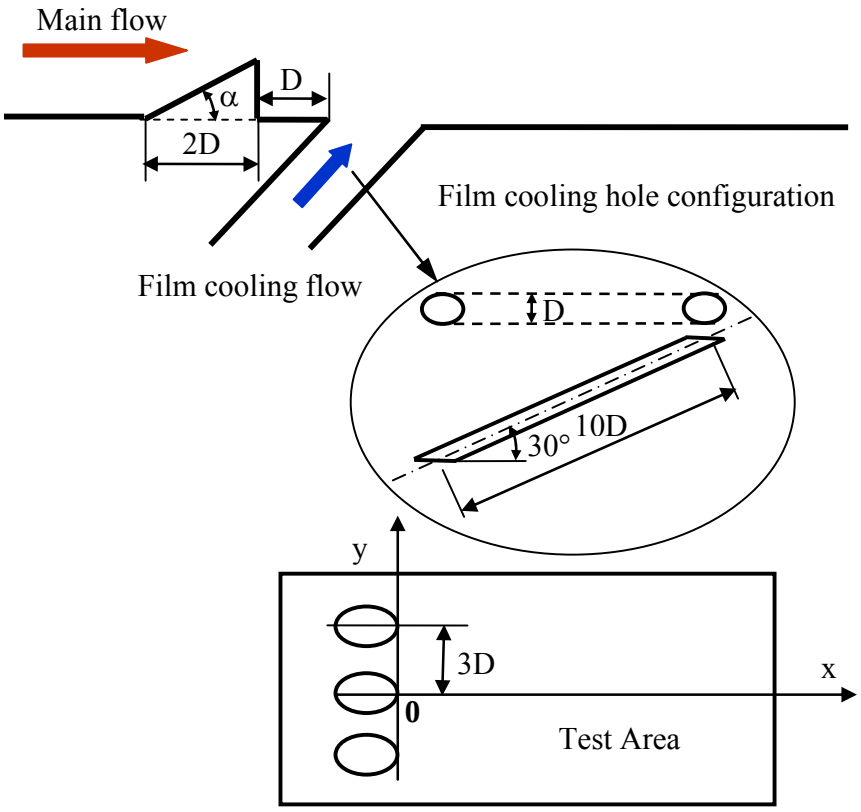

Figure 5.1 Schematic of the test model

The test plate is made of Plexiglas, which has very low thermal conductivity (0.187W/mK) and is a proper material for a transient test. Ramps are made separately, by machining a shallow groove on the test plate and tapping the ramp into the groove. Figure 5.2 shows the photos of the test plate with ramp models detached from the test plate.

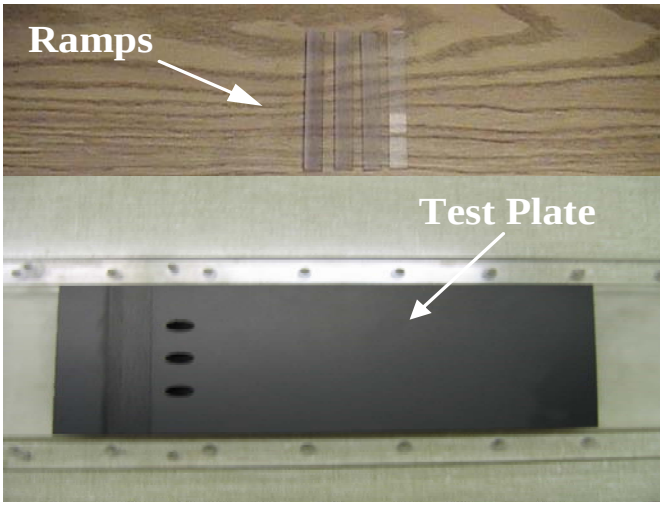

Figure 5.2 Photos of the test plate and ramps

5.2 RESULTS AND DISCUSSION

This section presents the measured data which quantity the effects of blowing ratio and ramp geometry on both film cooling effectiveness and heat transfer coefficient.

Film effectiveness Figures 5.3 and 5.4 show the effects of blowing ratio on the distribution of η along the center line and the values averaged across the span, respectively. One most distinct feature shown in both figures is the consistently high value of the film effectiveness in the region immediately behind the ramp and upstream to the film cooling hole (X/D ~ -2). This phenomenon is non-existent in the baseline case without a ramp.

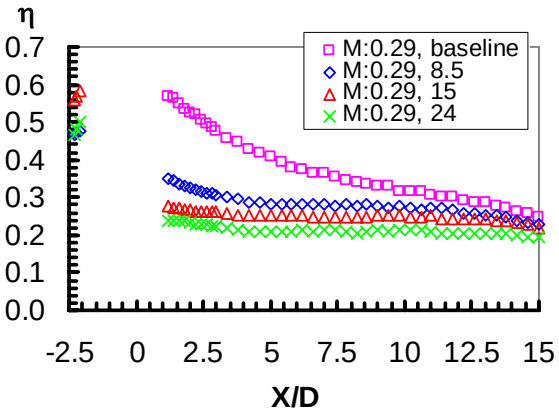

(a)M=0.29

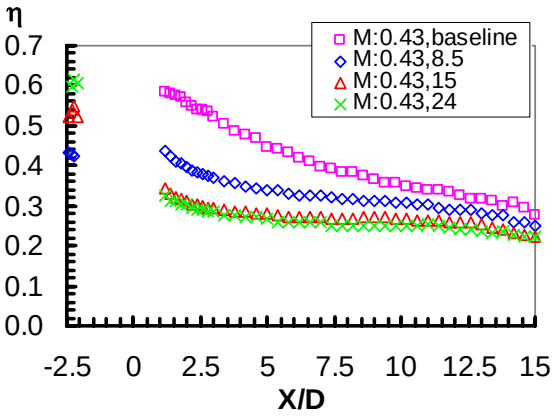

(b)M=0.43

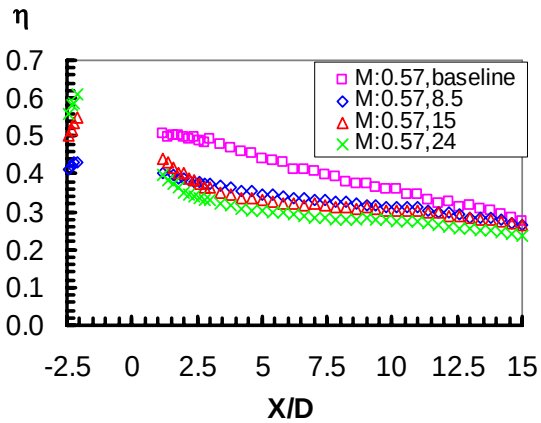

(c)M=0.57

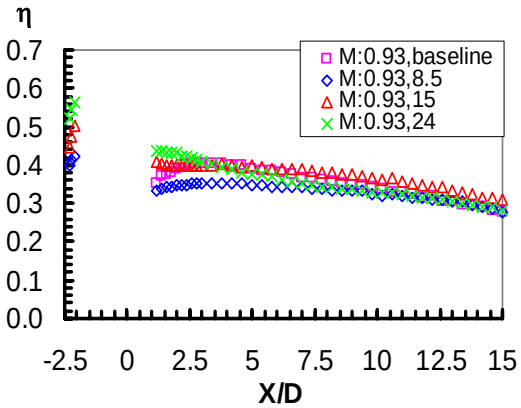

(d) M=0.93

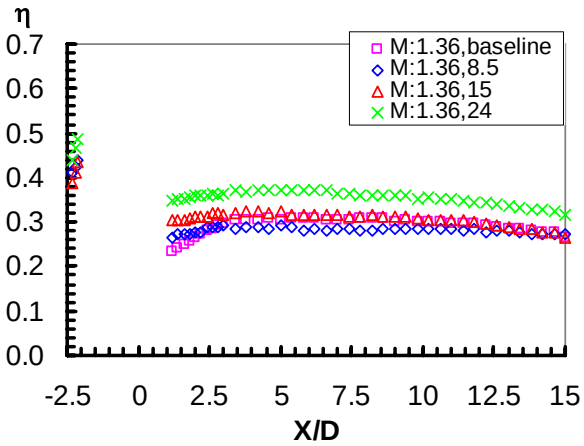

(e) M=1.36

Figure 5.3 Centerline film cooling effectiveness for different ramp angles at various blowing ratios

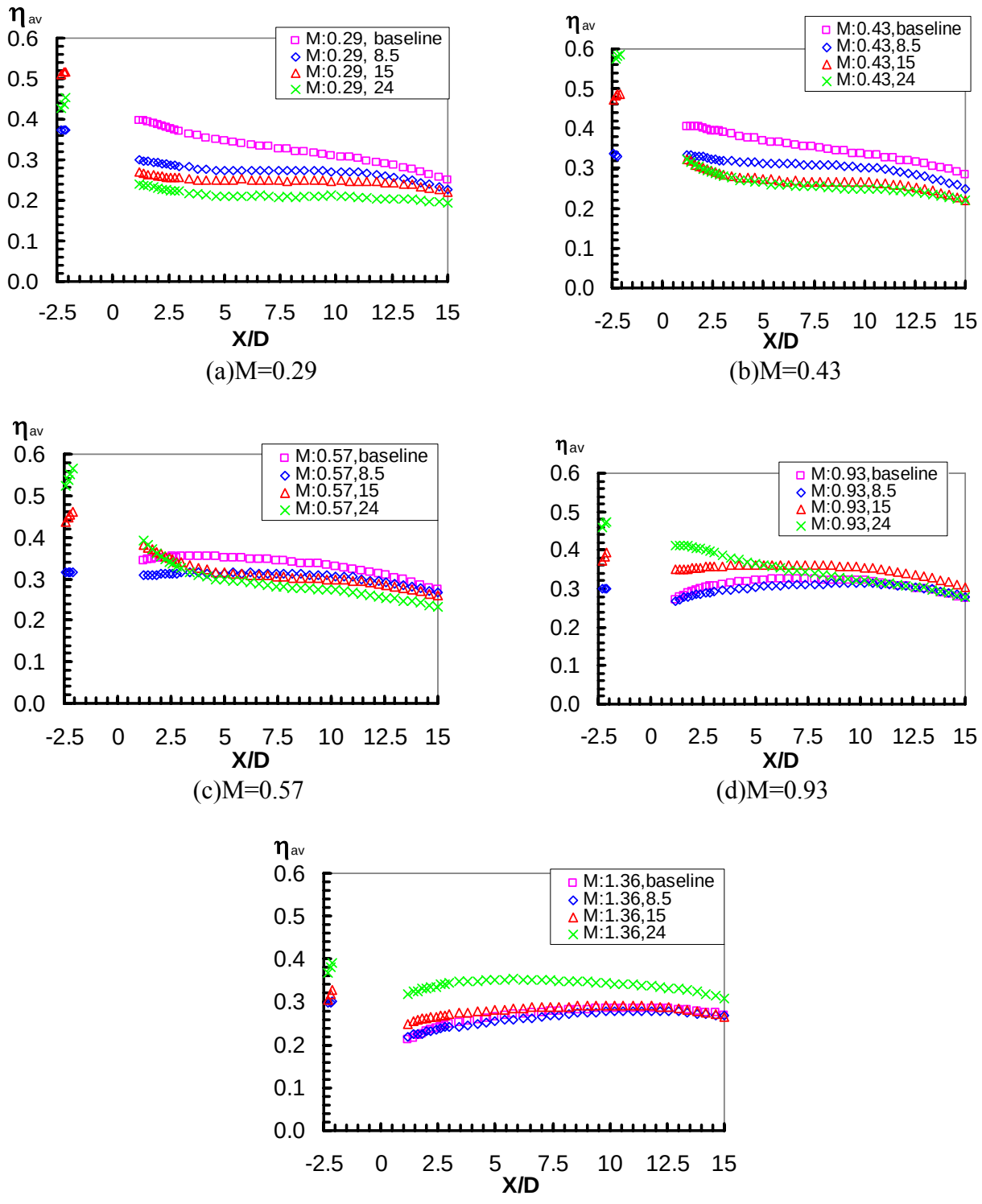

Figure 5.4 Spanwise averaged film cooling effectiveness for different ramp angles at various blowing ratios

Another distinct and probably more significant observation from both Figs. 5.3 and 5.4 is the effectiveness of the ramp in producing higher film cooling when the angle of the ramp is adequately large and the magnitude of the blowing ratio is sufficiently high, say M > 1. This finding is particularly evident for the case M = 1.36, as displayed in Figs. 5.3(e) and 5.4(e), where the ramp is of the steepest angle, 24^o. The value of η in this case is about 50% higher than its baseline without the ramp. On the other hand, when the blowing ratio is low, e.g. M < 0.6, in (a) to (c) of Figs. 5.3 and 5.4, the presence of the ramp consistently results in an η lower than the value without the ramp.

The flow separated from a backward-facing step has been a subject of extensive study in the fields of fluid dynamics, heat transfer, and combustion. While the ramp angle may induce certain differences in flow details, the general flow pattern behind a two-dimensional ramp would be dominated by a highly turbulent, shear layer separated from the tip of the ramp and a recirculation region immediately behind the ramp and underneath the separated shear layer. Figure 5.5 illustrates schematically such flow characteristics.

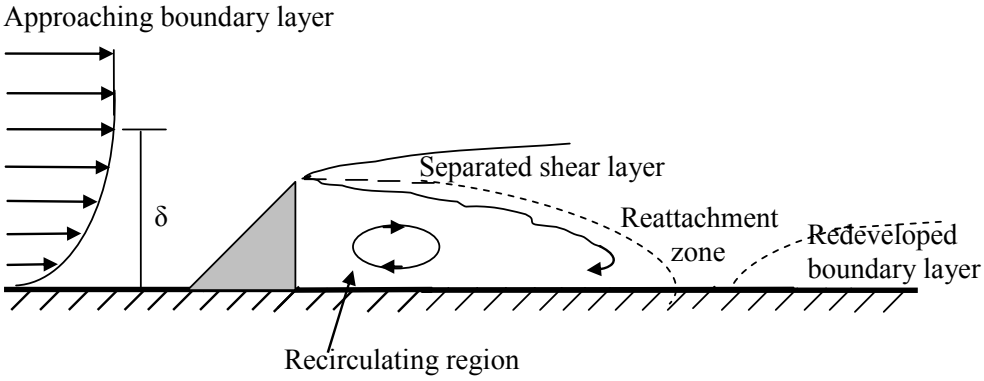

Figure 5.5 Schematic of the characteristics of flow over an upstream ramp

The region of recirculation diminishes as the shear layer expands in width toward downstream and eventually reattaches to the floor. The typical distance of reattachment under a fully turbulent flow condition is approximately 5 to 10 times the ramp height. Current geometry with the film holes located about 1.0D downstream to the ramp suggests that the film cooling injection would likely alter the separated flow field, particularly in the recirculating zone. With injection, the flow in the region would no longer be two-dimensional. Additional shear layers with elevated levels of turbulence would be generated due to the interaction between the injected coolant and the recirculating flow. Under this condition, the flow would be more active in lateral movement as well.

It is understandable that the aforementioned flow interaction depends strongly on the blowing ratio and the conditions of main stream. For cases with low blowing ratios, say M = 0.29, 0.43, and 0.57, the injected coolant, which lacks sufficient momentum, is immediately overwhelmed by the local recirculating flow at the exit of injection. As a result, the film effectiveness is relatively low. An increase in the ramp angle, as well as the ramp height, leads to a stronger dominance of recirculation and lower film cooling effectiveness downstream of the injection holes. The dominance of recirculation is also responsible for the evidently high value in η over the region upstream of the injection holes.

When the blowing ratio is sufficiently high, e.g., M = 1.36, the injected coolant inherits higher momentum and is capable of penetrating into the recirculation zone, and the film coverage could extend over the entire recirculating region. Again, the highly turbulent shear layer atop the recirculation zone acts as a crossflow, preventing the coolant from lift-off and leading to a better film protection in the region. Under this condition, a taller ramp typically

strengthens the levels of momentum and turbulence associated with the separated shear layer, which would favor coolant retention in the region.

Barigozzi et al. (2007) recently presented similar work. They studied the effect of an upstream ramp on cylindrical and fan-shaped hole film cooling. The comparison of the critical parameters in their study with those in the present study is shown in Table 5.1. Figure 5.6 shows their results. The highest blowing ratio with results they reported is M=1. Comparing their results of cylindrical hole with the present data for the ramp angle 15^{o}, the general characteristics of film cooling effectiveness is rather similar, except that their results show slight improvement with a ramp when M=0.3. When M=0.5, the film cooling effectiveness with a ramp is lower than that without a ramp. Further increase blowing ratio to M=1, the film cooling effectiveness with a ramp becomes comparable to that without a ramp. The general trend of the results of the fan-shaped hole in their study is also very consistent with that of the cylindrical hole in the present study. At all blowing ratios they tested, the ramp tends to lower film cooling effectiveness, but the difference becomes smaller as the blowing ratio increases. When the blowing ratio reaches 1.0, film cooling effectiveness with a ramp, again, similar to the cylindrical hole case, is at the same level as that without a ramp.

Table 5.1 The critical parameters in Barigozzi et al.'s study and the present study

		Barigozzi et al.	Present study
Hole	Injection angle α	Same	
	Hole length L/D	7	10
	Pitch	6D	3D
Ramp	Inclined angle	14^o	8.5^o, 15^o, 24^o
	Length	Same	
	Distance from film cooling hole	0.5D	D
Flow condition	U∞ (m/s)	20	34
	Boundary layer thickness δ	0.95D	2.2D
	Displacement thickness	0.09D	0.29D
	δ/ramp height	1.9	7.1, 4.1, 2.5

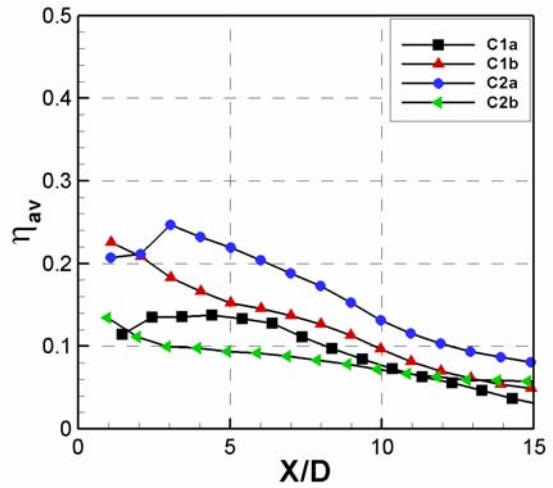

(a) M=0.3

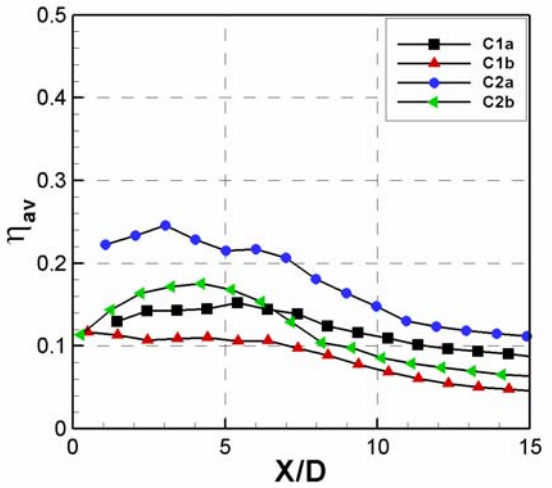

(b) M=0.5

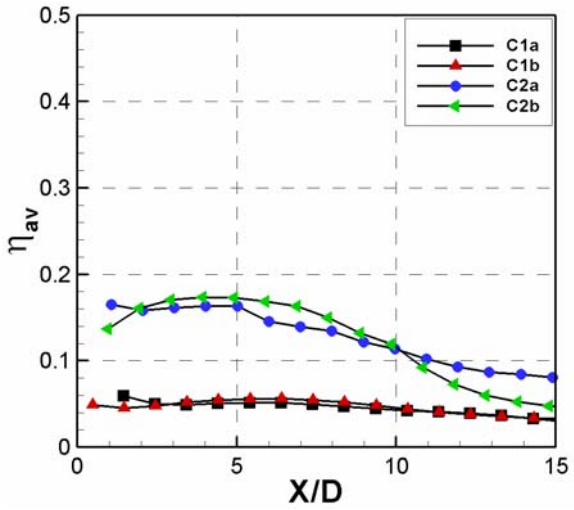

(c) M=1.0

Figure 5.6 Spanwise averaged film cooling effectiveness by Barigozzi et al. (2007),
C1a and C1b: cylindrical hole without and with an upstream ramp;
C2a and C2b: fan-shaped hole without and with an upstream ramp.

Heat transfer coefficient Figures 5.7 and 5.8 exhibit the distributions of heat transfer coefficient h measured along the center line and averaged across the span, respectively. The data presented here represent the ratio h/h_o, where h_o is the heat transfer coefficient measured over the test plate without coolant injection. The baseline shown in each figure represents the corresponding case with film cooling but without a ramp present. The results revealed in both figures suggest that the heat transfer coefficient for the cases with low blowing ratio, say $M \leq 0.57$, varies strongly with the ramp angle or ramp height. In contrast, the heat transfer coefficient becomes rather insensitive to the ramp geometry when the blowing ratio is sufficiently high, say $M \geq 0.93$. In fact, the magnitudes of the heat transfer coefficient with or without a ramp are very comparable in the region sufficiently downstream, say $X/D \geq 7.5$, provided that the blowing ratio is high, i.e., $M \geq 1$.

As the heat transfer coefficient is largely a direct measure of the local, near-wall turbulence level, the aforementioned observation implies the dominance of ramp-induced flow separation in the regime of low blowing ratios. A higher ramp results in a more turbulent separation, hence a higher heat transfer coefficient. On the other hand, when the blowing ratio is high, the near-wall turbulence, as well as the local heat transfer coefficient, is dominated by the injectant and its interaction with the boundary layer close to the wall. Accordingly, the influences of the ramp and its geometry become insignificant.

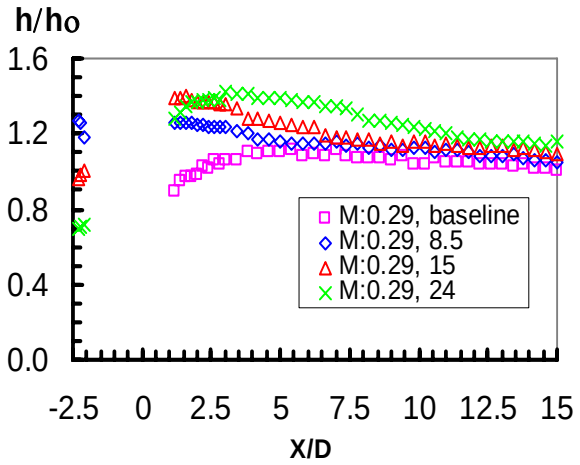

(a) M=0.29

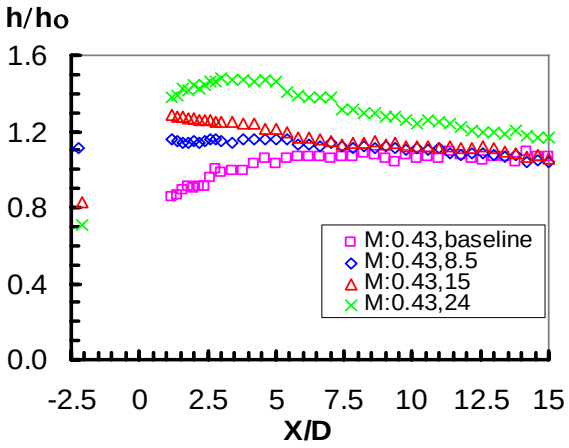

(b) M=0.43

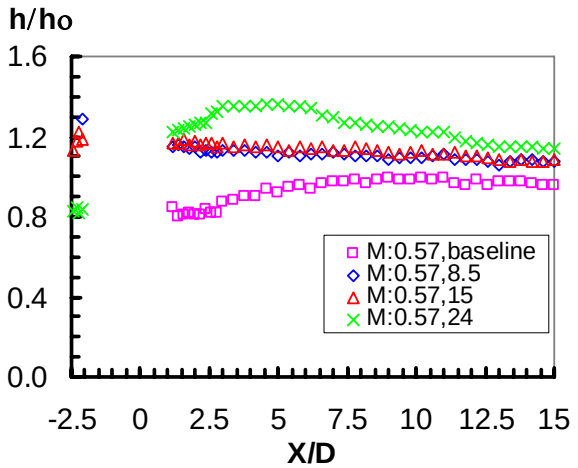

(c) M=0.57

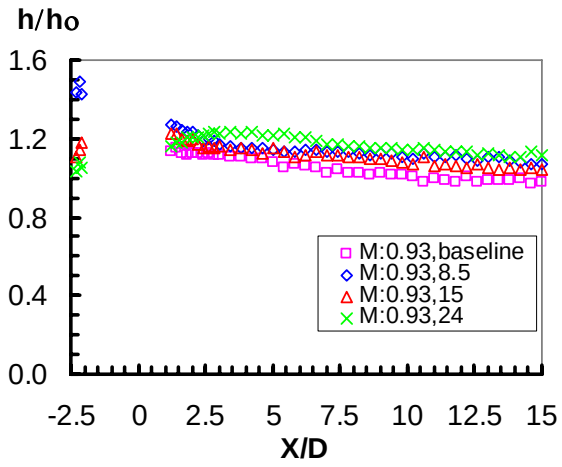

(d) M=0.93

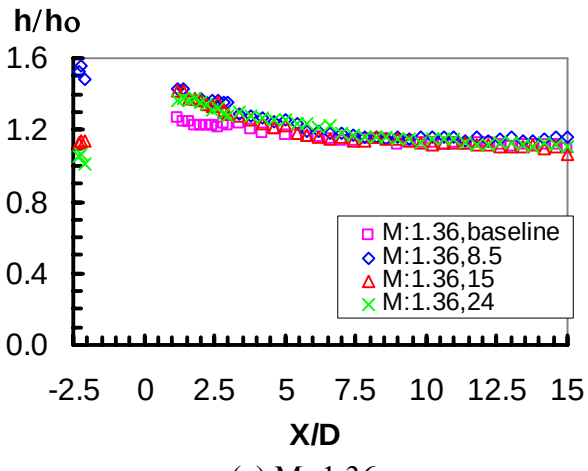

(e) M=1.36

Figure 5.7 Centerline heat transfer coefficient for different ramp angles at various blowing ratios

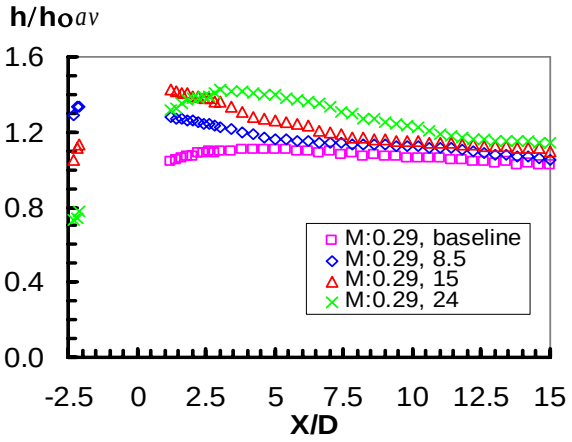

(a) M=0.29

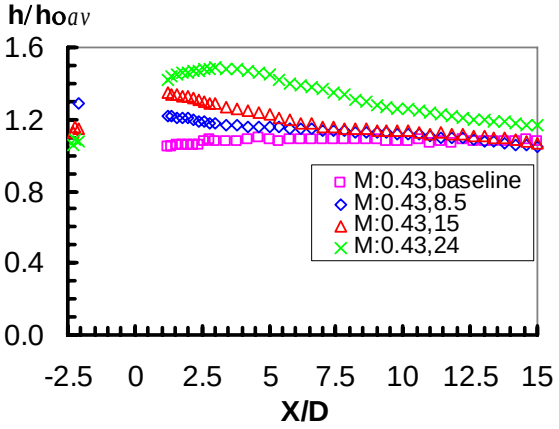

(b) M=0.43

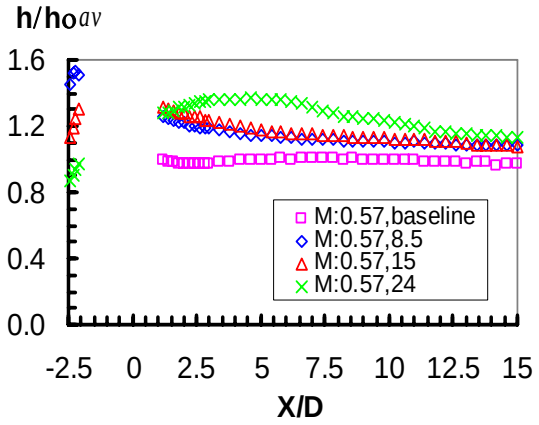

(c) M=0.57

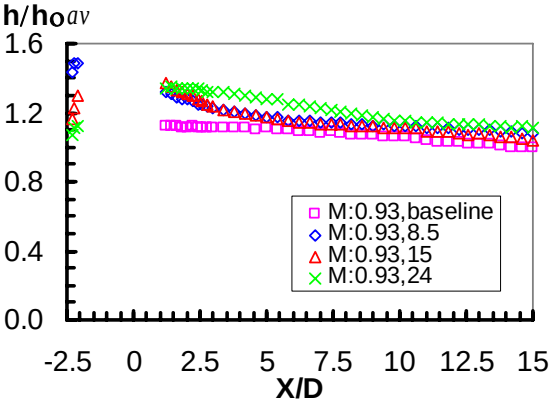

(d) M=0.93

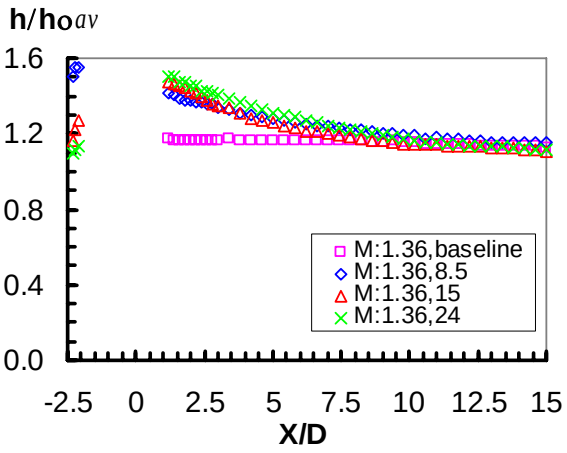

(e) M=1.36

Figure 5.8 Spanwise averaged heat transfer coefficient for different ramp angles at various blowing ratios

Reduced heat flux Figures 5.9 and 5.10 show the streamwise distribution of q/q_o along the center line and averaged across the span, respectively. Figures 5.11 and 5.12 present the centerline and spanwise averaged q/q_o for different blowing ratio M with a given ramp angle, correspondingly. The protection in the region between the downstream edge of the ramp and the upstream edge of film cooling holes is very effective, especially for cases with a low blowing ratio. Downstream of the film cooling hole, the ramp renders no improvement in overall heat reduction relative to the baseline case without the ramp until the blowing ratio reaches 0.93. According to the data presented earlier, this is fully expected, as the ramp, along with a low blowing ratio, leads to higher h and lower η, both of which adversely affect the reduction of heat transfer. However, the trend reverses as the blowing ratio increases. The value of q/q_o improves nearly 20% at the blowing ratio M=1.36 with a ramp of 24^o inclination.

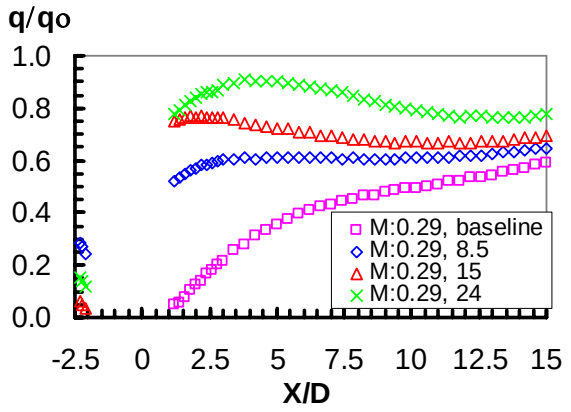

(a) M=0.29

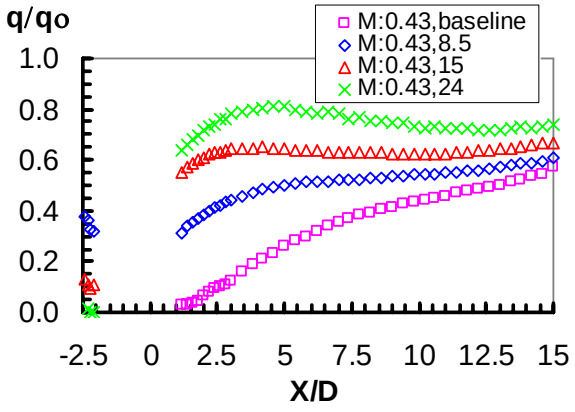

(b) M=0.43

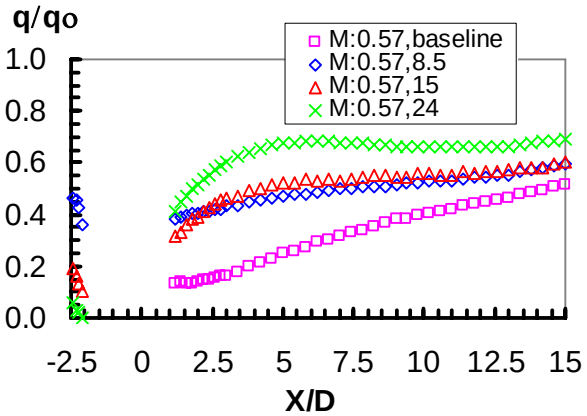

(c) M=0.57

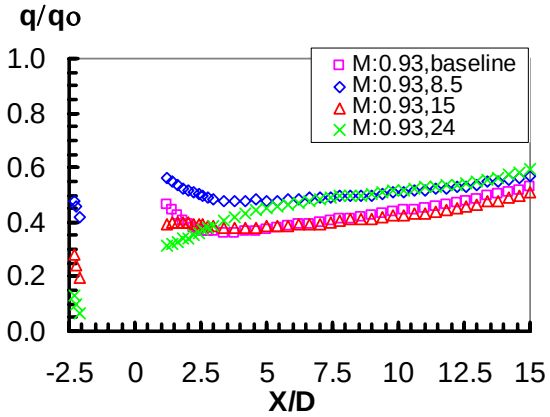

(d) M=0.93

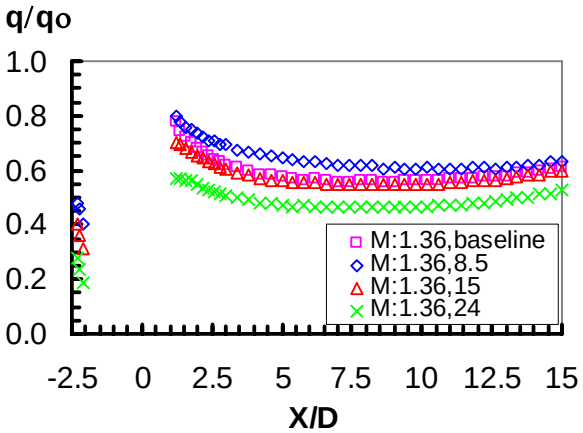

(e)M=1.36

Figure 5.9 Centerline heat flux reduction for different ramp angles at various blowing ratios

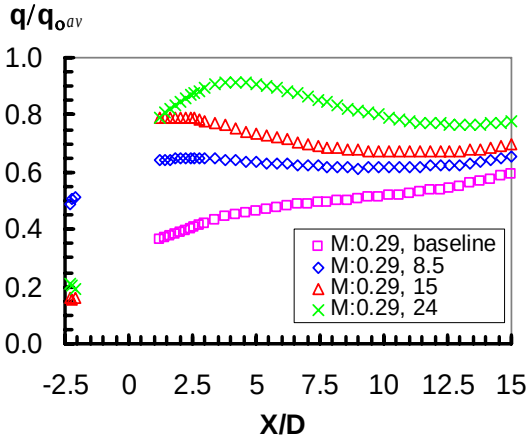

(a) M=0.29

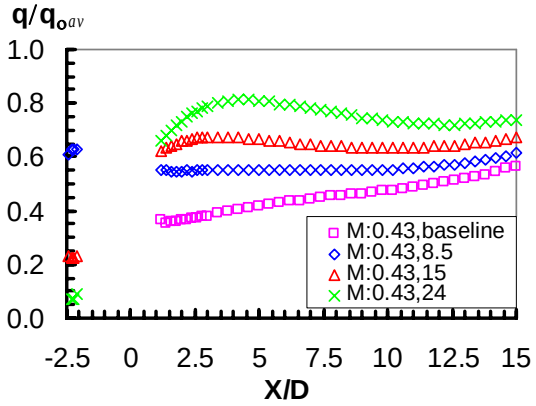

(b) M=0.43

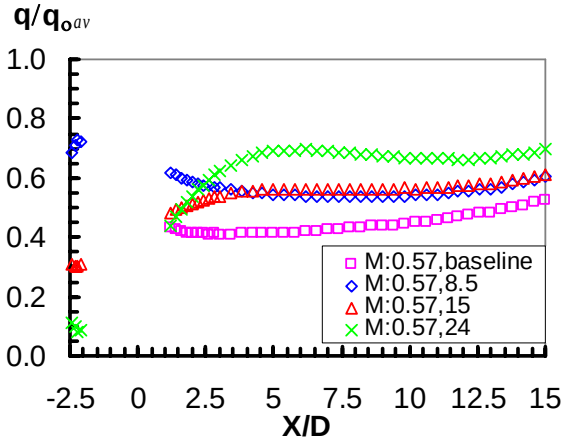

(c) M=0.57

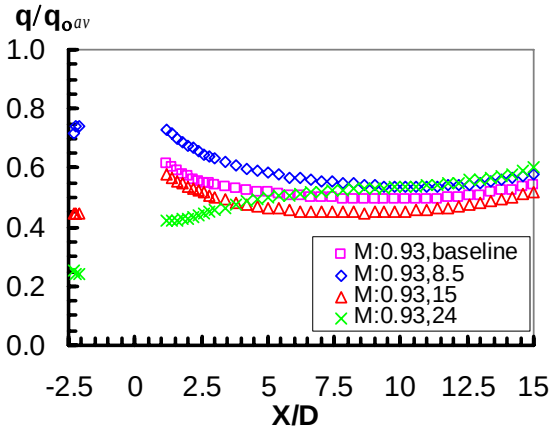

(d) M=0.93

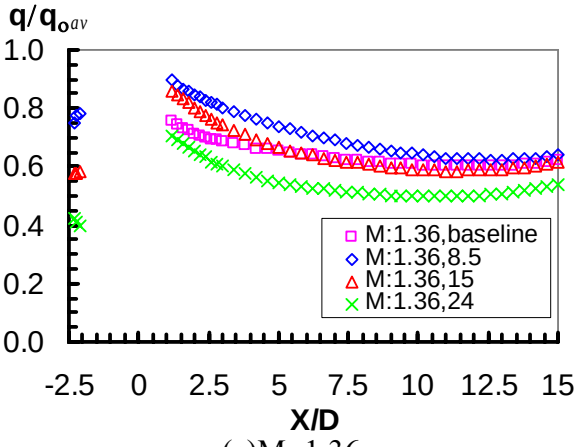

(e)M=1.36

Figure 5.10 Spanwise averaged heat flux reduction for different ramp angles at various blowing ratios

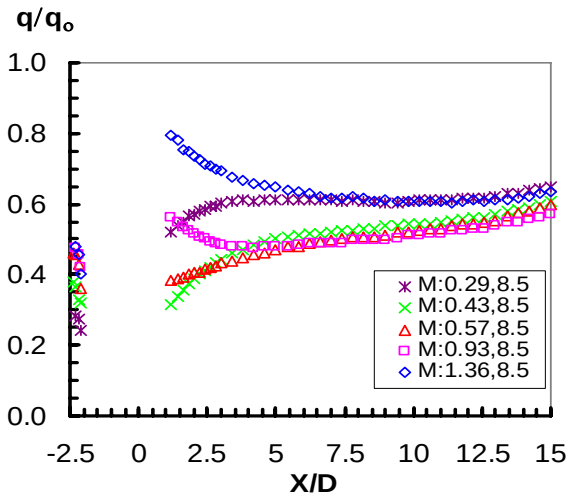

(a) Ramp angle 8.5^o

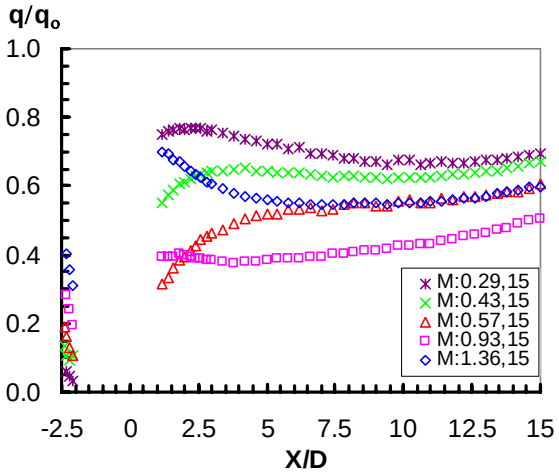

(b) Ramp angle 15^o

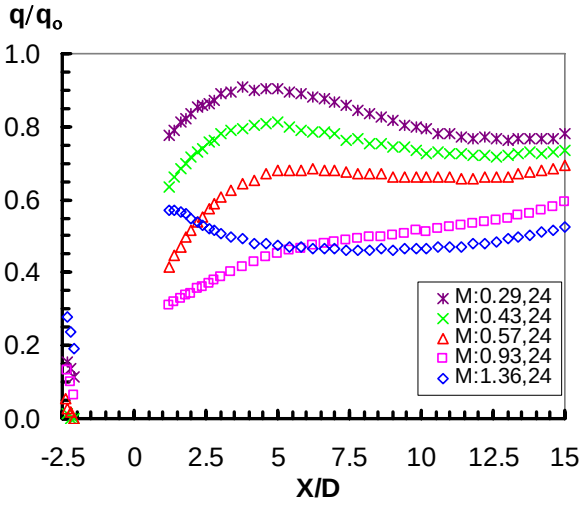

(c) Ramp angle 24^o

Figure 5.11 Centerline q/q_o for different blowing ratio M at a given ramp angle

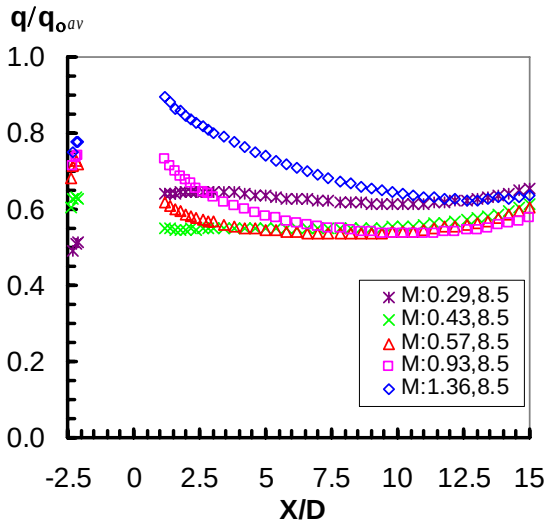

(a) Ramp angle 8.5^{o}

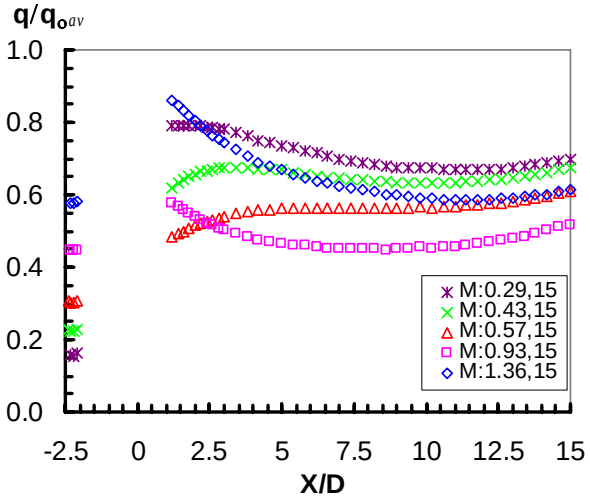

(b) Ramp angle 15^{o}

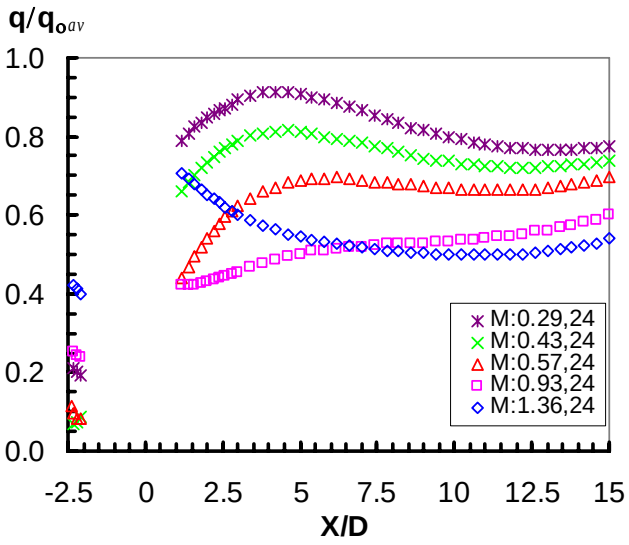

(c) Ramp angle 24^{o}

Figure 5.12 Spanwise averaged q/q_o for different blowing ratio M at a given ramp angle

5.3 CONCLUSIONS

The present studies experimentally evaluate the efficacy of placing an upstream ramp to enhance film cooling performance. Three ramp angles, 8.5^o, 15^o, and 24^o, with five blowing ratios ranging from 0.29 to 1.36, are tested. Local film cooling effectiveness and heat transfer coefficient distribution are measured using an IR imaging technique.

One of the most significant findings from the present study is that the upstream ramp increases film effectiveness only when the magnitude of the blowing ratio is sufficiently high, say $M \geq 1$. The presence of a ramp could be detrimental to film protection with higher q/q_o if the blowing ratio is lower than unity. Coolant would drift toward upstream with the recirculating flow immediately behind the ramp, resulting in a good film protection in the region downstream to the ramp. Lift-off of the coolant with a high blowing ratio would be tempered by the highly turbulent, shear layer separated from the downstream edge of the ramp. Current results reveal that placing a 24^o ramp upstream with a blowing ratio M=1.36 induces a nearly 50% increase in film effectiveness compared to the baseline case without a ramp. This implies that the efficacy of using an upstream ramp to enhance film cooling performance depends strongly on the nature of the interaction between the injected coolant and the separated flow field associated with the protrusion of a ramp. Presence of a ramp slightly increases the heat transfer coefficient, due mainly to additional shear-induced turbulence generated in the system. This, in turn, is detrimental to the overall reduction in surface heat transfer. Therefore, to establish a favorable cooling design with a ramp, the system must be operated in a regime where the mass flow of the injected coolant is not insignificant to affect the thermal characteristics of the recirculation zone, but its momentum is in-excessive, and the separated shear layer atop the recirculation zone could temper the coolant lift off or detachment.

6.0 FILM COOLING PERFORMANCE OF FILM COOLING HOLES EMBEDDED IN A TRENCH

6.1 TEST MODEL

The main objective of this phase of study is to determine the effect of blowing ratio on both heat transfer coefficient and film cooling effectiveness in an optimized film hole embedded in a trench geometry. Figure 6.1 shows the main geometry of the test model in the present study. The trench is 2D in width and 0.5D in depth.

D: Diameter of film cooling hole, 0.25”

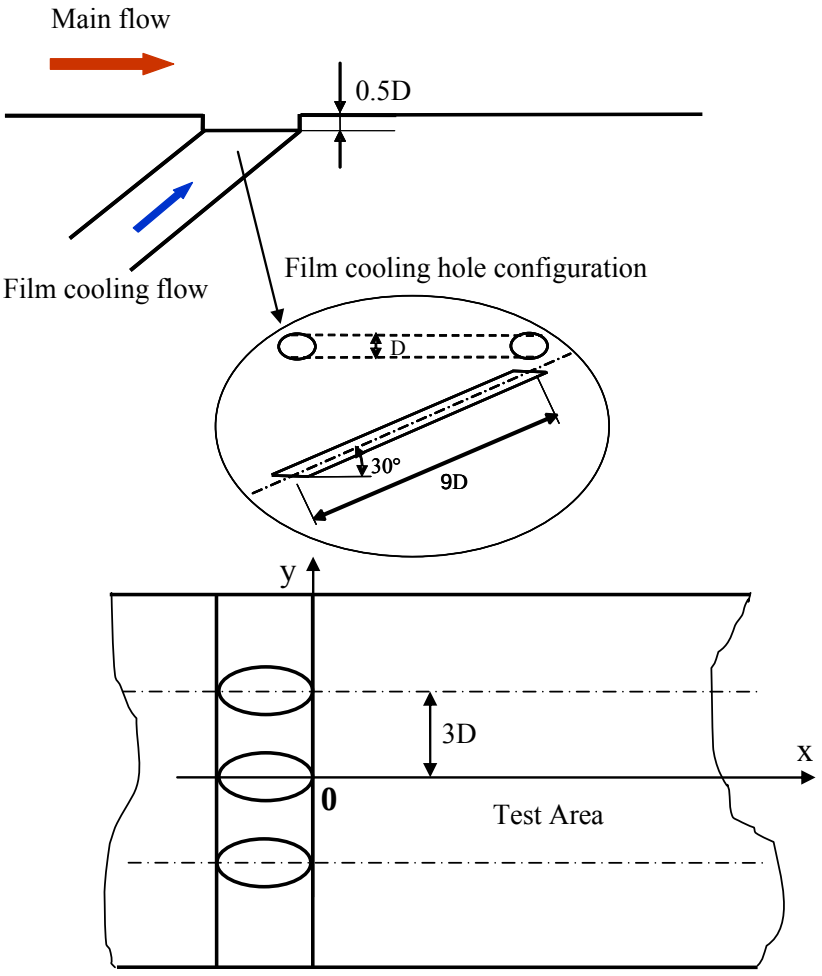

Figure 6.1 Schematic of the test model

Film cooling holes in this case have the same configuration as those for flow-aligned blocker and upstream ramp studied above. The length-to-diameter ratio is 9, still considerably greater than that of a modern turbine. This arrangement, again, is to allow a study exclusively focused on the effect of trench without much influence from the hole-inlet condition. A row of three holes with a 3D spanwise pitch is embedded in the trench. The test plate is made of Plexiglas. As mentioned before, the low thermal conductivity of Plexiglas (0.187W/mK) is technically suited for the measurements of η and h based on the transient conduction model over a semi-infinite solid domain. Figure 6.2 shows the photo of the test plate.

Figure 6.2 Photo of the test plate

6.2 RESULTS AND DISCCUSION

In this section, the results are presented and discussed. Similar to the cases of flow-aligned blockers and upstream ramp, this study tested the same five blowing ratio, i.e. M=0.29, 0.43, 0.57, 0.93, and 1.36.

Film effectiveness Figure 6.3 gives the contour plots of the local film cooling effectiveness of five blowing ratios for the trench and the corresponding baseline (without the trench). Such film effectiveness results reveal that the trench provides better protection in the region between neighboring holes, particularly in the near-hole region. The other notable feature is that the trench shows increased film cooling effectiveness at greater blowing ratios, say, M>0.57.

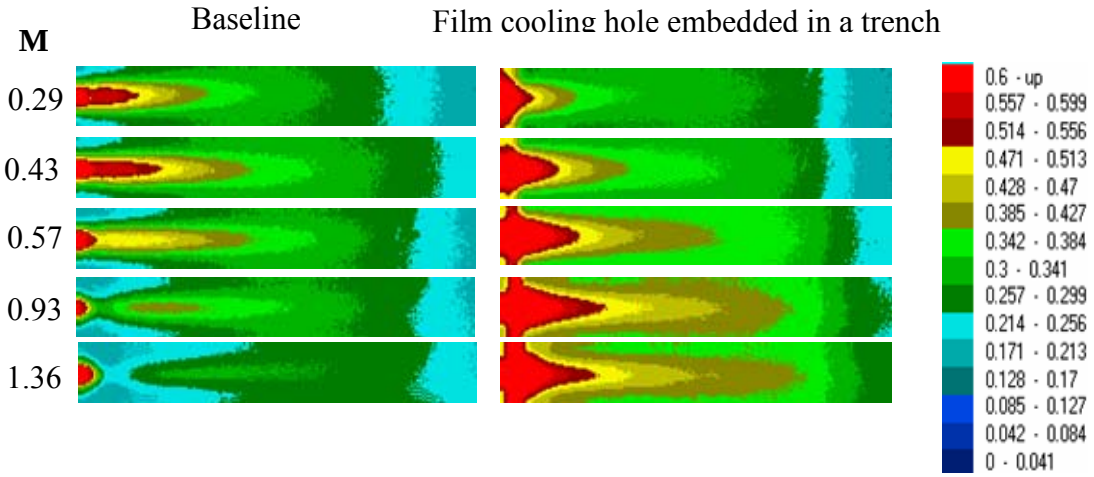

Figure 6.3 Local film cooling effectiveness distribution

To further characterize the film cooling performance of the trench, the streamwise distributions of the centerline and spanwise averaged film cooling effectiveness are given in Figs. 6.4 and 6.5, respectively. The corresponding baselines are also shown in the figures for comparison.

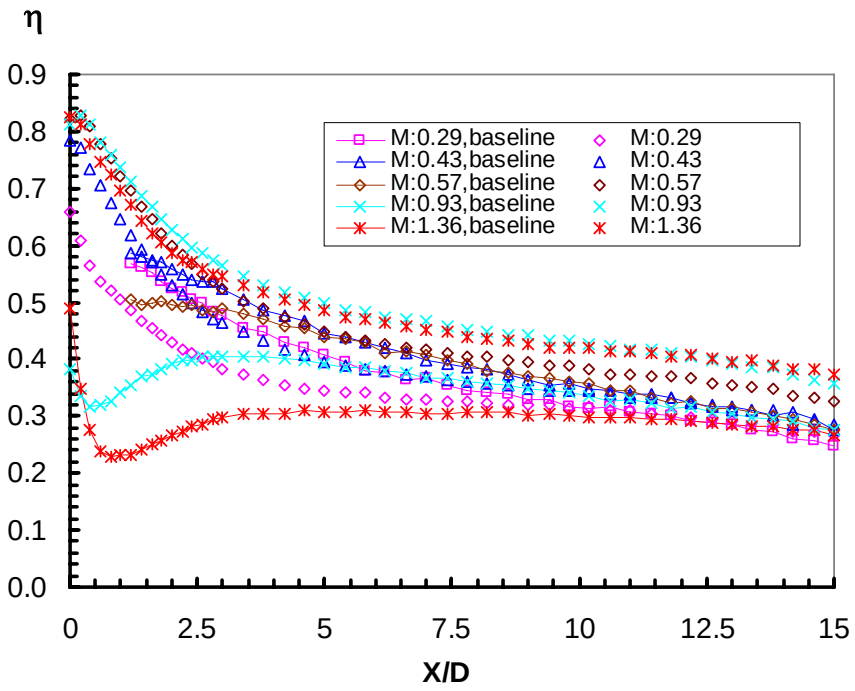

Figure 6.4 Streamwise distribution of the centerline film cooling effectiveness

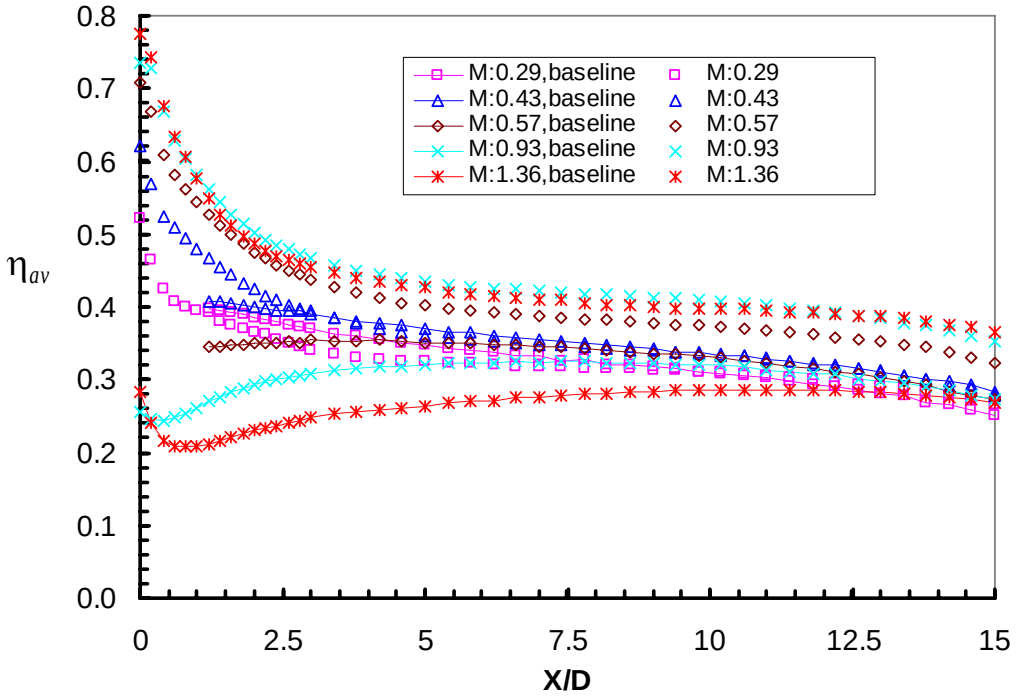

Figure 6.5 Streamwise distribution of the spanwise averaged film cooling effectiveness

Film cooling effectiveness along the centerline shows significant improvement as the blowing ratio M increases above 0.57. This is particularly notable for the values in the region immediately downstream to the trench; η is about 0.8 to 0.9, an improvement of 30% to 100% compared to the baseline. Improvement also reveals in spanwise averaged film cooling effectiveness for all the blowing ratios tested. However, for the cases with low blowing ratios, e.g. $M \leq 0.43$, the enhancement in η is limited to the near-trench region, and declines further downstream, as the value of η recovers to the same level as that of the baseline case. Nevertheless, the enhancement is very significant in the near-trench region, nearly 180%. In addition, as exhibited in Figs. 6.4 and 6.5, film effectiveness increases as the blowing ratio increases, but the same magnitude appears for the two higher blowing ratios M=0.93 and M=1.36. This phenomenon is consistent with that reported by Waye and Bogard (2006).

The trench modifies the injected coolant as the coolant spreads more laterally before reaching the protected surface. Therefore, a more uniform laterally distributed coolant flow, similar to that in the case of transverse slot, is obtained. At a low blowing ratio, because the amount of coolant is low, the effect of lateral flow may, in fact, deplete the coolant concentration sideway from the centerline. As a result, the magnitude of centerline effectiveness can be lower than that of the baseline case. However, the spanwise averaged film cooling effectiveness remains more or less the same level, and it can become even higher over the downstream portion of the trench. The trench-induced spreading effect becomes notably favorable when the blowing ratio increases, say $M>0.6$. In the baseline case without a trench, the coolant jet starts to lift off due to the high exiting coolant momentum or velocity. On the other hand, in the case with a trench, the coolant first fills the trench, spreading laterally, and then ejects out. This is evident from the temperature distribution in the trench, as displayed in Fig. 6.6. Coolant jets enter the

relatively relaxed space provided by the trench, which reduces the jet momentum, and coolant remains attached to the surface for better protection. However, this trend reaches a plateau at an M of about 1.0, as observed in both the present study and the work by Waye and Bogard (2006). This is because the space permitting lateral spreading becomes insufficient when the coolant mass increases and excessive coolant may penetrate and diffuse into the mainstream, diminishing the trench effect.

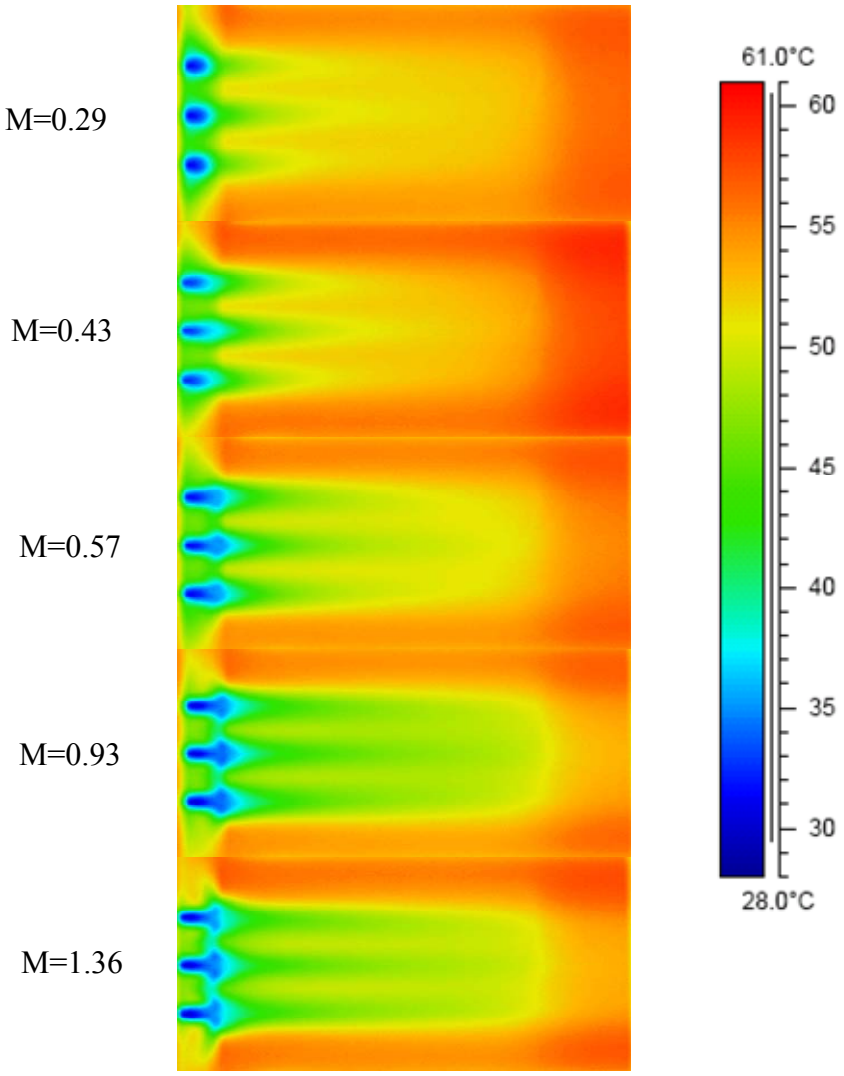

Figure 6.6 Contour plot of the local temperature distribution

The comparison of the present data with those reported in the literature is shown in Fig. 6.7. The configuration of the trench in Waye & Bogard's work is the same as the present one, but the trench is on the suction side of a turbine vane, thus with a convex curvature. The configuration studied by Lu et al. is different from the present one, as shown in Fig. 1.8 Case 2 in Section 1.2. The injection angle 35° in their study is also higher than that of the present configuration studied. Overall, the present data agrees well with those presented by both Waye & Bogard (2006) and Lu et al. Nevertheless, the effectiveness data from Lu et al. are generally lower when X/D<7.5.

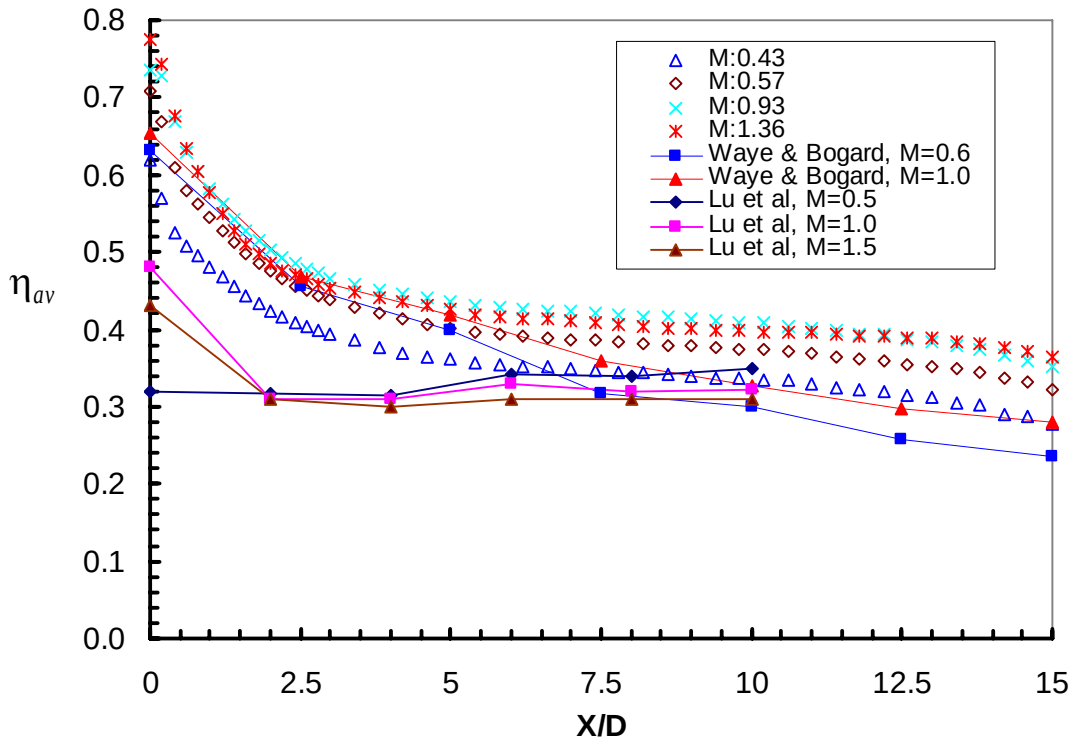

Figure 6.7 The comparison of the spanwise averaged film cooling effectiveness with those reported in the literature

Heat transfer coefficient Figure 6.8 shows the trench-affected results in heat transfer coefficient, h, along with the corresponding baseline data. The heat transfer coefficient near the trench shows a significant increase in magnitude, due mainly to the surface disturbance in the near-wall region. Further downstream, the value of the heat transfer coefficient remains more or less at the same level as that in the baseline case.

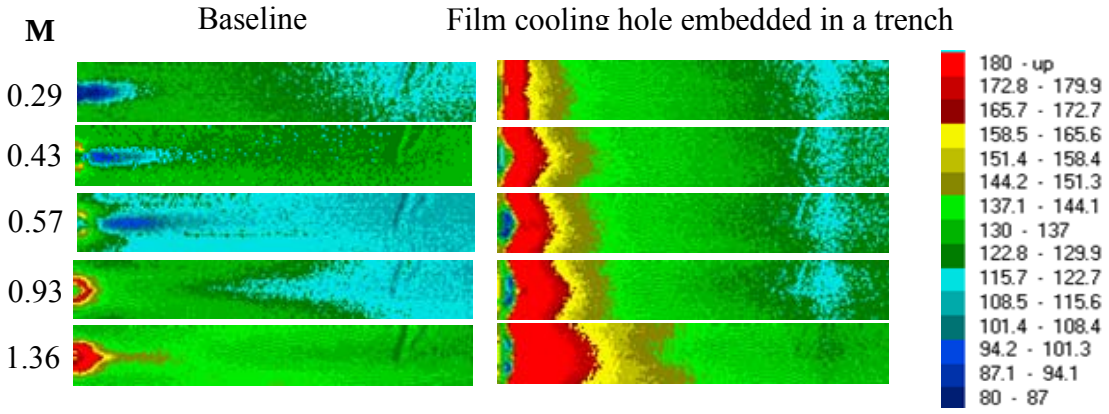

Figure 6.8 Contour plot of the heat transfer coefficient

To further analyze the data, the ratio of the heat transfer coefficient with film cooling to its counterpart h_o without film cooling is determined. Figures 6.9 and 6.10 reveal a normalized heat transfer coefficient distribution along the centerline and averaged across the span, respectively. The general trend is that, the magnitudes of heat transfer coefficients in the region sufficiently downstream, say X/D > 7.5, are of similar levels to those in the baseline cases. In the region immediately downstream to the trench, say X/D<5, the increase of heat transfer is evident for all the blowing ratios tested.

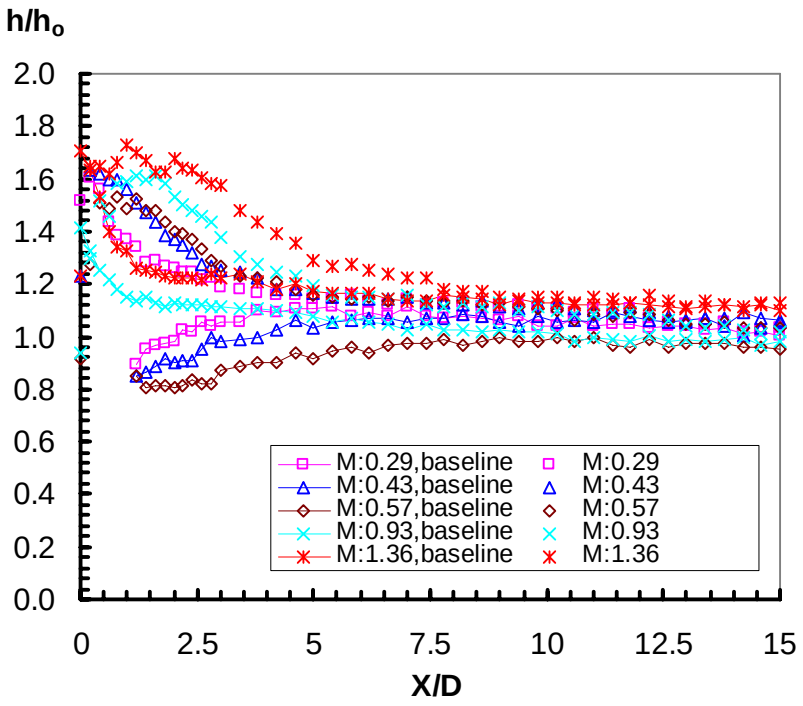

Figure 6.9 Streamwise distribution of the centerline heat transfer coefficient

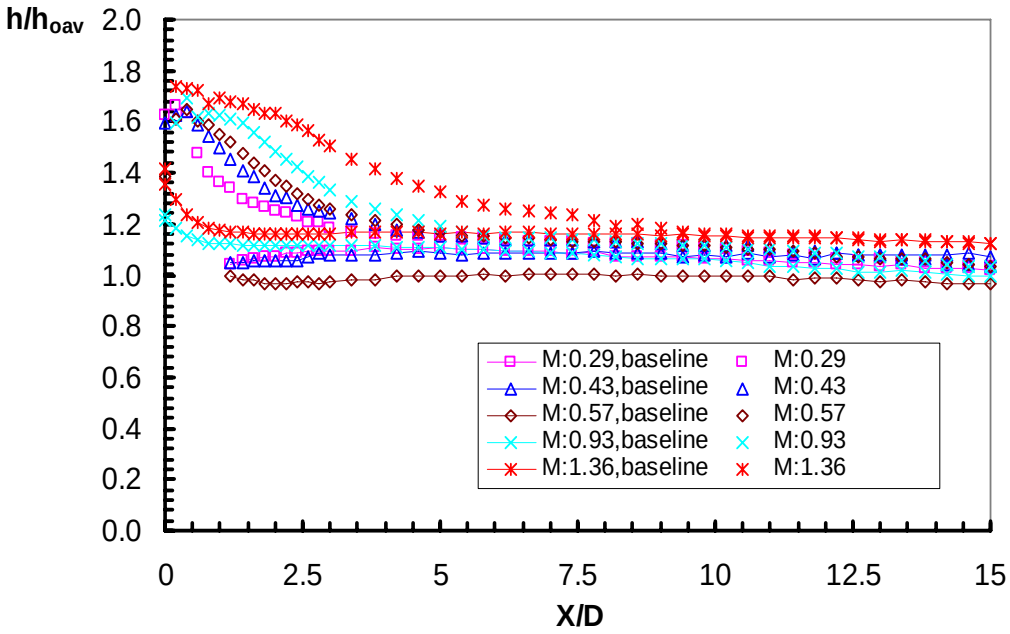

Figure 6.10 Streamwise distribution of the spanwise averaged heat transfer coefficient

The flow pattern in a trench is deemed to be more complex than that in a 2-dimentional slot without coolant ejection. The ejection of coolant from film cooling holes to a trench is similar to flow entering a sudden-expansion channel, except that a trench is a much shorter channel. Flow in a sudden-expansion channel is characterized by highly turbulent shear layer along with recirculation adjacent to the shear layer. Jet interactions further complicate the flow field, as multiple coolant jets enter the same trench. Therefore, coolant flow exiting a trench inherits high turbulence intensity, which is responsible for the increase of the local heat transfer coefficient. This effect is expected to elevate with an increase in blowing ratio or jet momentum. Further downstream, the turbulence dissipates and diminishes due to wall effects and the presence of main flow.

The heat transfer coefficient is also compared with that reported in the literature. As mentioned above, the configuration of the trench studied by Waye and Bogard (2006) are the same as the present one, but they did not measure heat transfer coefficient. Therefore, Harrison et al. (2007)'s result are chosen for comparison. The configuration they studied is the same as that in the present study, except the depth of the trench in their study is 1.0D, deeper than that of the present one. As shown in Fig.6.11, the present results are very consistent with theirs.

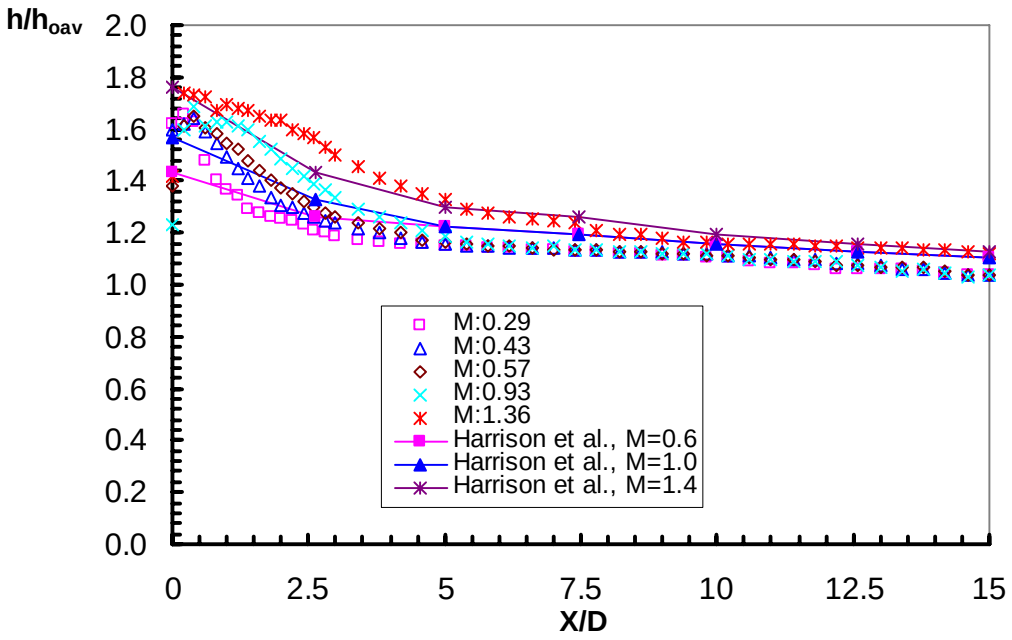

Figure 6.11 The comparison of the spanwise averaged heat transfer coefficient with that reported in the literature

Reduced heat flux The ratio of heat flux with film cooling injection to that without film cooling is based on the measured film effectiveness and heat transfer coefficient. The centerline and spanwise averaged heat flux ratios are plotted in Figs. 6.12 and 6.13, respectively. Compared to the corresponding baseline data, the centerline values of q/q_o are lower at blowing ratios M>0.57. Particularly, q/q_o is zero in the region X/D<2, which indicates a complete coolant protection. The spanwise-averaged result shows a similar trend as that of the center line, and the value of q/q_o decreases when blowing ratio M>0.57. The improvement of film cooling performance, measured by heat flux reduction, is rather substantial, up to 100%, regardless of a high heat transfer coefficient existing in the region close to the trench downstream edge. Such a reduction in heat transfer is attributable mainly to the significant increase in film effectiveness.

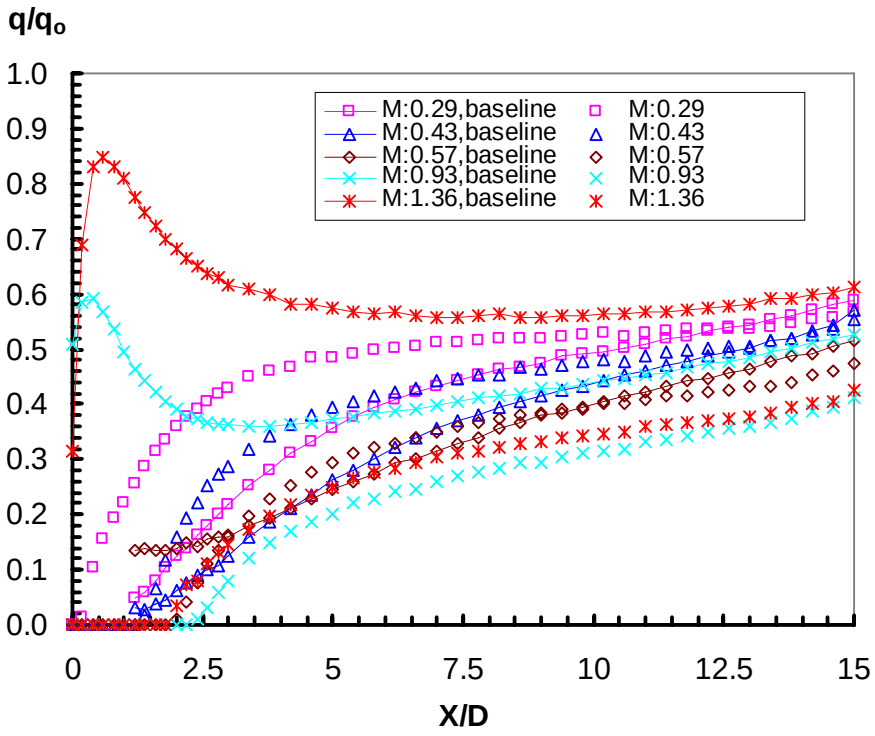

Figure 6.12 Streamwise distribution of the centerline heat flux ratio

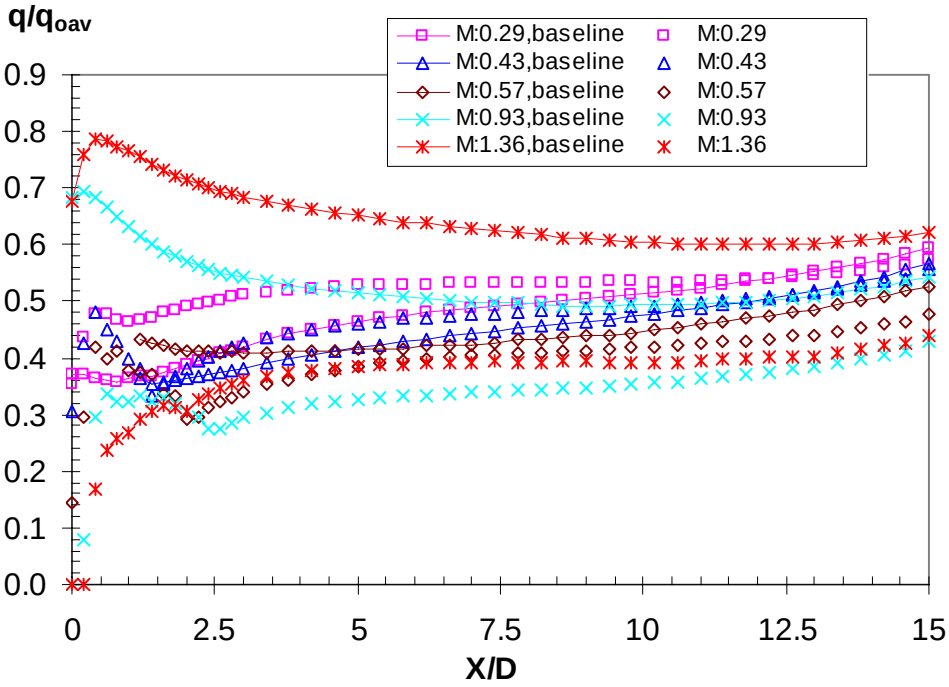

Figure 6.13 Streamwise distribution of the spanwise averaged heat flux ratio

6.3 CONCLUSIONS

The present study focuses on the cooling performance of film cooling holes embedded in a trench. Local film cooling effectiveness and heat transfer coefficient distribution are revealed by measurement using an IR imaging technique.

The experimental results show that a trench has a profound influence on increasing the film cooling effectiveness when M>0.43. This effect is particularly significant in the region immediately downstream from the trench, with an impressive 180% increase. This is due mainly to the lateral spreading of coolant induced by the trench, which also reduces the momentum of injected coolant and produces better coverage downstream. Therefore, the trench configuration is especially effective for film cooling when the blowing ratio is sufficiently high. However, the overall enhancement in film cooling effectiveness, based on the present study, reaches a plateau when the blowing ratio M ~1.0.

One of the significant contributions of the present study is the attainment of detailed local distribution of heat transfer coefficient, in addition to film effectiveness. The local heat transfer coefficient increases sharply in the region immediately downstream of the trench. Also, the magnitude of overall heat transfer coefficient increases with blowing ratio. At a region far downstream of the trench, the effect of the trench on the heat transfer coefficient becomes rather insignificant.

As a combined result of film cooling effectiveness and heat transfer coefficient, the reduced heat flux, q/q_o, decreases when blowing ratio M>0.57. Apparently the trench-induced enhancement in film effectiveness overwhelms the increase in heat transfer coefficient in the near-hole region. Up to a 100% reduction in the q/q_o is observed.

7.0 COMPARISON OF THE THREE FILM COOLING CONCEPTS

In this chapter, the three film cooling enhancement approaches investigated in this study are compared based on film effectiveness, heat transfer coefficient ratio and reduced heat flux. The comparison is made based on the same five blowing ratios tested. For the upstream ramp cases, only the results with 24^{o} angle inclination are selected for comparison, since it is the only ramp configuration that promises potential improvement in film cooling downstream from the injection holes.

7.1 COMPARISON OF FILM COOLING PERFORMANCE AT DIFFERENT BLOWING RATIO

Figures 7.1 and 7.2 presents the spanwise averaged film cooling effectiveness and heat transfer coefficient ratio of the three film cooling schemes at five blowing ratios, respectively. At all the blowing ratios tested, the trench provides the highest η_{av}, and the upstream ramp gives the lowest η_{av}, among the three approaches. Except for the highest blowing ratio, M=1.36, the presence of an upstream ramp, in fact, produces a lower film effectiveness than the baseline case. This is particularly evident for low blowing ratio, i.e. M<0.6. As for heat transfer coefficient ratio, the upstream ramp renders the highest h for blowing ratio $M \leq 1.0$. The heat transfer coefficient ratio of the trench is slightly higher than that of flow-aligned blocker except at the low blow ratio M~ 0.3. In general, all three approaches lead to higher heat transfer coefficients than the corresponding baseline cases.

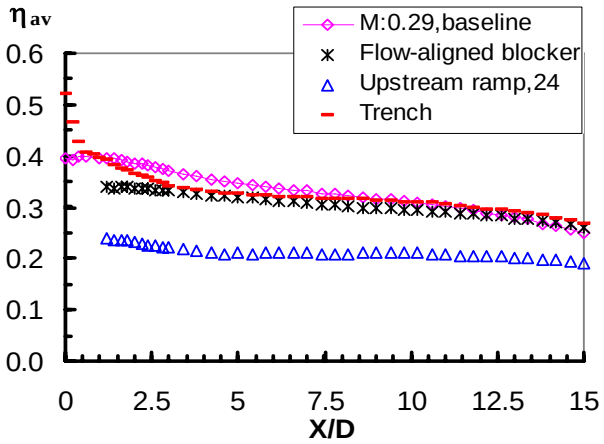

(a) M=0.29

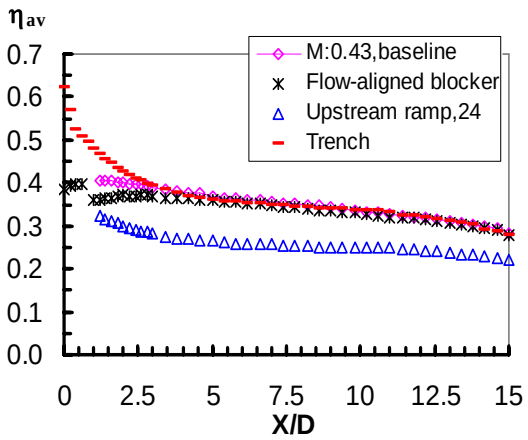

(b) M=0.43

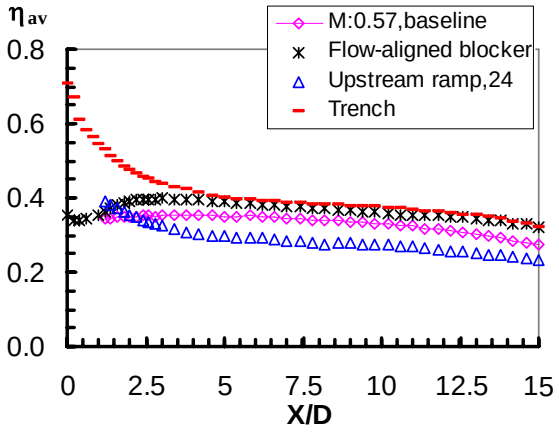

(c) M=0.57

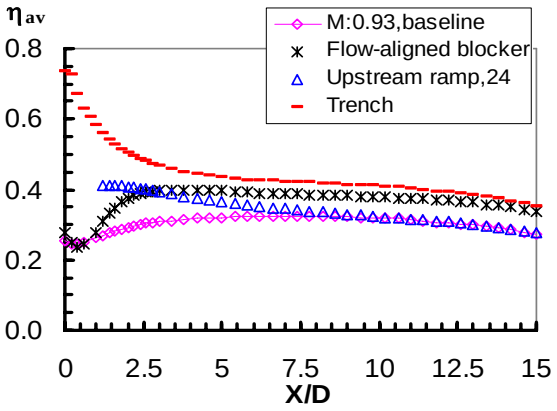

(d) M=0.93

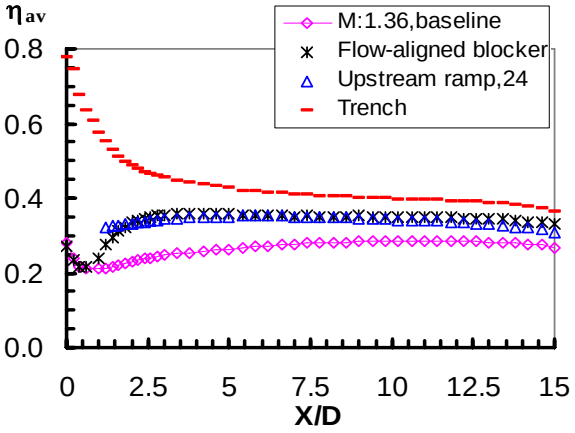

(e) M=1.36

Figure 7.1 The spanwise averaged film effectiveness for the three different approaches

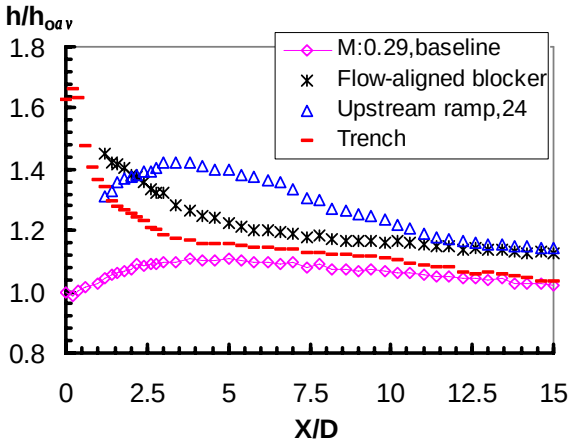

(a) M=0.29

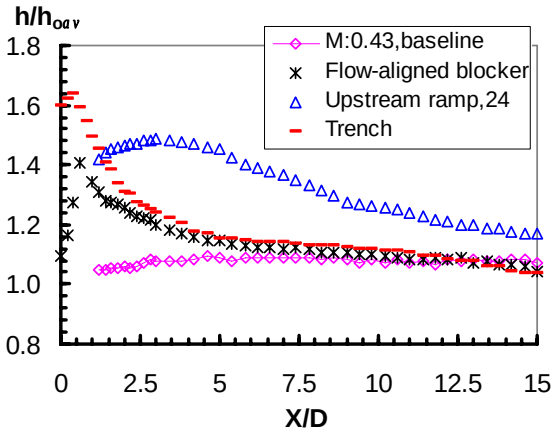

(b) M=0.43

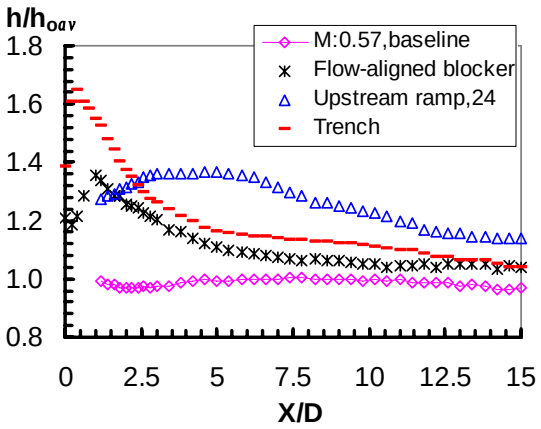

(c) M=0.57

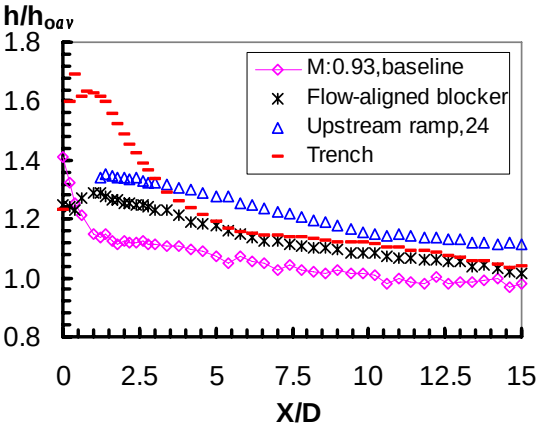

(d) M=0.93

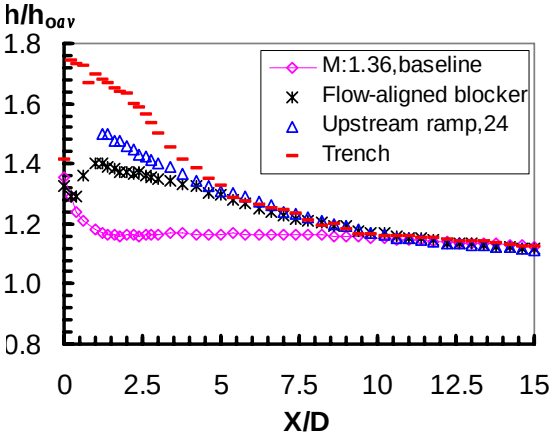

(e) M=1.36

Figure 7.2 The spanwise averaged heat transfer coefficient ratio for the three different approaches

The inter-hole and spanwise averaged heat flux ratios of the three different approaches at five blowing ratios are shown in Figs.7.3 and 7.4, respectively. The corresponding baseline data are also given for comparison. Overall, the performance of these three film cooling concepts improves with the blowing ratio.

Low range blowing ratio (M: ~ 0.3) (Figs. 7.3 and 7.4(a)) None of these three approaches offers any advantage at this low blowing ratio. In fact, film cooling performance is substantially degraded compared to the corresponding baseline case of cylindrical hole over a smooth plate. Specifically, upstream ramp gives the highest heat flux ratio, implying ineffective coolant protection. The performance of a trench is comparable to that of a cylindrical hole, with slightly higher heat flux ratio. The flow-aligned blocker renders a lower heat flux ratio than the upstream ramp does, yet higher than that of the trench.

Mid-range blowing ratio (M: 0.4 ~ 0.6) (Figs. 7.3 and 7.4(b) (c)) The performances of the three new film cooling concepts improve at this range of blowing ratio compared to those at the low range blowing ratio. However, there is still not any obvious advantage of using these new concepts, except that a trench improves lateral spreading of coolant. Particularly, flow-aligned blockers and a trench show comparable performance to that of the baseline. An upstream ramp has the worst performance, with an increase of 40~60% in q/q_o, compared to the baseline case.

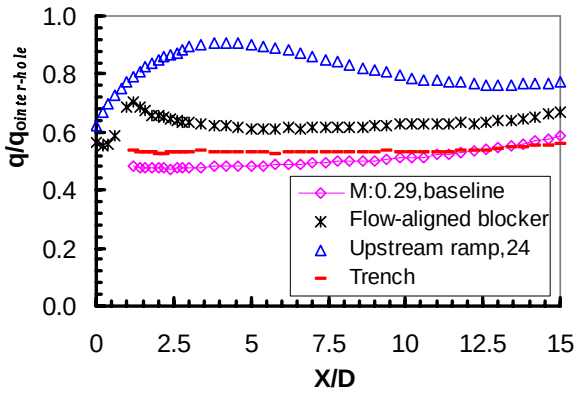

(a) M=0.29

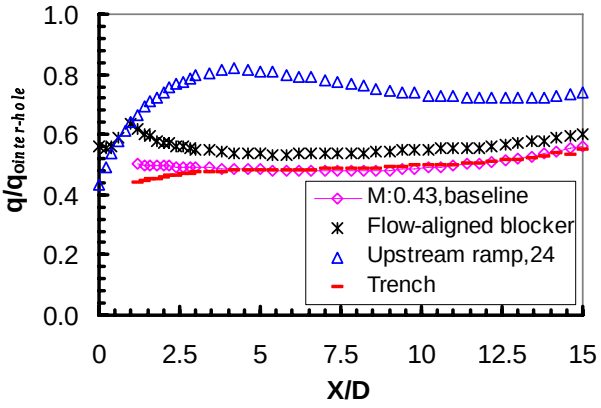

(b) M=0.43

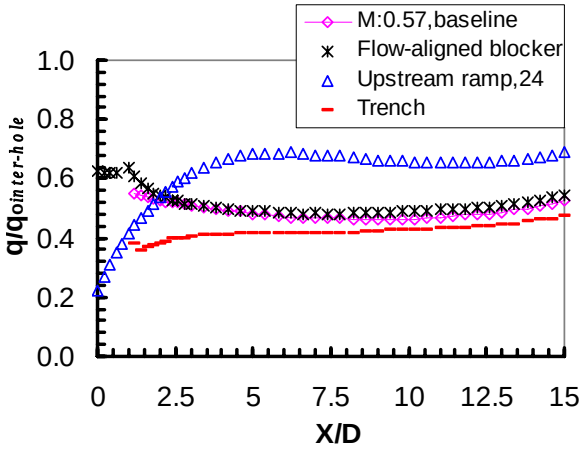

(c) M=0.57

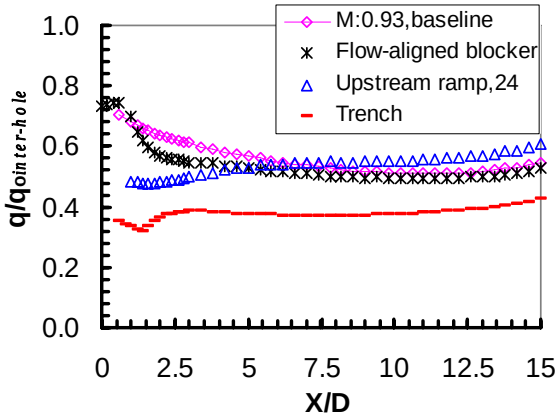

(d) M=0.93

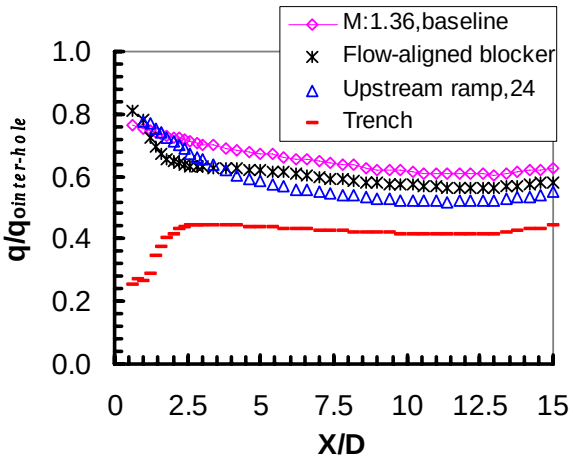

(e) M=1.36

Figure 7.3 The inter-hole averaged heat flux ratio distribution for the three different approaches

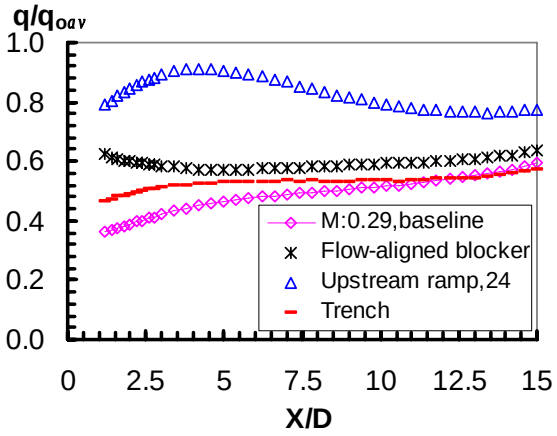

(a) M=0.29

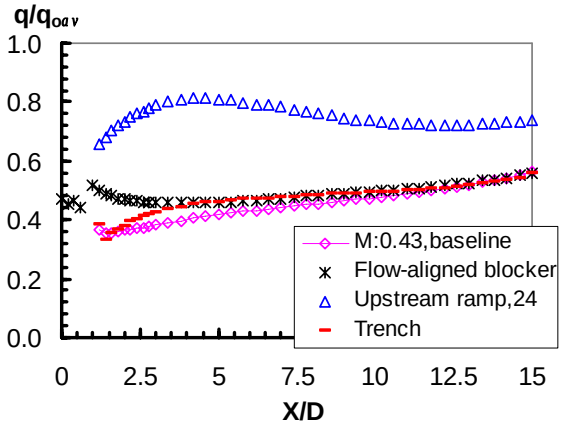

(b) M=0.43

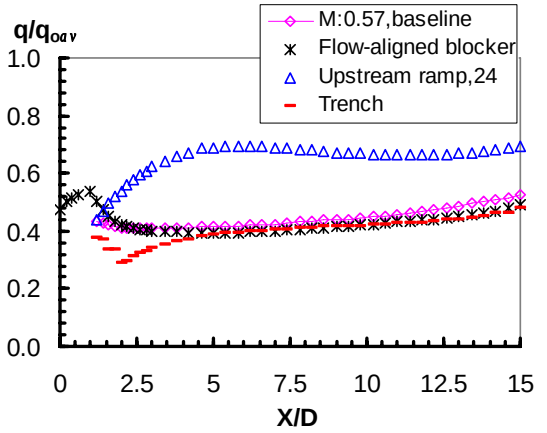

(c) M=0.57

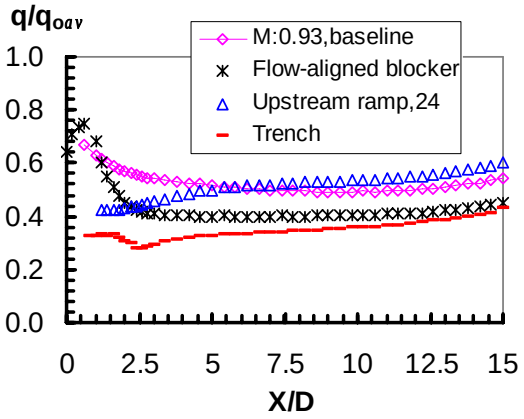

(d) M=0.93

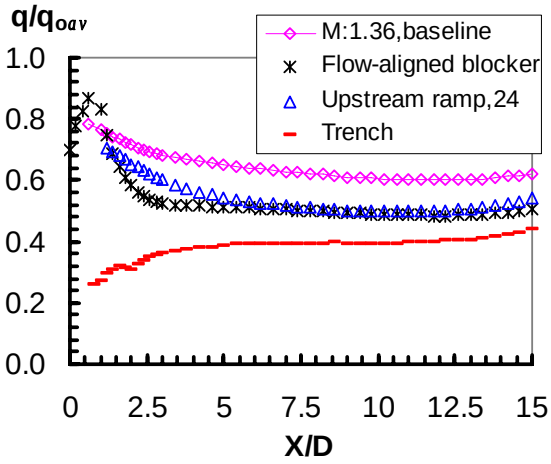

(e) M=1.36

Figure 7.4 The spanwise averaged heat flux ratio distribution for the three different approaches

High range blowing ratio (M: 0.9 ~ 1.4) (Figs. 7.3 and 7.4(d) (e)) The inter-hole and spanwise averaged heat flux ratios for the trench are much lower than the baseline, with a reduction of 20~100%. It suggests that the trench greatly improves film cooling in this high range blowing ratio. As for flow-aligned blockers, heat flux ratios are reduced by about 20% when X/D>1.2, but increased in the near-hole region, compared to the baseline. As described in the previous chapter, the reason is that leading edges of flow-aligned blockers cause heat transfer coefficient to increase in this region. The decrease of heat flux ratio for the upstream ramp is limited in the region X/D<5 when M=0.93, although it has the same level as that of flow-aligned blockers when M=1.36. Therefore, the trench concept appears to be a viable choice for film cooling improvement with high blowing ratios. Flow-aligned blockers may be used if the frontal configuration is modified to temper the high heat transfer coefficient near the leading edge regime. An upstream ramp could also be considered if the blowing ratio M ≥1.4.

7.2 CONCLUSIONS

The three approaches for improving film cooling performance are compared at all five different blowing ratios. The present data suggest that, the trench consistently provides the highest η_{av}, and the upstream ramp gives the lowest $\eta_{av.}$ The upstream ramp also renders a rather undesirable performance in heat transfer coefficient, which has the highest heat transfer coefficient until M reaches 1.4. The heat transfer coefficient of the trench is higher than that of flow-aligned blockers except at low blow ratio M ~ 0.3.

At low range blowing ratio (M: ~0.3), the heat flux ratios for all three methods are not lower than the baseline cases. This implies that these new concepts offer virtually no advantage in film cooling performance, and thus, should not be considered when the blowing ratio is low. At mid-range blowing ratio (M: 0.4 ~ 0.6), the spanwise averaged heat flux ratio for the trench is at the same level as the baseline cases, but the inter-hole averaged value is reduced. Thus, a trench is a good choice if the lateral spreading of coolant is of concern. The three new film cooling concepts show advantages at high range blowing ratio (M: 0.9 ~ 1.4). Particularly, the trench significantly decreases the heat flux ratio, up to 100%. It is a very good choice for improving film cooling performance. Flow-aligned blockers with modified leading edge configuration may be used for improving film cooling performance. An upstream ramp can also be considered if the blowing ratio $M \geq 1.4$.

8.0 CONCLUSIONS AND FUTURE WORK

8.1 MAJOR ACCOMPLISHMENTS

This dissertation presents experimental studies on three film cooling concepts with moderate surface reshapes. Experimental procedures, data analysis, and data reduction methodology for measurement of local heat transfer coefficient and film cooling effectiveness using IR imaging technique are established and documented via this work. The major findings are summarized below.

Film cooling performance of downstream flow-aligned blockers Downstream flow-aligned blockers seem to be effective in preventing the hot gas from entraining underneath the kidney vortices. The resulting film cooling effectiveness significantly improves when the blowing ratio M>0.43. The heat transfer coefficients are nearly identical to those in the baseline cases without blockers, except in the region near centerline, where a 20% reduction is observed. Heat transfer in the region near the leading edges of blockers increases, likely due to the high turbulence associated with flow separation and reattachment. Overall, flow-aligned blockers improve film cooling performance when the blowing ratio M>0.43. Several geometrical parameters of blocker design are expected to affect film cooling performance. The height of a blocker would be a significant factor, depending on the blowing ratio. Other parameters, such as a blocker's length and the space between two adjacent blockers, could also be important.

Effect of upstream ramp on film cooling performance The idea of placing a ramp with a back-facing step upstream of film cooling holes for film cooling enhancement is examined experimentally. The test matrix includes three ramp angles, i.e. 8.5^o, 15^o, and 24^o, and five blowing ratios. The extent of the upstream ramp to improve film cooling effectiveness strongly depends on the angle (height) of a ramp and blowing ratio. Film cooling data measured in the present study suggest that large angles combined with high blowing ratios are most favorable. Of the three ramp angles studied, the angle of 24^o at blowing ratio M=1.36 provides a 50% improvement in film cooling effectiveness and 20% of the reduced heat flux, q/q_o. However, the present ramp data with low blowing ratios show virtually no advantage, or even detrimental effects on overall film cooling performance.

The characteristics of flow over a ramp are responsible for the film cooling performance. Typically, the flow over a two-dimensional ramp is characterized by three different zones: recirculation region right behind the step, reattachment zone, and redeveloped boundary layer. At low blowing ratios, the coolant flow drifts upstream along with the recirculation flow and does not have enough momentum to penetrate into the recirculation zone. However, when the blowing ratio is high, the coolant penetrates into the recirculation zone, and the separated shear layer on top of it presses it down to the wall, leading to good protection. This complex flow phenomenon, in conjunction with the rather limited cooling enhancement observed in the present study, suggests that implementation of upstream ramp concept must be pursued with great caution.

Film cooling hole embedded in a transverse trench While previous studies have shown that a shallow and narrow trench greatly improves film cooling effectiveness, very limited heat transfer data exists. The use of an IR imaging technique reveals detailed distributions of both film cooling effectiveness and heat transfer coefficient for a shallow and narrow trench configuration. Particular emphasis is directed to characterize the effect of blowing ratio on both η and h. Film cooling effectiveness improves when blowing ratio M>0.43. A noticeable enhancement, up to 180% at M=1.36, is observed in the region near a trench exit. In addition, it is observed that the increase of film cooling effectiveness with blowing ratio reaches a plateau when M ~ 1.0.

The magnitudes of heat transfer coefficient vary rather insignificantly far downstream from a trench, but they rise sharply in the near-trench region. This level of augmentation in local heat transfer coefficient increases with the blowing ratio. The elevated turbulence associated with coolant blowing out of the trench may be responsible for this increase.

The reduced heat flux q/q_o decreases when the blowing ratio M>0.57. A reduction of up to 100% is observed at M=1.36, even though the heat transfer coefficient in the near-trench region is rather high.

Comparison of the performance of the three different approaches at different blowing ratio

The performance of the three different approaches studied is compared at all five blowing ratios tested. At low range blowing ratio (M: ~0.3), all three methods render no advantage, and in fact, degrade film cooling performance. However, such an undesirable trend reverses as the blowing ratio increases. At mid-range blowing ratio (M: 0.4 ~ 0.6), the trench and flow-aligned blockers show comparable film cooling performance to the baseline case, while the upstream ramp still reveals rather inferior performance. At high range blowing ratio (M: 0.9 ~ 1.4), all three

concepts render an improvement in overall cooling performance, with the trench being the most significant. The present data suggests that upstream ramp can be effective only when M~1.4 or higher.

Development of the IR imaging technique for heat transfer measurement As part of the major effort of this dissertation research, the experimental system, test procedures, and data reduction method for characterizing heat transfer for both two- and three- temperature problems using an IR imaging technique are developed. The framework of data reduction is a least square method for obtaining both η and h with minimized uncertainty for three-temperature problem.

8.2 FUTURE WORK

A significant level of research on three film cooling concepts has been accomplished in the present work. Further investigations may be directed towards a thorough study and maturity of the technologies for implementation in the state-of-the-art gas turbines.

The shape of flow-aligned blocker As discussed in Chapter 4, the blockers studied in the present work are prism-shaped with sharp corners. As a result, the heat transfer coefficient increases in the region near the leading edges of blockers. This leads to an increase in heat flux ratio, which is somewhat unexpected when the present blocker geometry was designed. Therefore, modification of the blocker shape is worthwhile, and research on optimal blocker geometry is recommended.

Data obtained from this study suggest that the height of the blocker is an important design parameter, as its effect on jet penetration height depends on the blowing ratios. Therefore, further studies and systematical exploration on this geometric parameter would be beneficial.

The height of a ramp relative to approaching boundary layer thickness The nature of flow separation depends strongly on the relative heights of obstacle and approaching boundary layer. The present study was performed with a boundary layer thickness δ about 2D, and the height of the steepest ramp is about 0.42δ. This overall suggests the present separation over a ramp occurs with a relatively thick approaching boundary layer. Further studies with a range of representative values of boundary layer thickness to ramp height ratio may be desirable.

Airfoil cascade test The present study on the film cooling performances of the three film cooling concepts is conducted via flat plate test. Tests on an airfoil streamlined surface and/or with a cascade similar to real engine configurations would be a reasonable extension of the current study.

APPENDIX A

THE LEAST SQUARE METHOD

The non-linear optimization problem is described as

$$f_i(x_1, x_2, \cdots, x_n) = 0, i = 1,2,\cdots, m; m \geq n \qquad (A.1)$$

where, x_1, x_2, …, x_n are independent variables, m is the number of equations, and n is the number of variables. When m=n, the equation represents a non-linear system of equations. Specifically, for the three-temperature problem, n=2, which includes film cooling effectiveness η and heat transfer coefficient h, and m depends on the number of frames used. In this dissertation, 15 frames are used, which gives m=15.

To find the optimal solutions of the unknowns in the above problem, first calculate its Jacobi matrix, which is written as

$$A = \begin{bmatrix} \frac{\partial f_1}{\partial x_1} & \frac{\partial f_1}{\partial x_2} & \cdots & \frac{\partial f_1}{\partial x_n} \\ \frac{\partial f_2}{\partial x_1} & \frac{\partial f_2}{\partial x_2} & \cdots & \frac{\partial f_2}{\partial x_n} \\ \vdots & \vdots & & \vdots \\ \frac{\partial f_m}{\partial x_1} & \frac{\partial f_m}{\partial x_2} & \cdots & \frac{\partial f_m}{\partial x_n} \end{bmatrix} \qquad (A.2)$$

The iteration formula for obtaining the least square solutions is

$$X^{(k+1)} = X^{(k)} - \alpha_k Z^{(k)} \qquad (A.3)$$

where $Z^{(k)}$ is the least square solution for the linear system of equations

$$A^{(k)}Z^{(k)} = F^{(k)} \qquad \text{(A.4)}$$

$$Z^{(k)} = (A^{(k)}) + F^{(k)} \qquad \text{(A.5)}$$

where

$$F^{(k)} = (f_1^{(k)}, f_2^{(k)}, \cdots, f_m^{(k)})^T \qquad \text{(A.6)}$$

$$f_i^{(k)} = f_i(x_1^{(k)}, x_2^{(k)}, \cdots, x_n^{(k)}), i = 1,2,\cdots,m \qquad \text{(A.7)}$$

α_k is the value for the function

$$\sum_{i=1}^{m} (f_i^{(k+1)})$$

reaching its minimum.

APPENDIX B

FORTRAN CODE FOR THE LEAST SQUARE METHOD

B.1 Main program

```
C-----------------------------------------------------------------------
C-----------------------------------------------------------------------
C     EXTERNAL   F, FJ
      PARAMETER  (JLINE=88, INUM=223, NUMT=180, NFILE=15,
     &      IHOL1=12,IHOU1=30,JHOL1=10,JHOU1=20,ITTS=20,
     &    IHOL2=12,IHOU2=30,JHOL2=40,JHOU2=48,
     &    IHOL3=12,IHOU3=30,JHOL3=67,JHOU3=77)
      DIMENSION  TWA(NFILE,INUM,JLINE),TAO(NUMT),TC(NUMT),TM(NUMT),
     &      TINI(INUM,JLINE),TIMTW(NFILE)
C-----------------------------------------------------------------
      DIMENSION X(2), P(NFILE,2), D(NFILE), PP(2,NFILE), DX(2),
     &      U(NFILE,NFILE), V(2,2), TW(NFILE)
      DIMENSION S(NFILE+1), E(NFILE+1), WORK(NFILE+1), ETA(INUM,JLINE),
     &      HTC(INUM,JLINE)
            COMMON AK,ALFA,NUMTM,TM,TC,TAO
      DATA X/ 0.01, 150 /
            XINT1=X(1)
            XINT2=X(2)
            NUMTM=NUMT
      M=NFILE
      N=2
      KA=NFILE+1
      EPS1=0.001
      EPS2=0.00001
C-------------------------------------------------------------
C-------------------------------------------------------------
      WRITE(*,*) 'Please input thermal conductivity of substrate'
      AK=0.187
      WRITE(*,*) 'Please input thermal diffusivity of substrate'
      ALFA=1.073E-7
C----------------Frame lines (JLINE) number of data in one line (INUM) ---
C-------------------------------------------------------------
      OPEN (1,FILE='t916fc11.csv')
      OPEN (2,FILE='t916fc12.csv')
      OPEN (3,FILE='t916fc13.csv')
      OPEN (4,FILE='t916fc14.csv')
```

```
OPEN (5,FILE='t916fc15.csv')
OPEN (6,FILE='t916fc16.csv')
OPEN (7,FILE='t916fc17.csv')
OPEN (8,FILE='t916fc18.csv')
OPEN (9,FILE='t916fc19.csv')
OPEN (10,FILE='t916fc110.csv')
OPEN (11,FILE='t916fc111.csv')
OPEN (12,FILE='t916fc112.csv')
OPEN (13,FILE='t916fc113.csv')
OPEN (14,FILE='t916fc114.csv')
OPEN (15,FILE='t916fc115.csv')
      OPEN (16,FILE='TESTRE.TXT')
READ (1,*) (  (TWA(1,ITE,JTE), ITE=1,INUM), JTE=1,JLINE)
READ (2,*) (  (TWA(2,ITE,JTE), ITE=1,INUM), JTE=1,JLINE)
READ (3,*) (  (TWA(3,ITE,JTE), ITE=1,INUM), JTE=1,JLINE)
READ (4,*) (  (TWA(4,ITE,JTE), ITE=1,INUM), JTE=1,JLINE)
READ (5,*) (  (TWA(5,ITE,JTE), ITE=1,INUM), JTE=1,JLINE)
READ (6,*) (  (TWA(6,ITE,JTE), ITE=1,INUM), JTE=1,JLINE)
READ (7,*) (  (TWA(7,ITE,JTE), ITE=1,INUM), JTE=1,JLINE)
READ (8,*) (  (TWA(8,ITE,JTE), ITE=1,INUM), JTE=1,JLINE)
READ (9,*) (  (TWA(9,ITE,JTE), ITE=1,INUM), JTE=1,JLINE)
READ (10,*) (  (TWA(10,ITE,JTE), ITE=1,INUM), JTE=1,JLINE)
READ (11,*) (  (TWA(11,ITE,JTE), ITE=1,INUM), JTE=1,JLINE)
READ (12,*) (  (TWA(12,ITE,JTE), ITE=1,INUM), JTE=1,JLINE)
READ (13,*) (  (TWA(13,ITE,JTE), ITE=1,INUM), JTE=1,JLINE)
READ (14,*) (  (TWA(14,ITE,JTE), ITE=1,INUM), JTE=1,JLINE)
READ (15,*) (  (TWA(15,ITE,JTE), ITE=1,INUM), JTE=1,JLINE)
CLOSE(1)
CLOSE(2)
CLOSE(3)
CLOSE(4)
CLOSE(5)
CLOSE(6)
CLOSE(7)
CLOSE(8)
CLOSE(9)
CLOSE(10)
CLOSE(11)
CLOSE(12)
CLOSE(13)
CLOSE(14)
CLOSE(15)
      TIMINI=20.42
TIMTW(1)=25.625-TIMINI
TIMTW(2)=30.697-TIMINI
TIMTW(3)=35.72-TIMINI
TIMTW(4)=40.841-TIMINI
TIMTW(5)=45.913-TIMINI
TIMTW(6)=50.983-TIMINI
      TIMTW(7)=56.055-TIMINI
      TIMTW(8)=61.127-TIMINI
TIMTW(9)=65.131-TIMINI
TIMTW(10)=70.203-TIMINI
TIMTW(11)=75.273-TIMINI
TIMTW(12)=80.346-TIMINI
      TIMTW(13)=85.684-TIMINI
```

```
      TIMTW(14)=90.756-TIMINI
      TIMTW(15)=95.828-TIMINI
C-------------------------------------------------------
c      DO 1 ITE=1,INUM
c            DO 1 JTE=1,JLINE
c 1    TINI(ITE,JTE)=28.3
C-------------------------------------------------------
            OPEN (21,FILE='t916fc10.csv')
            READ (21,*) (  (TINI(ITE,JTE), ITE=1,INUM), JTE=1,JLINE)
      CLOSE(21)
C-------------------
      OPEN (22,FILE='tmc09161.txt')
      DO 1005  ITIME=1,NUMT
      READ (22,*)  TAO(ITIME), TM(ITIME), TC(ITIME)
1005  CONTINUE
      CLOSE(22)
            OPEN (23,FILE='ETAFILE.TXT')
      OPEN (24,FILE='HFILE.TXT')
            WRITE(23,*)
      WRITE(24,*)
      WRITE(23,*)'eta'
      WRITE(24,*)'h'
      WRITE(23,*)INUM,JLINE
      WRITE(24,*)INUM,JLINE
C-----------------------------
      DO 1010   JTT=1,JLINE
      DO 1020   ITT=ITTS,INUM
            IF(JTT.GT.1) THEN
            X(1)=ETA(ITT,JTT-1)
            X(2)=HTC(ITT,JTT-1)
              IF ((JTT.EQ.(JHOU1+1)).AND.(ITT.GE.IHOL1.AND.ITT.LE.IHOU1)) THEN
                X(1)=XINT1
                X(2)=XINT2
              ENDIF
       IF ((JTT.EQ.(JHOU2+1)).AND.(ITT.GE.IHOL2.AND.ITT.LE.IHOU2)) THEN
                X(1)=XINT1
                X(2)=XINT2
              ENDIF
              IF ((JTT.EQ.(JHOU3+1)).AND.(ITT.GE.IHOL3.AND.ITT.LE.IHOU3)) THEN
                X(1)=XINT1
                X(2)=XINT2
              ENDIF
            GOTO 1015
            ELSE
            IF(ITT.GT.ITTS) THEN
      X(1)=ETA(ITT-1,JTT)
            X(2)=HTC(ITT-1,JTT)
            ENDIF
            ENDIF
1015        T0=TINI(ITT,JTT)
            DO 1000 I=1,NFILE
1000        TW(I)=TWA(I,ITT,JTT)
            IF (ITT.LT.IHOL1.OR.ITT.GT.IHOU1.OR.
     &      JTT.LT.JHOL1.OR.JTT.GT.JHOU1) THEN
      IF (ITT.LT.IHOL2.OR.ITT.GT.IHOU2.OR.
     &      JTT.LT.JHOL2.OR.JTT.GT.JHOU2) THEN
```

```
            IF (ITT.LT.IHOL3.OR.ITT.GT.IHOU3.OR.
     &      JTT.LT.JHOL3.OR.JTT.GT.JHOU3) THEN
            CALL NLGIN(M,N,X,EPS1,EPS2,L,P,D,PP,DX,U,V,KA,S,E,WORK,TW,
     &      TIMTW,T0,NFILE)
            ELSE
            L=0
            X(1)=1.
            X(2)=0.
            ENDIF
            ENDIF
            ENDIF
      WRITE (*,*)
            WRITE (*,5) L
5     FORMAT (1X,'L=', I4)
      WRITE (*,*)
c      IF (L.EQ.0) THEN
            WRITE (*,20) ITT,JTT
c      WRITE (16,*) ITT,JTT
      WRITE (*,10) X(1), X(2)
            WRITE (16,*)ITT,JTT,L, X(1), X(2)
            ETA(ITT,JTT)=X(1)
            HTC(ITT,JTT)=X(2)
            IF (ETA(ITT,JTT).LE.0.) THEN
            ETA(ITT,JTT)=0.01
            ENDIF
            IF (ETA(ITT,JTT).GT.1.) THEN
            ETA(ITT,JTT)=0.99
            ENDIF
            IF (HTC(ITT,JTT).LE.0.) THEN
            HTC(ITT,JTT)=150.
            ENDIF
      WRITE (*,*)
            WRITE(23,*)ETA(ITT,JTT)
      WRITE(24,*)HTC(ITT,JTT)
c      ENDIF
  10  FORMAT (1X, 'X(1)=', E13.6, 3X, 'X(2)=', E13.6)
  20        FORMAT (1X, 'ITE=', I5, 3X, 'JTE=', I5)
1020  CONTINUE
1010  CONTINUE
C
c      DO 1030 JTT=1,JLINE
c            DO 1030 ITT=1,INUM
c1030  CONTINUE
      CLOSE(23)
      CLOSE(24)
      STOP
      END
c-----------------------------------------------------------------
            INCLUDE "SUB-F-DF-CSP.FOR"
            INCLUDE "SUB-LEAST-SQUARE.FOR"
```

B.2 Subroutine "SUB-LEAST-SQUARE.FOR"

```
C-----------------------------------------------------------------------
C-----------------------------------------------------------------------
      SUBROUTINE EROFUN (W, ERFW, ERFDEW)
            DIMENSION  WI(54), ERFWI(54)
            DATA ERFWI/0.00000,0.02256,0.04511,0.06762,0.09008,0.11246,0.13476
     &        ,0.15695,0.17901,0.20094,0.22270,0.24430,0.26570,0.28690
     &        ,0.30788,0.32863,0.34913,0.36936,0.38933,0.40901,0.42839
     &        ,0.46622,0.50275,0.53790,0.57162,0.60386,0.63459,0.66378
     &        ,0.69143,0.71754,0.74210,0.76514,0.78669,0.80677,0.82542
     &        ,0.84270,0.85865,0.87333,0.88679,0.89910,0.91031,0.93401
     &        ,0.95228,0.96611,0.97635,0.98379,0.98909,0.99279,0.99532
     &        ,0.99814,0.99931,0.99976,0.99992,0.99998/
      WI(1)=0.0
            DO 2000 I=2,21
            WI(I)=WI(I-1)+0.02
2000  CONTINUE
      DO 2010 I=22,41
      WI(I)=WI(I-1)+0.04
2010  CONTINUE
      DO 2020 I=42,49
      WI(I)=WI(I-1)+0.1
2020  CONTINUE
      DO 2030 I=50,54
      WI(I)=WI(I-1)+0.2
2030  CONTINUE
      DO 2040 I=1,53
            IF (W.GT.WI(I).AND.W.LE.WI(I+1) ) THEN
            ERFW=ERFWI(I)+(W-WI(I))/(WI(I+1)-WI(I))*(ERFWI(I+1)-ERFWI(I))
            ERFDEW=2.0/(3.1415926)**0.5*EXP(-W**2)
            ELSE
            ENDIF
            IF (W.GT.3.0) THEN
            ERFW=1.0
      ERFDEW=2.0/(3.1415926)**0.5*EXP(-W**2)
            ELSE
            ENDIF
2040  CONTINUE
      RETURN
            END
C-----------------------------------------------------------------------
C-----------------------------------------------------------------------


C-----------------------------------------------------------------------
C-----------------------------------------------------------------------
      SUBROUTINE F(M,N,X,D,TW,T0,TIMTW,NN)
            DIMENSION  TW(NN),TIMTW(NN),X(N),D(M)
C
            VH=X(2)
            VETA=X(1)
            DO 1000 I=1,NN
            TIM=TIMTW(I)
            TEMP=TW(I)
            CALL FF(VH,VETA,VF,TIM,TEMP,T0)
```

```
          D(I)=VF
1000  CONTINUE
C
          RETURN
      END
C-------------------------------------------------------------
C-------------------------------------------------------------
      SUBROUTINE FJ(M,N,X,P,T0,TIMTW,NN)
      DIMENSION X(N),P(M,N),TIMTW(NN)
          VH=X(2)
          VETA=X(1)
          DO 1050 I=1,NN
          TIM=TIMTW(I)
          CALL FFJ(VH,VETA,VDFH,VDFETA,TIM,T0)
          P(I,1)=VDFETA
          P(I,2)=VDFH
1050  CONTINUE
      RETURN
      END
C---------------------------------------------------------------------

C---------------------------------------------------------------------
C---------------------------------------------------------------------
      SUBROUTINE NLGIN(M,N,X,EPS1,EPS2,L,P,D,PP,DX,U,V,KA,S,E,WORK,
     &      TW,TIMTW,T0,NN)
      DIMENSION TW(NN),TIMTW(NN)
      DIMENSION X(N), P(M,N),D(M),PP(N,M),DX(N),WORK(KA)
      DIMENSION U(M,M), V(N,N),Y(10),B(10), S(KA), E(KA)
C
      L=500
      ALPHA=1.0
C
 5    CALL F(M,N,X,D,TW,T0,TIMTW,NN)
      CALL FJ(M,N,X,P,T0,TIMTW,NN)
C
      CALL GINV(M,N,P,D,PP,DX,LL,EPS2,U,V,KA,S,E,WORK)
      IF(LL.NE.0) THEN
      L=1
      RETURN
      ENDIF
      J=0
10    IF(J.LE.2) THEN
      Z=ALPHA+J*0.01
      ELSE
      Z=H2
      ENDIF
      DO 20 I=1,N
20    V(I,1)=X(I)-Z*DX(I)
      CALL F(M,N,X,D,TW,T0,TIMTW,NN)
      Y1=0.0
      DO 30 I=1,M
30    Y1=Y1+D(I)*D(I)
      DO 40 I=1,N
40    V(I,1)=X(I)-(Z+0.00001)*DX(I)
      CALL F(M,N,X,D,TW,T0,TIMTW,NN)
      Y2=0.0
```

```
      DO 50 I=1,M
50    Y2=Y2+D(I)*D(I)
      Y0=(Y2-Y1)/0.00001
      IF (ABS(Y0).GT.1.0E-10) THEN
      H1=Y0
      H2=Z
      IF(J.EQ.0) THEN
      Y(1)=H1
      B(1)=H2
      ELSE
      Y(J+1)=H1
      KK=0
      DO 60 K=1,J
      IF(KK.EQ.0) THEN
      IF(ABS(H2-B(K))+1.0.EQ.1.0) THEN
      KK=1
      ELSE
      H2=(H1-Y(K))/(H2-B(K))
      END IF
            ENDIF
60    CONTINUE
      B(J+1)=H2
      IF(KK.NE.0) B(J+1)=1.0E+35
      H2=0.0
      DO 70 K=J,1,-1
70    H2=-Y(K)/(B(K+1)+H2)
      H2=H2+B(1)
      ENDIF
      J=J+1
      IF(J.LE.7) GOTO 10
      Z=H2
      ENDIF
      ALPHA=Z
      Y1=0.0
      Y2=0.0
      DO 80 I=1,N
      DX(I)=-ALPHA*DX(I)
      X(I)=X(I)+DX(I)
      Y1=Y1+ABS(DX(I))
      Y2=Y2+ABS(X(I))
80    CONTINUE
      IF (Y1.LT.EPS1*Y2) THEN
      L=0
      RETURN
      ENDIF
      L=L-1
      IF (L.GE.0) GOTO 5
      RETURN
      END
C-------------------------------------------------------------
C-------------------------------------------------------------
      SUBROUTINE GINV (M,N,A,B,AA,X,L,EPS,U,V,KA,S,E,WORK)
      DIMENSION A(M,N), U(M,M), V(N,N), B(M), AA(N,M), X(N)
      DIMENSION S(KA), E(KA), WORK(KA)
      CALL UAV(A,M,N,U,V,L,EPS,KA,S,E,WORK)
      IF (L.EQ.0) THEN
```

```
      K=1
10    IF(A(K,K).NE.0.0) THEN
      K=K+1
      IF(K.LE.MIN(M,N)) GOTO 10
      ENDIF
      K=K-1
      IF (K.NE.0) THEN
      DO 40 I=1,N
      DO 40 J=1,M
      AA(I,J)=0.0
      DO 30 II=1,K
30    AA(I,J)=AA(I,J)+V(II,I)*U(J,II)/A(II,II)
40    CONTINUE
      END IF
            DO 80 I=1,N
            X(I)=0.0
      DO 70 J=1,M
70    X(I)=X(I)+AA(I,J)*B(J)
80    CONTINUE
      ENDIF
      RETURN
      END
C-----------------------------------------------------------------------
C-----------------------------------------------------------------------
      SUBROUTINE UAV(A,M,N,U,V,L,EPS,KA,S,E,WORK)
      DIMENSION A(M,N), U(M,M), V(N,N), S(KA), E(KA), WORK(KA)
C
      IT=600
      K=N
      IF(M-1.LT.N) K=M-1
      L=M
      IF(N-2.LT.M) L=N-2
      IF(L.LT.0) L=0
      LL=K
      IF(L.GT.K) LL=L
      IF(LL.GE.1) THEN
      DO 150 KK=1,LL
      IF (KK.LE.K) THEN
      D=0.0
      DO 10 I=KK,M
10    D=D+A(I,KK)*A(I,KK)
      S(KK)=SQRT(D)
      IF(S(KK).NE.0.0) THEN
      IF (A(KK,KK).NE.0.0) S(KK)=SIGN(S(KK),A(KK,KK))
      DO 20 I=KK,M
20    A(I,KK)=A(I,KK)/S(KK)
      A(KK,KK)=1.0+A(KK,KK)
      END IF
      S(KK)=-S(KK)
      ENDIF
      IF (N.GE.KK+1) THEN
      DO 50 J=KK+1, N
      IF ((KK.LE.K).AND.(S(KK).NE.0.0)) THEN
      D=0.0
      DO 30 I=KK,M
30    D=D+A(I,KK)*A(I,J)
```

```
      D=-D/A(KK,KK)
      DO 40 I=KK,M
40    A(I,J)=A(I,J)+D*A(I,KK)
      ENDIF
      E(J)=A(KK,J)
50    CONTINUE
      ENDIF
      IF(KK.LE.K) THEN
      DO 60 I=KK,M
60    U(I,KK)=A(I,KK)
      ENDIF
      IF(KK.LE.L) THEN
      D=0.0
      DO 70 I=KK+1, N
70    D=D+E(I)*E(I)
      E(KK)=SQRT(D)
      IF (E(KK).NE.0.0) THEN
      IF (E(KK+1).NE.0.0) E(KK)=SIGN(E(KK),E(KK+1))
      DO 80 I=KK+1, N
80    E(I)=E(I)/E(KK)
      E(KK+1)=1.0+E(KK+1)
      ENDIF
      E(KK)=-E(KK)
      IF((KK+1.LE.M).AND.(E(KK).NE.0.0)) THEN
      DO 90 I=KK+1, M
90    WORK(I)=0.0
      DO 110 J=KK+1,N
      DO 100 I=KK+1,M
100   WORK(I)=WORK(I)+E(J)*A(I,J)
110   CONTINUE
      DO 130 J=KK+1,N
      DO 120 I=KK+1,M
120   A(I,J)=A(I,J)-WORK(I)*E(J)/E(KK+1)
130   CONTINUE
      ENDIF
      DO 140 I=KK+1, N
140   V(I,KK)=E(I)
      ENDIF
150   CONTINUE
      ENDIF
      MM=N
      IF(M+1.LT.N) MM=M+1
      IF(K.LT.N) S(K+1)=A(K+1,K+1)
      IF(M.LT.MM) S(MM)=0.0
      IF(L+1.LT.MM) E(L+1)=A(L+1,MM)
      E(MM)=0.0
      NN=M
      IF(M.GT.N) NN=N
      IF(NN.GE.K+1) THEN
      DO 190 J=K+1,NN
      DO 180 I=1,M
180   U(I,J)=0.0
      U(J,J)=1.0
190   CONTINUE
      ENDIF
      IF (K.GE.1) THEN
```

```
      DO 250 LL=1,K
      KK=K-LL+1
      IF (S(KK).NE.0.0) THEN
      IF(NN.GE.KK+1) THEN
      DO 220 J=KK+1, NN
      D=0.0
      DO 200 I=KK,M
200   D=D+U(I,KK)*U(I,J)/U(KK,KK)
      D=-D
      DO 210 I=KK,M
210   U(I,J)=U(I,J)+D*U(I,KK)
220   CONTINUE
      ENDIF
      DO 225 I=KK,M
225   U(I,KK)=-U(I,KK)
      U(KK,KK)=1.0+U(KK,KK)
      IF(KK-1.GE.1) THEN
            DO 230 I=1, KK-1
230   U(I,KK)=0.0
      ENDIF
      ELSE
      DO 240 I=1,M
240   U(I,KK)=0.0
      U(KK,KK)=1.0
      ENDIF
250   CONTINUE
      ENDIF
      DO 300 LL=1,N
      KK=N-LL+1
      IF((KK.LE.L).AND.(E(KK).NE.0.0)) THEN
      DO 280 J=KK+1,N
      D=0.0
      DO 260 I=KK+1,N
260   D=D+V(I,KK)*V(I,J)/V(KK+1,KK)
      D=-D
      DO 270 I=KK+1,N
270   V(I,J)=V(I,J)+D*V(I,KK)
280   CONTINUE
      ENDIF
      DO 290 I=1,N
290   V(I,KK)=0.0
      V(KK,KK)=1.0
300   CONTINUE
      DO 305 I=1,M
      DO 305 J=1,N
305   A(I,J)=0.0
      M1=MM
      IT=60
310   IF(MM.EQ.0) THEN
      L=0
      IF(M.GE.N) THEN
      I=N
      ELSE
      I=M
      ENDIF
      DO 315 J=1,I-1
```

```
      A(J,J)=S(J)
      A(J,J+1)=E(J)
315   CONTINUE
      A(I,I)=S(I)
      IF(M.LT.N) A(I,I+1)=E(I)
      DO 314 I=1, N-1
      DO 313  J=I+1, N
      D=V(I,J)
      V(I,J)=V(J,I)
      V(J,I)=D
313   CONTINUE
314   CONTINUE
      RETURN
      ENDIF
      IF (IT.EQ.0) THEN
      L=MM
      IF(M.GE.N) THEN
      I=N
      ELSE
      I=M
      ENDIF
      DO 316 J=1,I-1
            A(J,J)=S(J)
            A(J,J+1)=E(J)
316   CONTINUE
      A(I,I)=S(I)
            IF (M.LT.N) A(I,I+1)=E(I)
            DO 318 I=1,N-1
            DO 317 J=I+1,N
            D=V(I,J)
            V(I,J)=V(J,I)
      V(J,I)=D
317   CONTINUE
318   CONTINUE
      RETURN
            ENDIF
            KK=MM
320   KK=KK-1
      IF (KK.NE.0) THEN
      D=ABS(S(KK))+ABS(S(KK+1))
            DD=ABS(E(KK))
            IF (DD.GT.EPS*D)  GOTO 320
            E(KK)=0.0
            ENDIF
            IF (KK.EQ.MM-1) THEN
            KK=KK+1
            IF(S(KK).LT.0.0) THEN
            S(KK)=-S(KK)
            DO 330 I=1,N
330   V(I,KK)=-V(I,KK)
      ENDIF
335   IF (KK.NE.M1) THEN
      IF (S(KK).LT.S(KK+1)) THEN
            D=S(KK)
            S(KK)=S(KK+1)
            S(KK+1)=D
```

```
          IF (KK.LT.N) THEN
          DO 340 I=1,N
          D=V(I,KK)
          V(I,KK)=V(I,KK+1)
          V(I,KK+1)=D
340   CONTINUE
      ENDIF
          IF (KK.LT.M) THEN
          DO 350 I=1,M
          D=U(I,KK)
          U(I,KK)=U(I,KK+1)
          U(I,KK+1)=D
350   CONTINUE
      ENDIF
          KK=KK+1
          GOTO 335
          ENDIF
          ENDIF
          IT=60
          MM=MM-1
          GOTO 310
          ENDIF
          KS=MM+1
360   KS=KS-1
      IF (KS.GT.KK) THEN
          D=0.0
          IF (KS.NE.MM) D=D+ABS(E(KS))
          IF (KS.NE.KK+1) D=D+ABS(E(KS-1))
          DD=ABS(S(KS))
          IF(DD.GT.EPS*D) GOTO 360
          S(KS)=0.0
          ENDIF
          IF (KS.EQ.KK) THEN
          KK=KK+1
          D=ABS(S(MM))
          IF (ABS(S(MM-1)).GT.D) D=ABS(S(MM-1))
          IF (ABS(E(MM-1)).GT.D) D=ABS(E(MM-1))
          IF (ABS(S(KK)).GT.D) D=ABS(S(KK))
          IF (ABS(E(KK)).GT.D)  D=ABS(E(KK))
          SM=S(MM)/D
          SM1=S(MM-1)/D
          EM1=E(MM-1)/D
          SK=S(KK)/D
          EK=E(KK)/D
          B=((SM1+SM)*(SM1-SM)+EM1*EM1)/2.0
          C=SM*EM1
          C=C*C
          SHH=0.0
          IF ((B.NE.0.0).OR.(C.NE.0.0)) THEN
          SHH=SQRT(B*B+C)
          IF (B.LT.0.0) SHH=-SHH
          SHH=C/(B+SHH)
          ENDIF
          F=(SK+SM)*(SK-SM)-SHH
          G=SK*EK
          DO 400 I=KK,MM-1
```

```
          CALL SSS(F,G,CS,SN)
          IF (I.NE.KK) E(I-1)=F
          F=CS*S(I)+SN*E(I)
          E(I)=CS*E(I)-SN*S(I)
          G=SN*S(I+1)
          S(I+1)=CS*S(I+1)
          IF ((CS.NE.1.0).OR.(SN.NE.0.0)) THEN
          DO 370 J=1,N
          D=CS*V(J,I)+SN*V(J,I+1)
          V(J,I+1)=-SN*V(J,I)+CS*V(J,I+1)
          V(J,I)=D
370   CONTINUE
      ENDIF
          CALL SSS (F,G,CS,SN)
          S(I)=F
          F=CS*E(I)+SN*S(I+1)
          S(I+1)=-SN*E(I)+CS*S(I+1)
          G=SN*E(I+1)
          E(I+1)=CS*E(I+1)
          IF (I.LT.M) THEN
           IF ((CS.NE.1.0).OR.(SN.NE.0.0)) THEN
          DO 380 J=1,M
          D=CS*U(J,I)+SN*U(J,I+1)
          U(J,I+1)=-SN*U(J,I)+CS*U(J,I+1)
          U(J,I)=D
380   CONTINUE
      ENDIF
          ENDIF
400   CONTINUE
      E(MM-1)=F
          IT=IT-1
          GOTO 310
          ENDIF
          IF (KS.EQ.MM) THEN
          KK=KK+1
          F=E(MM-1)
          E(MM-1)=0.0
          DO 420 LL=KK,MM-1
          I=MM+KK-LL-1
          G=S(I)
          CALL SSS (G,F,CS,SN)
          S(I)=G
          IF (I.NE.KK) THEN
          F=-SN*E(I-1)
          E(I-1)=CS*E(I-1)
          ENDIF
          IF (( CS.NE.1.0).OR.(SN.NE.0.0)) THEN
          DO 410 J=1,N
          D=CS*V(J,I)+SN*V(J,MM)
          V(J,MM)=-SN*V(J,I)+CS*V(J,MM)
          V(J,I)=D
410   CONTINUE
      ENDIF
420   CONTINUE
      GOTO 310
          ENDIF
```

```
            KK=KS+1
            F=E(KK-1)
            E(KK-1)=0.0
            DO 450 I=KK,MM
            G=S(I)
            CALL SSS (G,F,CS,SN)
            S(I)=G
            F=-SN*E(I)
            E(I)=CS*E(I)
            IF (( CS.NE.1.0).OR.(SN.NE.0.0)) THEN
            DO 430 J=1,M
            D=CS*U(J,I)+SN*U(J,KK-1)
            U(J,KK-1)=-SN*U(J,I)+CS*U(J,KK-1)
            U(J,I)=D
430   CONTINUE
      ENDIF
450   CONTINUE
      GOTO 310
            END
C-------------------------------------------------
C-------------------------------------------------
            SUBROUTINE  SSS(F,G,CS,SN)
C
            IF (( ABS(F)+ABS(G)).EQ.0.0) THEN
            CS=1.0
            SN=0.0
            D=0.0
            ELSE
            D=SQRT(F*F+G*G)
            IF (ABS(F).GT.ABS(G))  D=SIGN (D,F)
            IF (ABS(G).GE.ABS(F))  D=SIGN (D,G)
            CS=F/D
            SN=G/D
            ENDIF
            R=1.0
            IF (ABS(F).GT.ABS(G)) THEN
            R=SN
            ELSE
            IF (CS.NE.0.0) R=1.0/CS
            ENDIF
            F=D
            G=R
            RETURN
            END
C-------------------------------------------------------------
```

B.3 Subroutine "SUB-F-DF-CSP.FOR"

```
C-----------------------------------------------------------------------
      SUBROUTINE FF(VH,VETA,VF,TIMTW1,TW1,T0)
            PARAMETER NUMT=180
            DIMENSION TM(NUMT),TC(NUMT),TAO(NUMT)
            COMMON AK,ALFA,NUM,TM,TC,TAO
C
            VCON=(VH/AK)**2*ALFA
```

```
          UTTAO=0.0
      DO 1010 ITIME=2,NUM
            IF(TAO(ITIME).LT.TIMTW1) THEN
              DTTAO=TIMTW1-TAO(ITIME)
              DTC=TC(ITIME)-TC(ITIME-1)
              DTM=TM(ITIME)-TM(ITIME-1)
        W=VH/AK*SQRT(ALFA*DTTAO)
              CALL EROFUN(W, ERFW, ERFDEW)
              UT=1-EXP(VCON*DTTAO)*(1-ERFW)
              UT=UT*( VETA*DTC+(1-VETA)*DTM )
              UTTAO=UTTAO+UT
       ELSE
            ENDIF
1010  CONTINUE
C
      DTTAO=TIMTW1-TAO(1)
          DTC=TC(1)-T0
          DTM=TM(1)-T0
      W=VH/AK*SQRT(ALFA*DTTAO)
          CALL EROFUN(W, ERFW, ERFDEW)
          UT=1-EXP(VCON*DTTAO)*(1-ERFW)
          UT=UT*( VETA*DTC+(1-VETA)*DTM )
          UTTAO=UTTAO+UT
          VF=TW1-T0-UTTAO
      RETURN
          END
C-------------------------------------------------------------
      SUBROUTINE FFJ(VH,VETA,VDFH,VDFETA,TIMTW1,T0)
          PARAMETER NUMT=180
          DIMENSION TM(NUMT),TC(NUMT),TAO(NUMT)
          COMMON AK,ALFA,NUM,TM,TC,TAO
      VDFETA=0.
          VDFH=0.
          VCON=(VH/AK)**2*ALFA
          DO 1010 ITIME=2,NUM
            IF(TAO(ITIME).LT.TIMTW1) THEN
              DTTAO=TIMTW1-TAO(ITIME)
              DTC=TC(ITIME)-TC(ITIME-1)
              DTM=TM(ITIME)-TM(ITIME-1)
        W=VH/AK*SQRT(ALFA*DTTAO)
              CALL EROFUN(W, ERFW, ERFDEW)
              P11=1-EXP(VCON*DTTAO)*(1-ERFW)
              P12=EXP(VCON*DTTAO)*(2*VH/AK**2*ALFA*DTTAO)*(1-ERFW)
     &        -EXP(VCON*DTTAO)*ERFDEW/AK*SQRT(ALFA*DTTAO)
        VDFETA=-P11*(DTC-DTM)+VDFETA
              VDFH=VDFH+P12*(VETA*DTC+(1-VETA)*DTM)
       ELSE
            ENDIF
1010  CONTINUE
      DTTAO=TIMTW1-TAO(1)
          DTC=TC(1)-T0
          DTM=TM(1)-T0
      W=VH/AK*SQRT(ALFA*DTTAO)
          CALL EROFUN(W, ERFW, ERFDEW)
          P11=1-EXP(VCON*DTTAO)*(1-ERFW)
          P12=EXP(VCON*DTTAO)*(2*VH/AK**2*ALFA*DTTAO)*(1-ERFW)
```

```
&        -EXP(VCON*DTTAO)*ERFDEW/AK*SQRT(ALFA*DTTAO)
 VDFETA=-P11*(DTC-DTM)+VDFETA
        VDFH=VDFH+P12*(VETA*DTC+(1-VETA)*DTM)
        RETURN
        END
```

BIBLIOGRAPHY

Ahn, J., Jung, I. S., and Lee, J. S., 2000, "Film Cooling from Two Rows of Holes with Opposite Orientation Angles: Heat Transfer", JSME International Journal, Series B, Vol.43, pp.706-711.

Ammari, H. D., Hay, N., and Lampard, D, 1990, "The Effect of Density Ratio on the Heat Transfer Coefficient from a Film-Cooled Flat Plate", Journal of Turbomachinery , Vol. 112, pp.444-450.

Barigozzi, G., Franchini, G., and Perdichizzi, A.,2007, "The Effect of an Upstream Ramp on Cylindrical and Fan-shaped Hole Film Cooling-Part I: Aerodynamic Results", GT2007-27077, ASME: Turbo Expo 2007, Montreal, Canada.

Barigozzi, G., Franchini, G., and Perdichizzi, A.,2007, "The Effect of an Upstream Ramp on Cylindrical and Fan-shaped Hole Film Cooling-Part II: Adiabatic Effectiveness Results", GT2007-27079, ASME: Turbo Expo 2007, Montreal, Canada.

Barlow, D. N., and Kim, Y. W., 1995, "Effect of Surface Roughness on Local Heat Transfer and Film Cooling Effectiveness", ASME Paper 95-GT-14.

Bergeles. G., Gosman, A. D., and Launder, B. E., 1977, " Near-Field Character of a Jet Discharged through a Wall at 30 Degrees to a Mainstream", AIAA Journal, Vol. 15, No. 4, pp. 499-504.

Berger, P. A., Liburdy, J. A., 1998, " A Near-Field Investigation into the Effects of Geometry and Compound Angle on the Flow Field of Film Cooling Holes", ASME Paper No. 98-GT-278.

Bunker, R. S., 2002, "Film Cooling Effectiveness Due to Discrete Holes Within a Transverse Surface Slot," Paper GT-2002-30178, IGTI Turbine Expo, Amsterdam, Netherlands.

Bunker, R. S., 2005, "Technology Review: A Review of Shaped Hole Turbine Film-Cooling Technology", Journal of Heat Transfer, Vol.121, pp.441-453.

Bunker, R. S., 2006, "Gas Turbine Heat Transfer: 10 Remaining Hot Gas Path Challenges," Proceedings of GT2006, ASME Turbo Expo 2006: Power for Land, Sea and Air, May 8-11, 2006, Barcelona, SPAIN.

Burd, S. W., Simon, T. W.,1997, "The Influence of Coolant Supply Geometry on Film Coolant Exit Flow and Surface Adiabatic Effectiveness", ASME Paper 97-GT_25

Chen,S. P., Li, P.W., Chyu, M. K., Cunha, F. J., and Messeh, W. A., "Heat Transfer in an Airfoil Trailing Edge Configuration with Shaped Pedestals Mounted Internal Cooling Channel and Pressure Side Cutback", Proceedings of GT2006, ASME Turbo Expo 2006: Power for Land, Sea and Air, May 8-11, 2006, Barcelona, SPAIN

Cho, H. H., Rhee, D. H., and Kim, B.G., 2001, "Enhancement of Film Cooling Performance Using a Shaped Film Cooling Hole with Compound Angle Injection", JSME International Journal, Series B, Vol. 44, No. 1, pp. 99-110.

Drost, U., Bőlcs, A., and Hoffs, A., 1997, "Utilization of the Transient Liquid Crystal Technique for Film Cooling Effectiveness and Heat Transfer Investigation on a Flat Plate and a Turbine Airfoil", ASME Paper 97-GT-26.

Ekkad, S. V., Zapata, D., and Han, J. C., 1997, "Film cooling effectiveness over a Flat Surface with Air and CO2 Injection through Compound Angle Holes Using a transient Liquid Crystal Image Method", Journal of Turbomachinery, Vol. 119, pp.587-593

Ekkad, S. V., Zapata, D., and Han, J. C., 1997, "Heat Transfer Coefficient over a Flat Surface with Air and CO2 Injection through Compound Angle Holes Using a transient Liquid Crystal Image Method", Journal of Turbomachinery, Vol. 119, pp.580-586

Ekkad, S. V., Ou, S., and Richard, B. R., 2004, "A Transient Infrared Thermography Method for Simultaneous Film Cooling Effectiveness and Heat Transfer Coefficient Measurements from a Single Test", ASME Paper GT2004-54236.

Eriksen, and Goldstein, R. J., 1974, "Heat Transfer and Film Cooling Following Injection Through Inclined Tubes", ASME Journal of Heat Transfer,116, pp. 239-245.

Forth, C. J. P., Jones, T. V., 1988, "Scaling Parameters in Film Cooling", Proceedings 8th International Heat transfer Conference, Vol.3, pp. 1271-1276.

Foster, N. W., Lampard, D., 1980, "The Flow and Film Cooling Effectiveness Following Injection through a Row of Holes", Journal of Engineering for Power, Vol.102, pp.584-588.

Fric, T. F., and Campbell, R. P., 2002, "Method for Improving the Cooling Effectiveness of a Gaseous Coolant Stream Which Flows Through a Substrate, and Related Articles of Manufacture," US Patent No. 6,383,602.

Fric, T. F., and Roshko, A., 1994, "Vortical Structure in the Wake of a Transverse Jet", Journal of Fluid Mechanics, Vol.279, pp.1-47.

Gillespie, D. R. H., Wang, Z., Ireland, P. T., and Kohler, S. T., 1996, "Full Surface Local Heat Transfer Coefficient Measurements in a Model of an Integrally Cast Impingement Cooling Geometry", ASME Paper 96-GT-200.

Goldstein, R. J., 1971, “Film Cooling”, Advance Heat Transfer, 7, pp.321-379.

Goldstein, R. J., Eckert, E. R. G., Burggraf, F., 1974, “Effect of Hole Geometry and Density on Three-Dimensional Film Cooling”, International Journal of Heat Mass Transfer, Vol. 17, pp. 595-607.

Goldstein, R. J., Eckert, E. R. G., Chiang, H. D., and Elovic, E., 1985,“Effect of Surface Roughness on Film Cooling Performance”, ASME Journal of Engineering for Gas Turbines and Power, Vol. 107, pp. 111-116.

Goldstein, R. J., and Jin, P., 2001 “Film Cooling Downstream of a Row of Discrete Holes with Compound Angles”, Journal of Turbomachinery, Vol. 123, pp. 222-230.

Gritsh, M., Schulz, A., and Wittig, S., 1998, “Adiabatic Wall Effectiveness Measurements of Film Cooling Holes with Expanded Exits”, Journal of Turbomachinery, Vol. 120, pp. 549-556.

Hale, C. A., Plesniak, M. W., and Ramadhyani, S., 2000, “Film Cooling Effectiveness for Short Film Cooling Holes Fed by a Narrow Plenum”, Journal of Turbomachinery, Vol. 122, pp.553-557.

Han, J.C., Dutta, S., and Ekkad, S.V., 1999, “Gas Turbine Heat Transfer and Cooling Technology”, Taylor & Francis.

Harrison, K. L., Dorrington, J. R., Dees, J. E., and Bogard, D. G., “Turbine Airfoil Net Heat Flux Reduction with Cylindrical Holes Embedded in a Transverse Trench”, GT2007-27996, ASME Turbo Expo 2007, Montreal, Canada.

Harrison, K. L., and Bogard, D. G., “CFD Predictions of Film Cooling Adiabatic Effectiveness for Cylindrical Holes Embedded in Narrow and Wide Transverse Trenches”, GT2007-28005, ASME Turbo Expo 2007, Montreal, Canada.

Hay, N., Lampard, D., and Saluja, C. L., 1985, “Effects of Cooling Films on the Heat Transfer Coefficient on a Flat Plate with Zero Mainstream Pressure Gradient”, ASME Journal of Engineering Gas Turbines Power, 107, pp. 104-110.

Haven, B. A., and Kurosaka, M., 1996. ”Improved Jet Coverage through Vortex Cancellation,” AIAA J., Vol. 34, No. 11, 1996, pp2443-2444.

Haven, B. A., and Kurosaka, M., 1997, “Kidney and Anti-kidney Vortices in Cross flow Jets”, Journal of Fluid Mechanics, Vol.352,pp. 27-64.

Haven, B. A., Yamagata, D. K., Kurosaka, M., Yamawaki, S., and Maya, T., 1997, “Anti-kidney Pair of Vortices in Shaped Holes and Their Influence on Film Cooling Effectiveness”, ASME Paper 97-GT-45.

Hyams, D. G., McGovern, K. T., and Leylek, J. H., 1997, “Effect of Geometry on Slot-Jet Film Cooling Performance”, ASME Paper 96-GT-187.

Jumper, G. W., Elrod, W. C., and Rivir, R. B., 1991, "Film Cooling Effectiveness in High-Turbulence Flow", Journal of Turbomachinery, Vol. 113,pp. 479-483.

Jung, I. S., and Lee, J. S., 2000, "Effect of Orientation Angles on Film Cooling Over a Flat Plate: Boundary Layer Temperature Distributions and Adiabatic Film Cooling Effectiveness", Journal of Turbomachinery, Vol. 122, pp. 153-160.

Kim, Y. W., Chad, C., and Moon, H. K., 2005, "Film Cooling Characteristics of Pressure Side Discharge Slots in an Accelerating Mainstream Flow," Proceedings of GT2005, ASME Turbo Expo 2005: Power for Land, Sea and Air, June 6-9, Reno-Tahoe, Nevada, USA

Kohli, A., and Bogard, D. G., 1999, "Effect of Hole Shape on Film Cooling with Large Angle Injection", ASME Paper 99-GT-165.

Lee, H.-W., Park, J. J., and Lee, J. S., 2002, "Flow Visualization and Film Cooling Effectiveness Measurements around Shaped Holes with Compound Angle Orientations", International Journal of Heat and Mass Transfer, Vol. 45, pp. 145-156.

Ligrani, P. M., Ciriello, S., and Bishop, D. T., 1992, "Heat Transfer, Adiabatic Effectiveness, and Injectant Distributions Downstream of a Single Row and Two Staggered Rows of Compound Angle Film-Cooling Holes", Journal of Turbomachinery, Vol. 114, pp. 687-700.

Lu, Y. , Nasir, H., and Ekkad, S. V., 2005, "Film Cooling from a Row of Holes Embedded in Transverse Trenches", ASME Paper GT2005-68598.

Lutum, E., Johnson, B. V., 1999, "Influence of the Hole Length-to-Diameter Ratio on Film cooling with Cylindrical Holes", Journal of Turbomachinery, Vol. 121, pp. 209-216

Makki, Y. H., and Jakubowski, G. S., 1986, "An Experimental Study of Film Cooling from Diffused Trapezoidal Shaped Holes", AIAA Paper AIAA-86-1326.

Martini, P., and Schulz, A., 2004, "Experimental and Numerical Investigation of Trailing Edge Film Cooling by Circular Coolant Wall Jets Ejected from a Slot with Internal Rib Arrays," Journal of Turbomachinery, 126, pp.229-236

Mehendale, A. B., and Han, J. C., 1992, "Influence of High Mainstream Turbulence on Leading Edge Film Cooling Heat Transfer", Journal of Turbomachinery, Vol. 114, pp. 707-715.

Na, S., and Shih, T. I-P., 2006, "Increasing Adiabatic Film Cooling Effectiveness by Using an Upstream Ramp," Proceedings of GT2006, ASME Turbo Expo 2006: Power for Land, Sea and Air, May 8-11, 2006, Barcelona, SPAIN.

Obot, N. T., Majumdar, A. S., and Douglas, W. J. M., 1979, "The Effect of Nozzle Geometry on Impingement Heat transfer under a Round Turbulent Jet", ASME Paper 79-WA/HT-53.

Okita, Y., and Nishiura, M., 2006, "Film Effectiveness Performance of an Arrowhead-Shaped Film Cooling Hole Geometry," Proceedings of GT2006, ASME Turbo Expo 2006: Power for Land, Sea and Air, May 8-11, 2006, Barcelona, SPAIN

Papell, S. S, 1984, "Vortex Generating Coolant Flow Passage Design for Increased Film Cooling Effectiveness and Surface Coverage", NASA Technical Paper 2388.

Pedeson, D. R. , Eckert, E. R. G., and Goldstein, R. J., 1977, "Film Cooling with Large Density Differences Between the Mainstream and the Secondary Fluid Measured by the Heat-Mass Transfer Analogy", Journal of Heat Transfer, Vol. 99, pp. 620-627.

Pietrzyk, J. R., Bogard, D. G., and Crawford, M. E., 1989, "Hydrodynamic Measurements of Jets in Cross Flow for Gas Turbine Film Applications", Journal of Turbomachinery, Vol. 111, pp.139-145.

Salcudean, M., Gartshore, I., Zhang, K., and Barnea, Y, 1994, "Leading Edge Film Cooling of a Turbine Blade Model Through Single and Double Row Injection: Effect of Coolant Density", ASME paper 94-GT-2.

Saumweber, C. A., Schulz, A., and Wittig, S., 2003 "Free-Stream Turbulence Effects on Film Cooling with Shaped Holes", Journal of Turbomachinery, Vol. 125, pp. 65-72.

Schmidt, D. L., Sen, B., and Bogard, D. G., 1996, "Film Cooling with Compound Angle Holes: Adiabatic Effectiveness", Journal of Turbomachinery, Vol. 118, pp. 807-813.

Schmidt, D. L., Sen, B., and Bogard, D. G., 1996,"Effect of Surface Roughness on Film Cooling", ASME Paper 96-GT-299.

Schwarz, S. G., Goldstein, R. J., and Eckert, E. R. G., 1990," The influence of Curvature on Film Cooling Performance", ASME Journal of Turbomachinery, Vol. 112. pp. 472-478.

Shih, T. I-P, Lin, Y.-L., Chyu, M.K., and Gogineni, S., 1999, ''Computation of Film Cooling From Holes with Struts'', ASME Paper 99-GT-282, June 1999

Shih, T. I-P. Na, S., and Chyu, M. K., 2006, "Preventing Hot Gas Ingestion by Film-cooling Jets via Flow-aligned Blockers," Proceedings of GT2006, ASME Turbo Expo 2006: Power for Land, Sea and Air, May 8-11, 2006, Barcelona, SPAIN

Sinha, A. K., Bogard, D. G., and Crawford, M. E., 1991, "Film Cooling Effectiveness Downstream of a Single Row of Holes with Variable Density Ratio", Journal of Turbomachinery, Vol. 113, pp.442-449.

Somawardhana, R. P., and Bogard, D. G., "Effects of Obstructions and Surface Roughness on Film Cooling Effectiveness with and without a Transverse Trench", GT2007-28003, ASME Turbo Expo 2007, Montreal, Canada.

Teekaram, A. J. H., Forth, C. J. P., and Jones, T. V., 1989, "The Use of Foreign Gas to Simulate the Effects of Density Ratios in Film Cooling", Journal of Turbomachinery, Vol. 111, pp. 57-62.

Thole, K., Gritsch, M., Schulz, A., and Wittig, S., 1998, "Flow Field Measurement of Film Cooling Holes with Expanded Exits", Journal of Turbomachinery, Vol.120, pp327-336.

Vedula, R. J., and Metzger, D. E., 1991, "A Method for Simultaneously Determination of Local Effectiveness and Heat Transfer Distribution in Three-Temperature Convection Situations," ASME paper 91-GT-345.

Waye, S. K., and Bogard, D. G., 2006, "High Resolution Film Cooling Effectiveness Measurements of Axial Holes Embedded in a Transverse Trench with Various Trench Configurations", Proceedings of GT2006, ASME Turbo Expo 2006: Power for Land, Sea and Air, May 8-11, 2006, Barcelona, SPAIN

Wilfert, G., and Wolff, S., 2000, "Influence of Internal Flow on Film Cooling Effectiveness", Journal of Turbomachinery, Vol.122, pp327-333.

Yu, Y., and Chyu, M. K., 1998, "Influence of Gap Leakage Downstream of the Injection Holes on Film Cooling Performance", ASME Journal of Turbomachinery, Vol. 120., pp.779-807.

Yu, Y., Yen, C.-H., Shih, T.I.-P., Chyu, M. K., and Gogineni, S., 2002 "Film Cooling Effectiveness and Heat Transfer Coefficient Distributions Around Diffusion Shaped Holes," Transaction of ASME, 124, Oct.. pp. 820-827.

Yu, Y., 1993, "Film Cooling Measurements with a Transverse Gap Downstream of the Injection Holes", Ph.D dissertation.

Zaman, K.B.M.Q and Foss, J. K., 1997, "The Effect of Vortex Generators on a Jet in a Cross-Flow," Phys. Fluids, 9(1), January 1997, pp.106-114